**Republic of Iraq**
**Ministry of Higher Education**
**and Scientific Research**
**University of Misan**
**College of Science**
**Department of Chemistry**

# Synthesis and Study of Electrical and Thermal Properties of Some Polyurea nanocomposite

Thesis Submitted to
The College of Science / University of Misan as Partial Fulfillment
of the Requirements for the Master Degree of Science in Chemistry

**By**

## Zainab Kadhim Hamod

B.Sc. Chemistry College of Science / University of Misan
(2019)

Supervisors

Assistant Professor Dr.

**Ahmed Majeed Abbas**

**Mundher Abdul-Hassan**

**2026** **1447**

بسم الله الرحمن الرحيم

﴿ مَا كَانَ لِيَأْخُذَ أَخَاهُ فِي دِينِ الْمَلِكِ إِلَّا أَن يَشَاءَ اللَّهُ نَرْفَعُ دَرَجَاتٍ مَّن نَّشَاءُ وَفَوْقَ كُلِّ ذِي عِلْمٍ عَلِيمٌ ﴾

صدق الله العلي العظيم

سورة يوسف/ الآية ٧٦

# ***Supervisor Certificate***

I am the supervisor of **Ms. Zainab Kadhim Hamod,** certify that the thesis (**Synthesis and Study of Electrical and Thermal Properties for Some Poly urea Polymers)** was done and written under my supervision as a fulfillment of the requirement for the master degree of science in chemistry.

Signature……

**Assistant Professor**

**Dr. Ahmed Majed Abass**

Signature……

**Assistant Professor**

**Dr. Mundher Abdul-Hassen**

*College of Science*

*Misan University*

Date: / 4 /2026

## ***Head of Chemistry Department Recommendation***

According to the recommendation of the supervisor, this thesis is forwarded to the examination committee for approval.

Signature……

***Dr. Mohammed Abdul Raheem Saeed***

H*ead of Chemistry Department*

*College of Science*

*Misan University*

Date: / 4 /2026

# Dedication

All praise is due to **Allah**, and may peace and blessings be upon the most noble of all creation, the Messenger sent as a mercy to the worlds, supported by the victory of the Lord of the worlds. Seeking knowledge has always been our path for the sake of Allah Almighty, and by His grace, we were granted success in this endeavor.

Our pursuit of knowledge was a tribute to my beloved parents—may Allah reward them abundantly—and especially to my dear

Mother and Father

whose love, prayers, and unwavering support sustained me throughout this journey. My sincere appreciation also goes to my dear

Colleagues and Close Friends

whose support and camaraderie made this academic journey both enriching and memorable.

To the one who gave me his Time and Knowledge…

My supervisors

# ***Acknowledgement***

I would like to express my deep gratitude to my esteemed professors, who were the guiding lights illuminating my path toward knowledge and understanding, particularly Asst. Prof. Dr. Ali Taha, Prof. Dr. Jasim Abbas, and Asst. Prof. Dr. Osama Ali. Special thanks and profound appreciation are extended to my supervisor, **Asst. Prof. Dr. Ahmed Majid Abbas**, for his guidance, supervision, and continuous support throughout all stages of this research. I am also deeply grateful to **Asst. Prof. Dr. Mundher Abdul-Hassan** for his assistance and follow-up during the completion of this study.

Finally, I wish to express my heartfelt thanks to the Dean of the College of Science, and to the Head of the Department of Chemistry for their continuous support and for facilitating all requirements necessary for the completion of this work.

***Zainab***

## ***Abstract***

Polymer nanocomposites have attracted considerable scientific attention in recent decades due to their tunable structural, thermal, and electrical properties, making them highly promising for advanced technological applications. In this context, the present study focuses on the synthesis and characterization of eight based polyurea polymers derived from Schiff base monomers, employing selected aromatic monomers and four different diisocyanates (TDI, MDI, HDI and PDI). These polymers were subsequently reinforced with silver and copper nanoparticles to achieve high electrical conductivity combined with excellent thermal stability.

The first monomer, terephthaldehyde bis(thiosemicarbazone) (TBT), was synthesized via the reaction of terephthaldehyde with thiosemicarbazide in ethanol, as shown below:

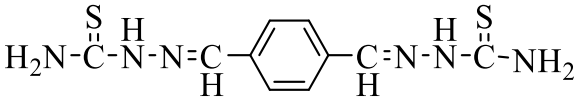

Terephthaldehyde bis(thiosemicarbazone) (TBT)

whereas the second monomer, 5,5′-[(1,4-phenene) bis(1,3,4-thiadiazol-2-amine)] (TDA), was prepared through the reaction of terephthalic acid with thiosemicarbazide using concentrated sulfuric acid as catalyst. As in the following structural formula:

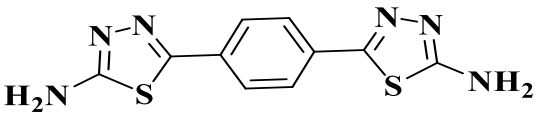

5,5′-[(1,4-phenene) bis(1,3,4-thiadiazol-2-amine)] (TDA)

These monomers served as key building blocks for the polycondensation reactions with the selected diisocyanate in dry N-methyl-2-pyrrolidone (dry-NMP), leading to the formation of polyurea polymers as shown:

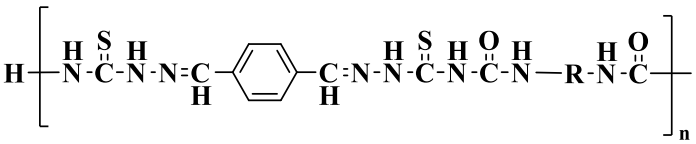

R= 2a= 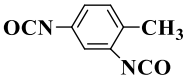 , 2b= 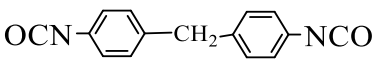 , 2c= 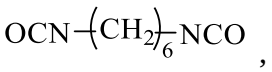 ,

2d= 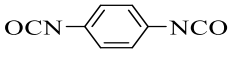

Whereas polyurea polymers were prepared from the TDA:

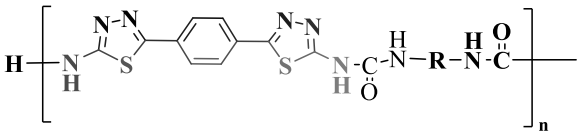

R= 3a= 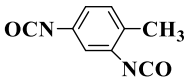 , 3b= 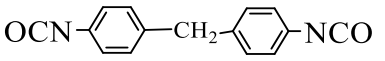 , 3c= 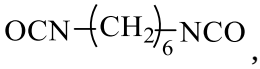 ,

3d= 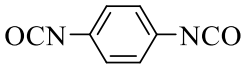

Hybrid polyurea nanocomposites were fabricated by incorporating silver and copper nanoparticles into the polymer matrix using ultrasonic dispersion. FT-IR spectroscopy confirmed the successful formation of polyurea linkages, while thermogravimetric analysis (TGA) revealed a multi-step thermal degradation behavior with high thermal stability, particularly for PDI-based polymers. X-ray diffraction (XRD) analysis verified the crystalline nature of the embedded nanoparticles, whereas FESEM and TEM observations demonstrated a relatively uniform dispersion of silver nanoparticles and the formation of interconnected metallic pathways by copper nanoparticles, contributing significantly to enhanced electrical conductivity. EDX and zeta potential analyses further confirmed effective nanoparticle incorporation and high colloidal stability, especially in copper-containing composites and PDI-based systems. Electrical measurements showed a high conductivity to polyurea-nanocomposite polymers, with silver-based nanocomposites exhibiting superior performance, highlighting their potential for applications in flexible electronics, conductive inks, and thermal management systems.

# Contents

# List of Tables



# List of Figures

# ***List of Abbreviations***

| Abbreviations | Key |
|---|---|
| PVC | Polyvinyl chloride |
| $D_p$ | Degree of polymerization |
| $M_n$ | The number average molecular weight of the polymer |
| M | Molecular weight of the monomer |
| $T_g$ | Glass transition temperature |
| PE | Polyethylene |
| PS | Polystyrene |
| PVA | Polyvinyl alcohol |
| MgO | Magnesium oxide |
| PMMA | Polymethyl methacrylate |
| CGPs | Chain–growth polymerization |
| SGPs | Step-growth polymerizations |
| PUs | Polyurea |
| RIM | Reaction injection molding |
| HS | Hard segment |
| DETDA | Diethyl toluene diamine |
| MDI | Methylene diphenyl diisocyanate |
| TDI | Toluene diisocyanate |
| HDI | Hexamethylene diisocyanate |
| TS | Tensile strength |
| $\varepsilon_B$ | Elongation at break |
| MLD | Molecular layer deposition |
| PDIC | 1,4-Phenylene diisocyanate |
| ED | Ethylenediamine |
| EOC | Ethylene–octene copolymer |
| DFT | Density Functional Theory |
| TSDC | Thermally Stimulated Depolarization Current |
| A | Absorbed |
| $I_o$ | Incident radiation |
| $I_A$ | Intensity of radiation absorbed |
| $I_R$ | Incident of radiation reflection |
| $I_T$ | Incident of radiation transmission |
| XRD | X-ray diffraction |
| β | Full width at half maximum (FWHM) |
| D | The size of the particles |
| λ | The wavelength of the X-rays |
| K | The Scherrer constant |

| | |
|---|---|
| T | Transmittance |
| k | Thermal conductivity |
| $T_m$ | Melting temperature |
| $T_c$ | Crystallization temperature |
| TGA | Thermogravimetric analysis |
| $K_{th}$ | Thermal conductivity coefficient |
| DTG | Derivative thermogravimetry |
| σ | Electrical conductivity |
| n | Carrier concentration |
| μ | Carrier mobility |
| q | Electrical charge |
| S | Sulfur |
| N | Nitrogen |
| HOMO | Highest occupied molecular orbital |
| LUMO | Lowest unoccupied molecular orbital |
| CTCs | charge transfer complexes |
| NPs | Nanoparticles |
| NCs | Nanocomposites |
| FT-IR | Fourier transform infrared spectrophotometry |
| NMR | Nuclear Magnetic Resonance Spectrometer |
| FESEM | Field Emission Scanning Electronic Microscope |
| TEM | Transmission Electron Microscopy |
| EDX | Energy Dispersive X-ray Spectroscopy |
| MP | Melting Point |
| TSC | Thiosemicarbazide |
| TPA | Terephthalic Acid |
| TPAL | Terephthalaldehyde |
| TBT | Terephthaldehyde Bis(thiosemicarbazone) |
| TDA | 5,5'[(1,4-phenelene) bis(1,3,4-thiadiazol-2-amine)] |
| NMP | N-Methyl-2-pyrrolidone |
| DMF | Dimethylformamide |
| TMS | Tetramethylsilane |
| FCC | Face-centered cubic |
| AgNPs | Silver nanoparticles |
| CuNPs | Copper nanoparticles |
| \|ζ\| | Zeta potential |
| CV% | Coefficient of variation of conductivity |

# List of Abbreviations for the Synthesized Chemical Compounds

| *Structural Formula* | *Key* |
|---|---|
| 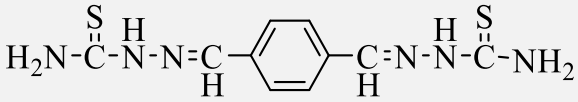 <br>Terephthaldehyde bis(thiosemicarbazone) | **TBT** |
| 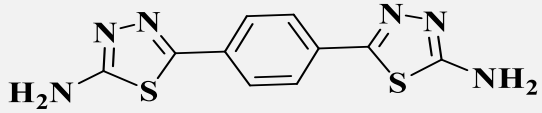 <br>5,5'-(1,4-phenylene) bis(1,3,4-thiadiazol-2-amine) | **TDA** |
| 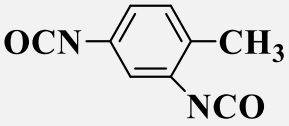 <br>2,4-diisocyanato-1-methylbenzene | **TDI** |
| 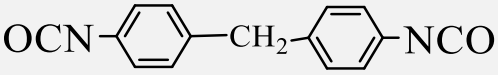 <br>bis(4-isocyanatophenyl)methane | **MDI** |
| 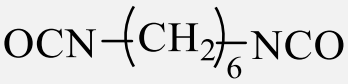 <br>1,6-diisocyanatohexane | **HDI** |
| 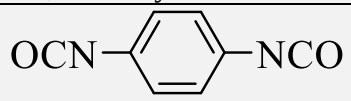 <br>1,4-diisocyanatobenzene | **PDI** |
| 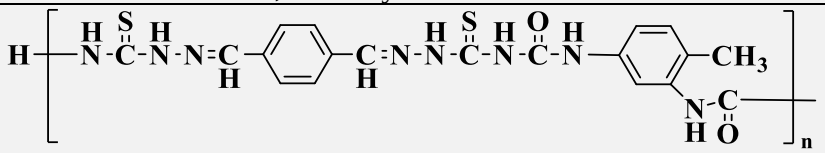 <br>***N*-(5-(3-(2-(4-((2-carbamothioylhydrazineylidene)methyl)benzylidene)hydrazine-1-carbonothioyl)ureido)-2-methylphenyl)acetamide** | **2a** |
| 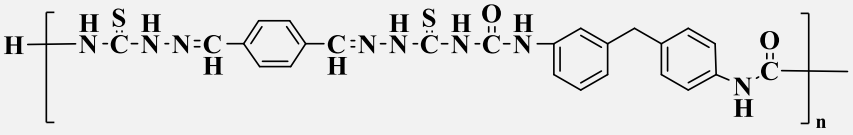 <br>***N*-(4-(3-(3-(2-(4-((2-carbamothioylhydrazineylidene)methyl)benzylidene)hydrazine-1-carbonothioyl)ureido)benzyl)phenyl)acetamide** | **2b** |
| 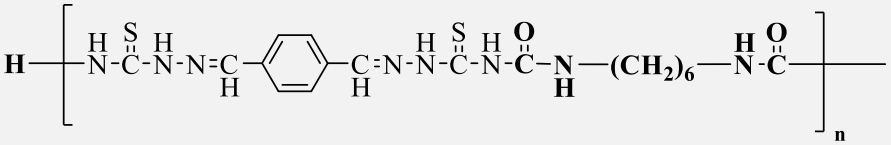 <br>***N*-(6-(3-(2-(4-((2-carbamothioylhydrazineylidene)methyl)benzylidene)hydrazine-1-carbonothioyl)ureido)hexyl)acetamide** | **2c** |

| | |
|---|---|
| 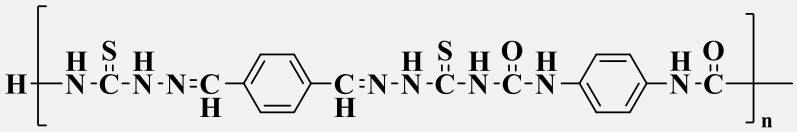 <br>*N*-(4-(3-(2-(4-((2-carbamothioylhydrazineylidene)methyl)benzylidene)hydrazine-1-carbonothioyl)ureido)phenyl)acetamide | **2d** |
| 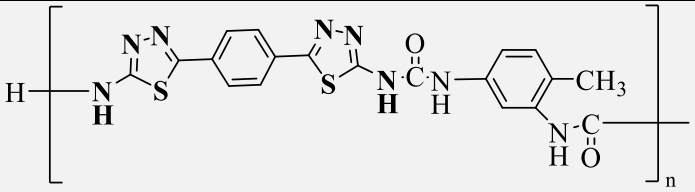 <br>*N*-(5-(3-(5-(4-(5-amino-1,3,4-thiadiazol-2-yl)phenyl)-1,3,4-thiadiazol-2-yl)ureido)-2-methylphenyl)acetamide | **3a** |
| 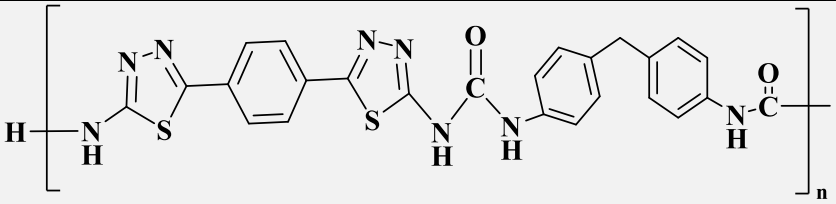 <br>*N*-(4-(4-(3-(5-(4-(5-amino-1,3,4-thiadiazol-2-yl)phenyl)-1,3,4-thiadiazol-2-yl)ureido)benzyl)phenyl)acetamide | **3b** |
| 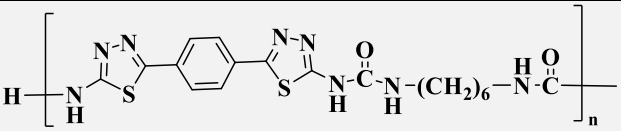 <br>*N*-(6-(3-(5-(4-(5-amino-1,3,4-thiadiazol-2-yl)phenyl)-1,3,4-thiadiazol-2-yl)ureido)hexyl)acetamide | **3c** |
| 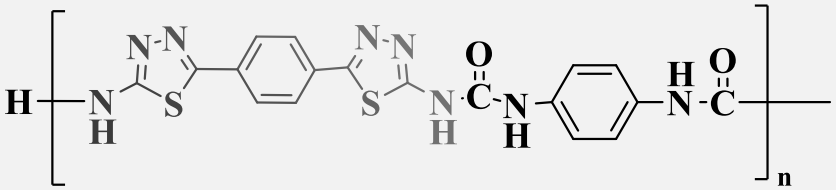 <br>***N*-(4-(3-(5-(4-(5-amino-1,3,4-thiadiazol-2-yl)phenyl)-1,3,4-thiadiazol-2-yl)ureido)phenyl)acetamide** | **3d** |

# *Chapter One*

## *Introduction and previous studies*

## 1.1 General Introduction

The scientific origins of polymer laboratory research trace back to the early twentieth century, specifically to Schrödinger's (1920) pioneering investigations into the long molecular chains constituting polymer structures, which laid the foundation of polymer science [1]. Since then, polymer technology has experienced remarkable progress, driven by the unique physical and mechanical properties of these materials, their high mouldability, the ability to tailor such properties, and the pressing demand for alternatives with superior technological characteristics compared to certain conventional materials [2].

Polymerization and polymers materials have attracted significant attention from both scientific and industrial communities. Extensive research has been devoted to investigating their properties, developing fabrication methods, and enhancing performance, thereby expanding their application rang across diverse sectors. Today, polymers are integral to the manufacture of most industrial products, ranging from children's toys to automotive and aerospace components. Their importance in the energy sector is evident through their use in the production of solar cells and electrochemical cells. Furthermore, a subset of polymers is classified as insulating materials, making them ideal for applications in the electronics industry, including printed circuit boards, electrical insulation materials, and coatings for wires and connectors, consistent with the intrinsic insulating behavior of most polymers. Certain polymers types exhibit notable resistance to elevated temperatures and mechanical stresses, enabling them to serve as effective alternatives to various traditional metals in the construction sector. Reinforced polymers, in particular, have demonstrated considerable utility in prefabricated construction, thermal and acoustic insulation, and in providing durable resistance to diverse environmental conditions [3].

Ongoing research endeavors aim to further improve the resistance of polymers to challenging environmental factors, such as high temperatures and ultraviolet radiation, while enhancing their capacity to withstand shocks and mechanical loads. Additional research objectives include refining their optical, electrical, thermal, mechanical, hardness, and other critical properties. A central focus in polymer science is the development of novel, industrially desirable characteristics through the incorporation of specific additives or the blending of two or more distinct polymers a process known as synthesis. This technology has gained increasing interest in recent years due to its wide-ranging applications, spanning from multicolor photolithography and advanced coatings to adhesives and protective films [4].

## 1.2 Polymers

In the eighteenth century, polymers were classified as colloids, as the colloidal state was regarded as an independent state of matter alongside the solid and liquid states. At that time, the precise composition of these substances was unknown, as the molecular structure of the giant molecules, later referred to as polymers, was not elucidated until 1920 [5]. The majority of polymers are of organic origin, as many organic compounds are classified as hydrocarbons, meaning they are composed primarily of carbon and hydrogen, with their chemical bonds

characterized predominantly by covalent interactions [6]. A polymer is thus defined as a macromolecule composed of repeating smaller chemical units, known as monomers, which serves as the fundamental building block of polymer. These monomers are linked by chemical bonds to form extended molecular chains, imparting polymers with a high molecular weight compared to other compounds [7 , 8]. The term polymer derives from the Latin poly meaning "many" and mer meaning "unit" or "part", thus signifying "many-units" or "many-parts". Representative examples include polyethylene and polyacrylic acid. Polymer molecules are typically held together, along with internal molecular forces commonly referred to as secondary forces or van der Waals forces [9], which act either between distinct polymer chains or within a segment of the same chain. These secondary interactions play a critical role in determining the physical properties of polymers. Polymers can also be classified based on the configuration of their chains, as illustrated in Figure (1-1).

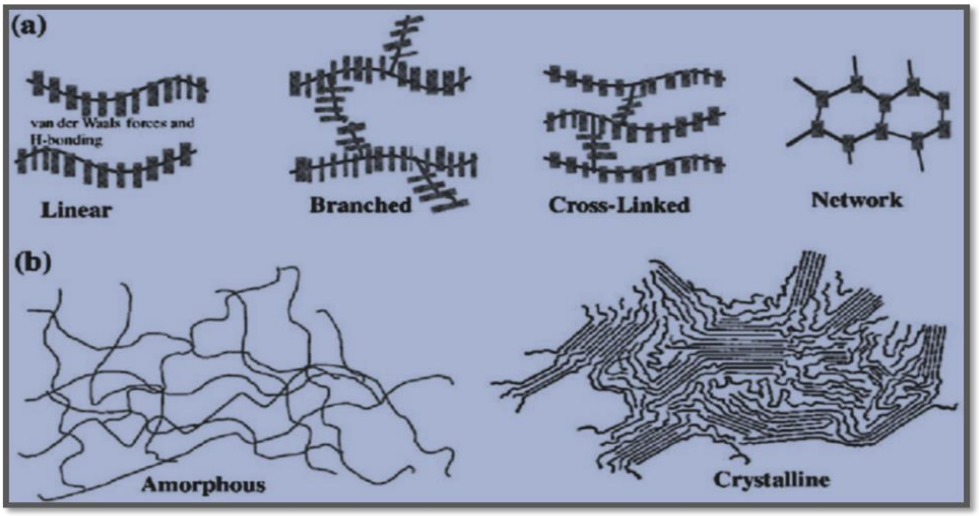


Figure (1-1): (a) polymers molecular structures; (b) polymer chains showing amorphous and crystalline structures [10].

Polymer molecules may be arranged in a linear configuration, in which case the resulting polymer is referred to as a linear polymer. Examples include nylon, polyethylene, polyvinyl chloride (PVC). Alternatively, the chains may be branched, producing a branched polymer, as in the case of amylopectin and low-density polyethylene. In some cases, polymers may adopt a ladder-like structure, or the branches may be interconnected, forming a cross-linked polymer, such as vulcanized rubber (Bakelite) and polyphenol-formaldehyde resins [11, 12]. Network Polymers are three-dimensional structures characterized by a high degree of cross-linking, which imparts hardness and mechanical strength. A notable example is thermosetting plastics, which, upon heating, undergo degradation or combustion rather than melting. These polymers typically possess three active functional groups, as seen in epoxy resins and phenol formaldehyde polymers [13, 14].

The degree of polymerization ($D_p$) is defined as the number of repeating units present within a polymer chain. When the degree of polymerization is relatively low, typically in the range of (10 - 20), the resulting material is referred to as oligomer. In contrast, common industrial

polymers exhibit high degrees of polymerization, with values around ($D_p \approx 100$) for glues and adhesive pastes, and ($D_p \approx 1000$) or higher for synthetic rubber and solid plastics. Consequently, the degree of polymerization serves as an indicator of the polymer's molecular weight, which can be calculate by knowing both $D_p$ and the molecular weight of the corresponding monomer, according to the following relationship [8]. The average molecular weight of all the polymer's chains is usually what people mean when they talk about its molecular weight. The number average molecular weight of the polymer (Mn) is directly related to the degree of polymerisation (Dp). The equation below shows how they are related [15].

$$\mathbf{M_n = D_p \times M} \quad \text{..... (1-1)}$$

M: molecular weight of the monomer.

Polymers possess numerous characteristics, among which the most significant are [16]:

1- They are low-cost materials that are easy to mold and manufacture, requiring minimal or no subsequent processing.
2- They exhibit flexibility and low density, making them lightweight.
3- Most polymers demonstrate low electrical and thermal conductivity, as well as a low modulus of elasticity.
4- Their molecular structures are more complex compared to metals and ceramics.
5- Certain polymers are noted for their color stability and transparency.
6- Some polymers resistance to weak acids, weak bases, and saline solutions.
7- Due to their low density, high specific strength, and excellent corrosion resistance, polymers are highly suitable for applications where extremely high mechanical strength is not a prerequisite.
8- Although they generally have superior chemical resistance compared to metals, extended exposure to ultraviolet radiation and certain solvents can lead to degradation of their properties.
9- Polymers typically have low moisture absorption and maintain favorable electrical properties.

## 1.3 Texture of Polymers

The geometric structure of polymer chains is primarily determined by the type of bonds connecting the atoms within the chain. Due to the potential for rotation around single bonds, particularly when the polymer is in a solution or molten state, polymer chains can adopt multiple geometric configurations, referred to as conformations [17]. The localized motion of specific segments of the polymer chain, and the resulting conformations, plays a crucial role in defining the physical and mechanical properties of the polymer, such as the elasticity of rubber and the hardness of other types. Vulcanization is a notable example of a process that reduces the mobility of polymer chains, thereby increasing hardness and decreasing degree of elasticity. The localized mobility of polymer chains is highly dependent on temperature. In the molten state, polymer behave like viscous liquid due to the unrestricted movement of their chains. This

property is utilized in polymer manufacturing, where the material is heated to a molten state and pressed into molds of specific geometries. Upon cooling, the polymer solidifies into the mold's shape, a process known as molding. As temperature decreases, the translational freedom of the polymer chains becomes limited, allowing only localized motions, such as the movement of side groups and chain ends [18]. These changes are accompanied by fundamental transformations in the polymer's physical properties, transitioning from a molten, viscous material to a rigid solid. The temperature at which this transition occurs is known as the glass transition temperature ($T_g$). Below $T_g$, the mobility of chain segments and substituent groups is significantly restricted, resulting in a hard and brittle polymer. Above $T_g$, the enhanced segmental mobility imparts an elastic response to the polymer [17].

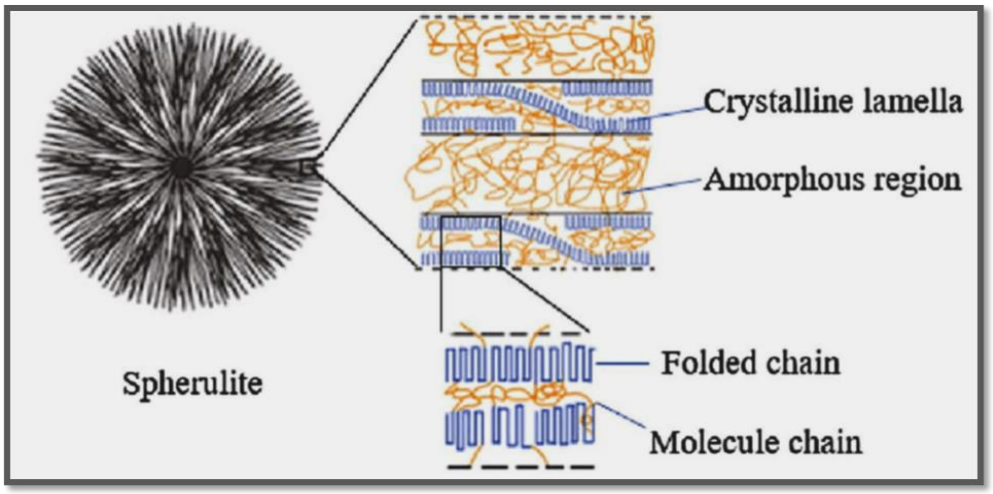


Figure (1-2): Representation of the structure of the polymer spherulite [19].

The physical and mechanical properties of polymers are governed by three principal factors, the most significant of which are the chemical bonds and binding forces. These bonds can be categorized into two types primary bonds. The first type comprises primary bonds, namely covalent bonds, which connect atoms within the polymer chains and account for the vast majority of bonds in a polymer. The second type includes secondary forces, which arise either between different chains or within the same chain, exerting a considerable influence on the physical and mechanical properties. A third type of bond also arises, originating from the physical entanglement of long chains. Secondary forces are sometimes known as van der Waals forces or intermolecular forces. Several forms of these forces influence polymer properties, including dipole forces, which occur due to the presence of polarized molecules or groups within the polymer chain. These groups possess a permanent dipole moment that generates attraction between opposite poles, with their influence being temperature dependent. Induction forces arise when polarized groups in the polymer chain act upon neighboring nonpolar molecules or groups, inducing partial polarization. They are independent of temperature. Dispersion forces result from instantaneous fluctuations in the dipole moment caused by electron mobility.

They occur between most molecules but are weakened in the presence of strong polarizers. These forces are also independent of temperature. Hydrogen bonds represent another important

category of interactions, formed between hydrogen atoms and groups containing an electron pair. Such bonds may be either intramolecular or intermolecular, influencing the physical and mechanical properties of polymers, particularly in the presence of active groups such as carboxyl (-COOH), amide (-$CONH_2$), amine (-NH-), and hydroxyl (-OH). Polarized groups capable of forming hydrogen bonds exert a pronounced effect on polymer properties, with bond energies ranging from (12.6–29.4 kJ/mol), and bond distances in the range of (2.4–3.2 × $10^{-8}$ cm) [20]. Another major factor significant influencing the physical and mechanical properties of polymers is their molecular weight.

High-molecular-weight of polymers exhibit superior strength, toughness, and resistance to solvents, making them suitable for rubber applications. In contrast, low-molecular-weight of polymers (less than 10,000) are typically used in adhesives due to their poor toughness. Precise control of molecular weight during production is therefore critical. The concept of molecular weight in polymers differs from that in organic and inorganic compounds due to the variability in chain lengths, and is thus expressed as an average molecular weight. Several approaches are used to calculate this value, including the number-average molecular weight, the weight-average molecular weight, and the viscosity-average molecular weight [21]. Thirdly, polymers that are organized in space have certain structures in their chains called cis and trans isomers. In the cis configuration, all of the carbon atoms are on the same side of the plane that contains the double bond. In the trans configuration, on the other hand, the carbon atoms are arranged in a such that they are either above or below this plane [22, 23].

## 1.4 Solubility of Polymers

The solubility of polymers in solvents constitutes a pivotal parameter influencing both their synthesis and industrial applications. Manufacturing processes such as the production of synthetic fibers, films, coatings, and adhesives rely fundamentally on this property, and these materials are often used in the form of polymer solutions. As with small molecules, polymers do not dissolve in all solvents; some display spontaneous solubility in specific solvents while being insoluble in others. The swelling phase is the first step in the dissolving process. During this phase, the polymer's volume and weight increase as it takes in solvent molecules. This happens when the intermolecular interactions in the polymer chains are strong, like when there are highly organized crystalline regions or hydrogen bonds. Strong polymer and solvent connections can help these interactions go away [23, 24], ultimately leading to a true solution once complete mixing between the polymer and solvent is achieved. The dissolution process is influenced by several key factors, including: Firstly, the polymer and solvent's properties:

The chemical makeup of the polymer and the polarity of the solvent determine how well it dissolves. Polar polymers, which have functional groups with partial charge, only dissolve in polar solvents. Nonpolar polymers, on the other hand, only dissolve in nonpolar solvents.[21]. Secondly, the flexibility of the polymer chain: This denotes the ability of polymer chains to move and displace relative to one another. Greater chain flexibility facilitates the dissociation of long chains and their penetration by solvent molecules, thereby enhancing solubility [25]. Thirdly, the polymer's molecular weight: Polymers with higher molecular weights are less soluble because their chains have more energy to connect with each other. Longer chains have

more links, which makes it harder to separate them in the solvent [26]. Moreover, the chemical composition: The quantity and type of functional groups within the polymer backbone, such as hydroxyl (-OH), carboxyl (-COOH), and amine (-$NH_2$) groups, affect solubility, as these groups promote the formation of bonds with solvents molecules [27].

In addition, the crystal structure: Crystalline polymers display lower solubility compared to amorphous counterparts due to strong chain interconnection. Even with a solvent of matching polarity, crystalline polymer often resist dissolution at ambient temperature. For instance, polyethylene (PE) swells in hexane at 20°C without complete dissolution but dissolves at elevated temperatures. Similarly, crystalline polystyrene (PS) dissolves only upon heating [28]. Equally important, chemical crosslinking: Covalent crosslinks between polymer chains hinder chain separation and mobility, rendering the polymer insoluble even when only a small number of such bonds are present [29]. Finally, the temperature: Thermal conditions influence solubility, as increasing the temperature can either enhance or reduce polymer solubility depending on its chemical nature and structural characteristics [30].

## 1.5 Polymers Classification

### 1.5.1 Classification Depending on the Origins of Polymers

Polymers can be classified according to their sources into three principal categories: The first category comprises natural polymers, which are compounds obtained from plant or animal sources, such as cellulose, starch, natural rubber, wool, silk, and leather. These materials are generally characterized by their high cost and limited availability, which restricts their widespread utilization [31]. The second category includes modified natural polymers, derived from natural polymers that have undergone chemical modifications, such as the introduction of functional groups or grafting with synthetic polymers. Representative examples include synthetic wool and cotton grafted with acrylic fibers [32]. The third category encompasses synthetic polymers, which are produced industrially from simple monomers via chemical reactions, with notable examples being polyvinyl alcohol (PVA) and polyethylene (PE) [31].

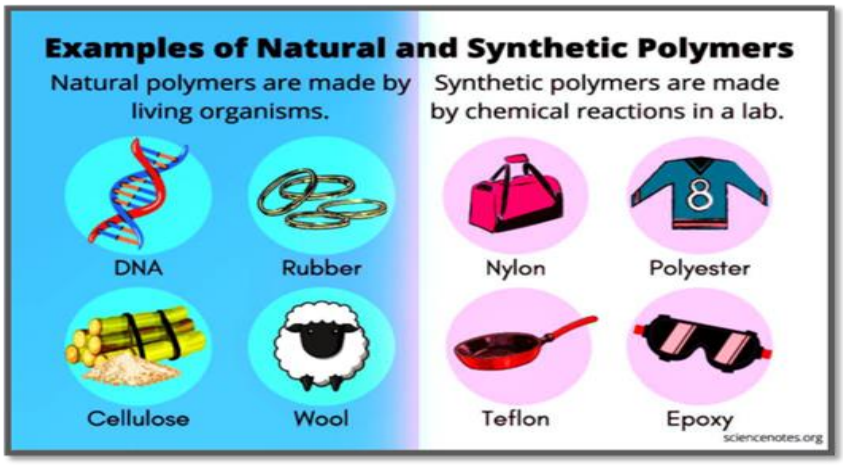


Figure (1-3): Examples of natural polymers and their monomers [33].

### 1.5.2 Classification Depending on the Chemical Nature of the Polymers

The chemical classification of polymers includes organic polymers, which are carbon-based compounds typically containing elements such as hydrogen, nitrogen, oxygen, and sulfur, and represent the most common in industrial applications [32]. It also comprises inorganic polymers, which are composed of non-carbon-based elements such as silicon, phosphorus, and nitrogen, are characterized by high thermal resistance and a three-dimensional network structure, as in the case of magnesium oxide (MgO) polymers [33, 34]. Furthermore, it encompasses organic-inorganic polymers, which incorporate units containing metal elements along with organic groups, and are notable for their high heat resistance, as exemplified by polysulfide [35].

## 1.5.3 Classification Depending on the Thermal Behavior

#### 1.5.3.1 Thermoplastics

This classification includes a group of polymers whose physical properties undergo significant changes under the influence of heat. As the temperature increases and approaches the glass transition temperature ($T_g$), these polymers progressively lose their rigidity, transforming first into soft, flexible materials, and subsequently into viscous melts. This behavior is attributed to reverse transformation sequence, returning to its solid, mechanically strong state. This reversal occurs due to the restriction of the translational chain motion, limiting it to localized movements [36]. In general, the physical performance of thermoplastic polymers is influenced by several factors, including the length of individual polymer chains, their shape and conformation, the functional groups present, and the structural or substituent characteristics of the main chain. Moreover, strong van der Waals interactions between polymer chains can significantly elevate the melting temperature. Representative examples of such polymers include polymethyl methacrylate (PMMA), polyethylene (PE), polypropylene (PP), and polystyrene (PS) [37].

#### 1.5.3.2 Thermosets Polymers

These polymers are cross-linked, as the presence of such cross-linking impedes molecular recrystallization while increases the energy required to the movement of polymer chains segments, resulting in a high glass transition temperature ($T_g$). Among the most notable characteristics of these materials are their insolubility and inability to melt, as well as their poor thermal and electrical conductivity [38]. Polymerization in this class through the formation of strong chemical bonds linking the molecules. Due to the robustness of the covalent bonds between chains, thermosetting plastics do not soften upon heating, except at temperatures sufficiently high to break these bonds, which consequently leads to material charring [32]. Accordingly, these materials are inherently brittle with low ductility, examples of which include unsaturated polyester and epoxy resins. This class of polymers does not melt upon

heating; instead, heat exposure stabilizes them in their final shapes. Under the influence of heat and pressure, their pastes are shaped into the desired forms using specialized molds [39].

### 1.5.3.3 Elastomers

This material is classified as a rubber polymer, distinguished by its capability to elongate up to twice its original length and subsequently recover its initial dimensions. Typical examples of this type include natural rubber and polyurethane [40]. These polymers are characterized by a low glass transition temperature ($T_g$) and demonstrate a higher mechanical response when subjected to stress. They are also capable of recovering their original dimensions upon the release of stress. The flexibility of this class of polymers is attributed to the structure of their long, flexible molecular chains, which are randomly coiled around each other, such that the average distance between the two ends of a polymer chain is considerably shorter than the distance observed when the chain is in a fully extended conformation [9].

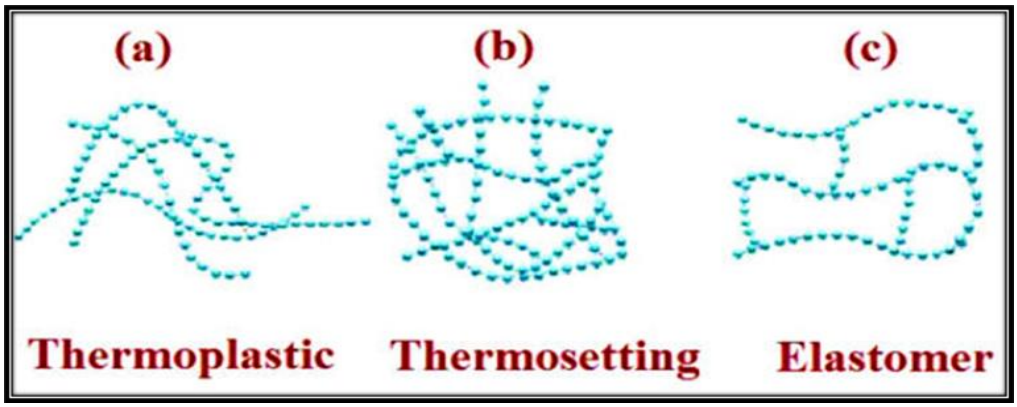


Figure (1-4): Types of polymer chain structures according to technical (technological) properties [41].

## 1.5.4 Polymers Can be Classified According to the Type of Monomer as Follows

A polymer molecule consists of repeating units that may be of similar or different chemical compositions. A polymer composed of identical repeating units is referred as a homopolymer, whereas one composed of different repeating units is termed a copolymer [42- 44].

### 1.5.4.1 Homopolymers

If a polymer is composed of a single type of monomer, it is classified as a homopolymer, as exemplified by poly (ethylene terephthalate), polyvinylchloride, polystyrene, polypropylene etc. To overcome such limitations, composite polymers derived from homopolymers are developed. The primary targeted properties of the composite polymer derived from the homopolymer include enhanced stiffness and tensile strength, improved stability, increased impact resistance, and elevated heat distortion temperature. Addition objectives comprise

improved mechanical damping capacity, reduced permeability to gases and liquids, modification of specific electrical properties, and a reduction in the overall production cost of the polymer [44].

### 1.5.4.2 Copolymers

Copolymers are defined as polymers composed of more than one type of building block (monomer). The way the different structural units in a copolymer chain are put together determines what kind of copolymer it is and has a big effect on its physical and mechanical properties. First, there are random polymers, which are made up of different monomer units that are not in any particular order along the polymer chain. The structure of alternating copolymers is the same all the way through because they are made up of two different types of monomer units that alternate periodically along the polymer chain. Some polymers, like nylon 66, are made up of two different monomers that need to be exchanged in a certain order. These polymers are called homopolymers because their structure is quite homogeneous. Block copolymers are also linear polymers made up of long sequences (blocks) of repeating units of the same kind. Each block has a different type of repeating unit. In addition, graft copolymer is formed when a second type of monomer, different from those in the main chain, is chemically bonded as side chains to the polymer backbone [45].

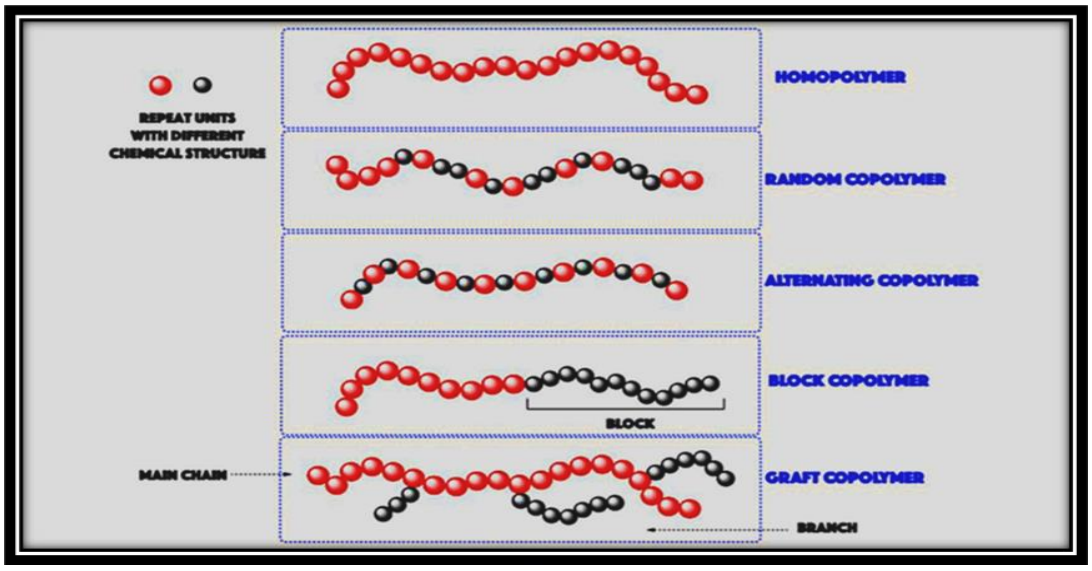


Figure (1-5): Classification of copolymers [46].

## 1.6 Polymerization

Polymerization is a fundamental chemical process in the polymer industry, wherein small molecules, known as monomers, are transformed into large macromolecules called polymers, while retaining the basic structural framework of the monomers without any fundamental alteration [18]. This process proceeds through the covalent linking of monomer units to form extended polymer chains. The methods of polymerization vary according to the nature of the reaction and the mechanism of linkage. Flory (1953) and Carothers (1940) classified polymerization processes into two principal categories [13, 14]: The first categories is addition polymerization**,** also called chain–growth polymerization (CGPs). This mechanism involves the successive addition of monomer molecules through three distinct stages. The initiation stage generates an active center, which may exist as an ion or as free radical containing an unpaired electron. This is followed by propagation stage, during which the active center extends via a series of symmetric reactions [32, 42]. The process concludes with the termination stage, wherein chain growth ceases when two free radicals react, each terminating the other [31]. In this polymerization, the reaction rate rises from zero to a maximum within a short period, before reaching equilibrium, as observed in the synthesis of low-density polyethylene [31, 42]. CGPs are produced by the repeated sequential addition of monomer units, where monomers react exclusively with the active end of the chain and do not interact directly with each other. Examples include Teflon, Orion, polyethylene, PVC, and polypropylene. General, alkenes and their derivatives serve as the typical monomer units for these polymers. The second category is condensation polymerization, also termed step-growth polymerizations (SGPs), which contrasts with addition polymerization in that the polymer is formed predominantly during the final stages of the process, as in exemplified by polyester stearate [32]. This mechanism involves condensation reactions between two molecules containing multiple functional groups, resulting in the formation of a new molecule, typically with the release of a small by product molecule at each step [32]. The reaction proceeds until one of the reactants is completely consumed. In this type of polymerization, the reaction rate is highest at the initial stages, owing to the maximum concentration of reactants, and gradually decreases over time, as seen in polyurea synthesis [47].

## 1.7 Polyurea

Polyurea (PUs) was first mentioned in 1948, when several researchers investigated the thermal properties and melting points of variety polymer systems, including polyester, linear polyethylene, polyurethane, polyamide, and polyurea [48]. The results revealed that polyurea exhibited superior thermal stability and significantly higher melting point compared to the other systems. It is noteworthy that these polymers were synthesized under laboratory conditions and were not yet applicable for practical uses in coating or linings. Figure (1-6) presents a comparative graph of the melting points of different polymers. Subsequently, the two-component flexible coating/lining technology based on polyurea was developed from

reaction injection molding (RIM) technology, which had emerged in the early 1980s. The polyurea RIM process was employed in the production of several automotive exterior components, including body panels and bumper covers. The cross-linking of polyurea results from the chemical reaction between amine-terminated resins and an isocyanate component. This reaction leads to the formation of a polymer consisting of repeating urea linkages; hence, the term "polyurea" is used to describe the resulting material [49].

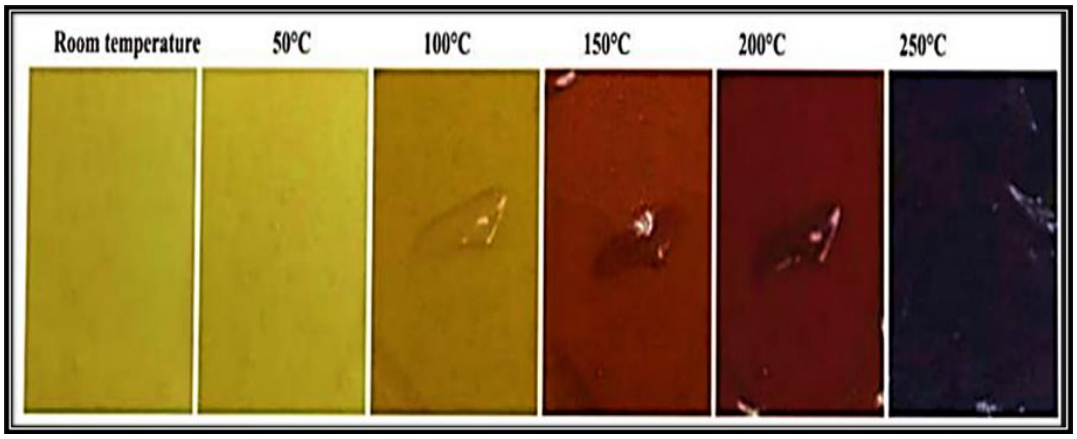


Figure (1-6): Color change in polyurea with increasing temperature; aromatic polyurea (isonate 143L/Versalink P650) [49].

In the process of making polyureas (PUs), a low-equivalent-weight polyamine is usually used as a chain extender. Adding more of this extender to the polyurea formulation makes the material stiffer and stronger by encouraging longer polymer chains to form [50]. However, although higher chain extender content contributes to greater stiffness, excessive amounts may result in brittle and mechanically weak elastomers. In practice, chain extenders are commonly incorporated into systems that require a high flexural modulus, such as structural applications and protective coatings for concrete surfaces [51]. Their addition not only elongates the polymer chains but also increases the hard segment (HS) content of the material, which plays a critical role in improving the overall tensile strength of the polyurea. The theoretical hard segment (HS), which primarily governs the hardness, strength, and toughness of the cured material, can be estimated using equation (1-2). This segment is mainly composed of urea bonds formed through the reaction between isocyanates and amines. Theoretically, low-molecular-weight amines (chain extenders) are considered to contribute more significantly to the hard segment compared to high-molecular-weight amines, such as polyether amines [49]. As shown in Figure (1-7).

$$\textbf{Hard segment (\%)} = \frac{m_{isocyanate} + m_{chain\ extender}}{m_{isocyanate} + m_{amine}} \times 100 \quad \text{..... (1-2)}$$

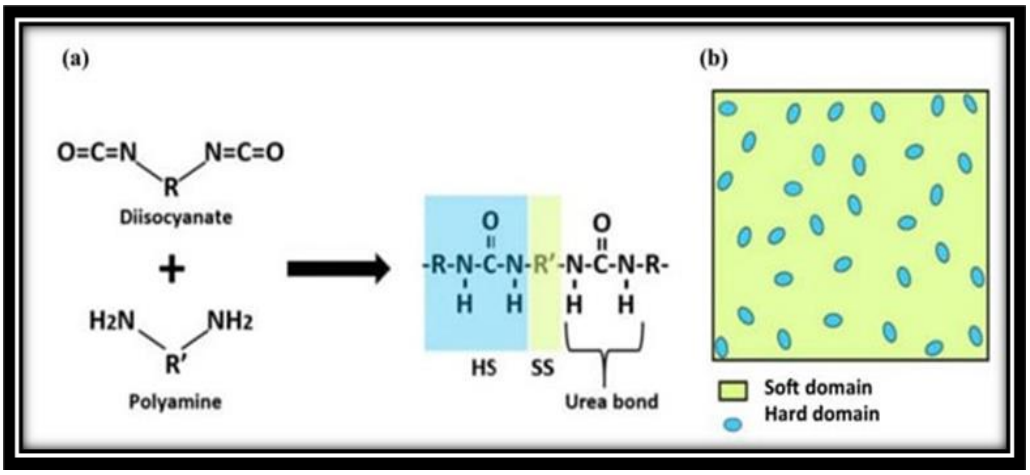


Figure (1-7): (a) Reaction between diisocyanate and diamine producing polyurea consisting of hard segment (HS), soft segment (SS) and urea bond, (b) microphase separation in polyurea forming hard and soft domains [51].

Diethyl toluene diamine (DETDA) is commonly employed as a chain extender, whereas the triamine T-5000 serves as a crosslinker, linking two or more polyurea chains to generate a three-dimensional polymeric network [52]. According to experimental results, DETDA replaces high-molecular-weight amino polymers like D2000 and reduces the intermolecular distance between neighboring urea groups. Furthermore, the growth of high $T_g$ hard domains depends on the production of bidentate hydrogen bonds, which are made easier by the addition of chain extender linkers, as shown in Figure (1-8).

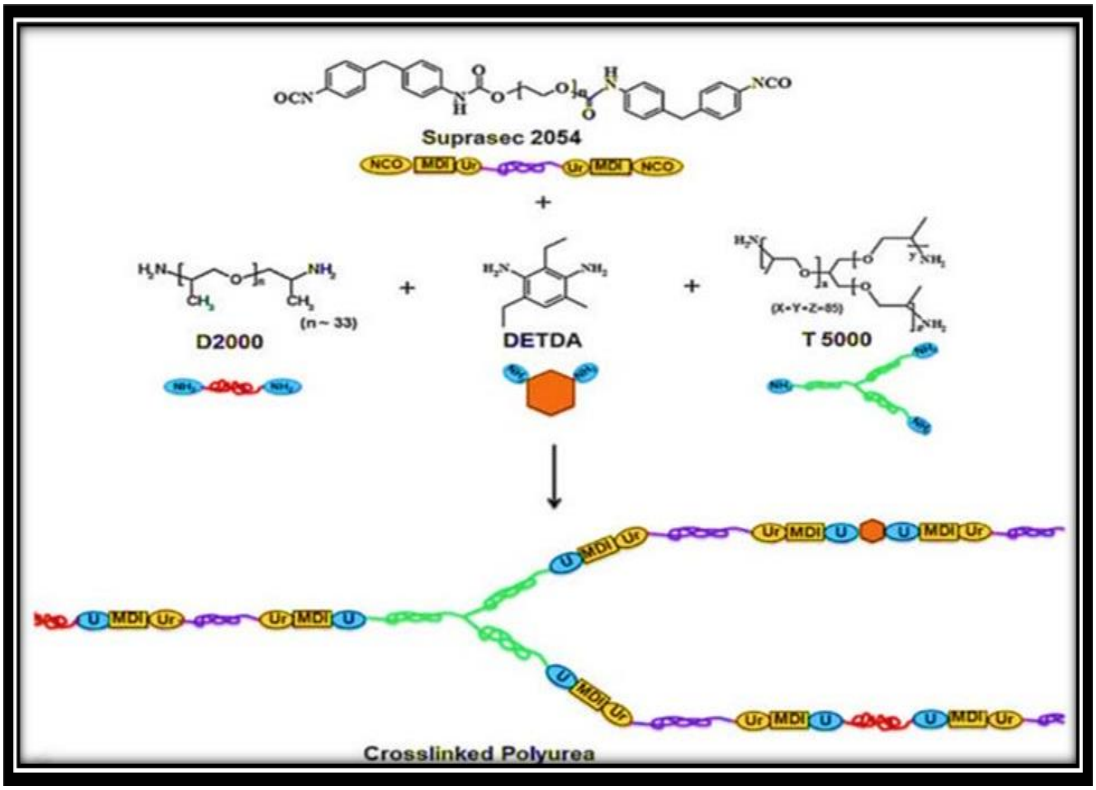


Figure (1-8): Schematic of formation of crosslinked polyurea with the help of low molecular weight amines [52].

Table (1-1) summarizes the different types of chain extenders utilized in polyurea manufacturing. It should be emphasized that both aromatic and aliphatic chain extenders may be employed in diverse polyurea systems, depending on the specific performance and application requirements.

**Table (1.1) Comparison of aromatic polyurea with aliphatic polyurea [49].**

| *Type of polyurea* | *Examples of Isocyanate* | *UV stability* | *Properties* | *Applications* |
|---|---|---|---|---|
| Aromatic 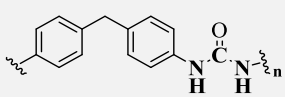 Aliphatic 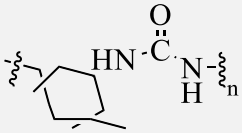 | Methylene diphenyl diisocyanate (MDI)<br><br>Toluene diisocyanate (TDI)<br><br>Hexamethylene diisocyanate (HDI) | Discoloration and microscopic cracks known as "crazing" are observed on the outer surface of the material, often resulting from mechanical stress or excessive exposure to ultraviolet radiation. Microscopic voids and irregularities in the surface structure have also been observed, negatively affecting surface homogeneity and resistance. The discoloration process is extremely slow, indicating a gradual deterioration in optical properties over a long period of time. | Tensile strength (TS): 35-60 MPa Elongation at break ($\varepsilon_B$): Over 400%<br><br>TS: 2.2-31.1 MPa Elongation at break ($\varepsilon_B$): 293% - 1000%.<br><br>The melting point is above 210°C. | *These materials are widely used in the manufacture of automotive parts and in ballistic protective coatings applications due to their high mechanical resistance.*<br><br>*They are also used as topcoats in environments exposed to high levels of ultraviolet (UV) radiation, particularly on exterior roofs and floors, where UV resistance is a critical factor in long-term performance stability.* |

Isocyanates are extensively in the synthesis of polyurea's, and the choice of the appropriate type represents a crucial factor in tailoring the properties of the resulting polymer. Among the most commonly used isocyanates is methylene diphenyl diisocyanate (MDI), which possesses an isocyanate group content of 31–32.9%, and a bifunctionality of 2.7, and a dynamic viscosity of (13–21 Pa·s). MDI is typically utilized in low-reactivity, single- and two-component systems with superior dynamic performance [53]. Another widely used isocyanate is toluene diisocyanate (TDI), characterized by an NCO content of up to 48.2%, a bifunctionality, and a very low viscosity of (0.305 Pa·s). TDI is mainly applied in highly flexible molding processes and specialty foams. While low-viscosity formulations (0.7 Pa·s) are also available for waterproofing purposes. Hexamethylene diisocyanate (HDI), with an NCO content of 22.5–23.5% and a viscosity of (1.5 Pa·s), is predominantly employed in industrial coatings as well as in automotive and transportation refinishing. Collectively, these properties underscore the significance of carefully isocyanate selection in controlling the reactivity, mechanical and electrical characteristics, and application areas of polyurea [49].

## 1.8 Polyurea Preparation Methods

There are three widely employed techniques for processing and mold polyurea: spray coating, reaction injection molding (RIM), and casting. Each method exhibits distinct operational characteristics that directly influence both preparation efficiency and the quality of the final product. Spray coating is particularly suitable for producing thin, homogeneous layers on a various of substrates. It is characterized by rapid curing and the ability to cover large surface areas; however, it requires high-pressure systems, costly equipment, and advanced operational expertise. Moreover, the quality of the application is highly dependent on proper surface preparation and environmental conditions. RIM is typically applied in the industrial scale production of large or precision parts, due to its capability of producing high quality surfaces free from air cavities.

Nonetheless, this technique demands precise control over mold temperature and mixing pressure, in addition to significant equipment investment. RIM derived polyurea has been extensively used in the fabrication of automotive exterior components, including body panels and bumper covers. Casting, is contrast, is a comparatively simple and low-cost technique that does not require complex equipment or high pressure. It is advantageous for incorporating additives, such as nanoparticles, into the polymer matrix and can be performed under standard laboratory conditions without the need for industrial scale facilities. Despite these benefits, casting suffers from limitations including a relatively slow processing time and the potential formation air bubbles or voids within the sample. Careful control of mixing and processing parameters is therefore required. This technique provides greater flexibility for nanoparticles incorporation while maintaining low operational requirements, making it particularly suitable for laboratory applications and for evaluating functional properties such as electrical conductivity and thermal behavior.

Polyurea is generally prepared by casting through the stoichiometric mixing of two main components, namely component A and component B. In many cases, component A is introduced gradually and dropwise to mitigate its toxicity and sensitivity to environmental factors, thereby reducing emissions and ensuring safe processing. Mixing is typically carried out using an external device, such as a mechanical stirrer or magnetic stirrer, to ensure formulation homogeneity before pouring the mixture either into an open mold or directly onto a substrate surface. Because casting represents an open system, it is highly sensitive to environmental conditions, particularly temperature and humidity. Critical factors that determine casting quality and final material properties include: the nature of the polymerization process, whether solvent- or non-solvent-based; the type of substrate or mold employed during casting; and the curing time required to achieve complete polymerization. Proper consideration of these factors helps minimize void formation, improve molecular bonding, and ultimately enhance the mechanical performance of the material. If solvents are used during fabrication, complete evaporation prior curing is necessary, with the evaporation temperature determined by the solvent's nature. Care must be taken to avoid temperatures that could soften or melt the polyurea films, as this would compromise its structural integrity. Residual solvents within the matrix significantly deteriorate tensile properties.

In previous studies, polyurea microspheres were integrated into polyurea sheets using Versalink P1000 and isocyanate 143L, which resulted in the formation of polyurea composites. This procedure, illustrated in Figure (1-9), involved combining isocyanates and diamines with a solution of acetone and polyurea microspheres before pouring the mixture into a polypropylene mold. The composite liquid was then poured through a funnel in a thin stream to eliminate air bubbles that had formed during mixing. The final samples were first cured for 24 hours at 80°C under vacuum. After that, they were cured at room temperature for five days [47], [53].

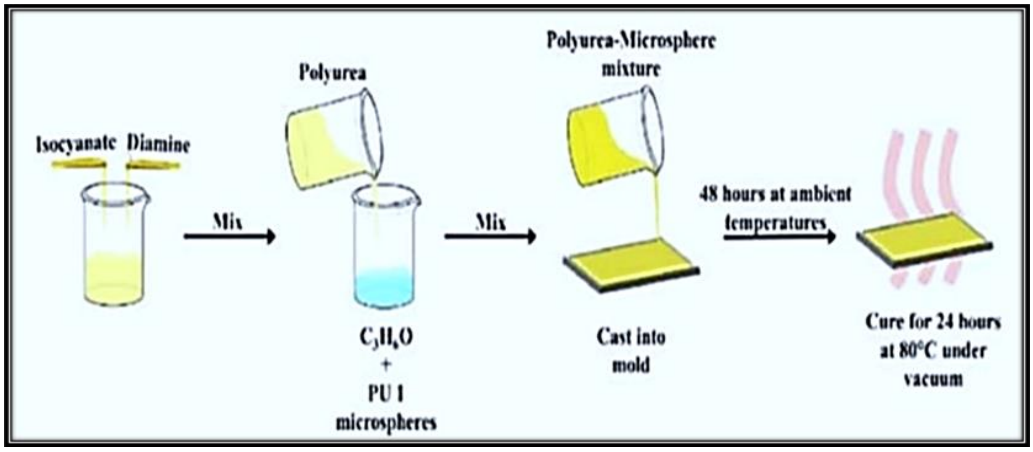


Figure (1-9): Schematic of production of polyurea films by casting method [54].

## 1.9 Literature Review

Polyurea systems possess a wide range of industrial applications owing to their unique combination of rapid curing, as well as thermal and chemical stability. They have demonstrated high efficiency in reaction injection molding (RIM) processes, with curing times as short as 2–3 seconds and drying times of less than 10 seconds. These features significantly reduce the occurrence of defective parts and enable compatibility with electrophoretic coating (ELPO) processes, which requires heating to approximately 205°C, a temperature that conventional or hybrid polyurethane systems are unable withstand. Since 1989, polyurea has also been applied in roofing and insulation systems, particularly for encapsulating rigid polyurethane foam, due to its durability, solvent-free nature (100% solids), and fast curing capability [55- 57].

In a (2021) study, (Ahmad Zarour, Suheir Omar), and colleagues proposed a method for synthesizing polyurea-coated microcapsules using a non-aqueous emulsion. These microcapsules were loaded with palladium nanoparticles, which rendered them effective catalysts for the hydrogenation of alkenes and alkynes. The prepared microcapsules exhibited high catalytic activity and reusability for up to nine cycles with consistent performance, while also allowing facile separation and demonstrating excellent structural stability. These findings highlight the potential of polyurea in the development of innovative and sustainable catalytic

systems, particularly in non-aqueous environments, thereby opening broad prospects for industrial applications [58].

In a (2023) study, (Mingyang Li, Gaoyang E), and colleagues developed a lignin-modified polyurea adhesive for coating potassium chloride granules to produce a controlled-release potassium fertilizer. The formulation was based on combining lignin with polyurea at an optimal ratio of 2:1, resulting in an effective coating layer with enhanced mechanical performance. Experimental results reveals that the modified adhesive provided the agricultural granules with a 139% increase in mechanical strength compared to humic acid-treated granules, while also improving the flowability of the final material. With respect to agricultural performance, the system achieved a cumulative potassium release rate of approximately 28% over 28 days, representing a 42% reduction compared to conventional release systems. This demonstrates its high efficiency in controlling nutrient release over extended periods. Overall, the study underscores the significance of modified polyurea in agricultural applications, particularly in the development of smart fertilizer systems that enhance agricultural productivity while reducing environmental waste [59].

In a (2023) study, (Amirhossein Mahtabani, Damiano La Zara), and colleagues employed molecular layer deposition (MLD) to deposit fine layers of polyurea onto silica nanoparticles using the monomers PDIC and ED. Following this, the modified particles were embedded within a polymer matrix composed of polypropylene and ethylene-octane copolymer (PP/EOC). Using a combination of advanced techniques, including DFT calculations, TSDC, and BDS analyses, the researchers observed that the grafted polyurea layer on the filler surface generated bi-modal trap depths, effectively reducing the accumulation of electrical charges at the filler-matrix interface and significantly enhancing the dielectric properties of the nanocomposite. This study confirms the vital role of polyurea in improving the electrical performance of nanocomposite materials, making them a strong candidate for advanced electronic applications and highly efficient electrical insulation systems [60].

In a (2023) study, (Jiupeng Du, Pablo Canamas), and colleagues investigated the use of polyurea for encapsulating the chemical UV filter Octyl Salicylate, commonly used in sunscreens. Microcapsules were fabricated using microfluidics technology, producing polyurea shell of varying thicknesses to shield the filter from direct skin contact, thereby reducing irritation and enhancing safety. The results indicated that the polyurea-coated capsules retained their UV absorption efficiency regardless of shell thickness, demonstrating that polyurea can provide effective protection without compromising functional performance. The study highlighted the compatibility of polyurea with sunscreen components, suggesting its potential as a promising material for developing safe and effective products that protect against harmful UV rays [61].

In a (2024) study, (Le Li, Huajie Shen), and colleagues explored the performance of polyurea coatings in enhancing the blast resistance of reinforced concrete structures. A (5mm) thick polyurea coating was applied to concrete surfaces to evaluate its effect on blast and fragmentation resistance. The results demonstrated that polyurea significantly reduced structural damage by absorbing a substantial portion of the blast energy through its superior

elastic and high expansion before reaching the fracture limit. The coating also limited the dispersal of concrete fragments and maintained structural integrity. The researchers explained that the polyurea possesses a high capacity to store and gradually release impact energy, thereby reducing the direct force on the structure. Numerical models were also used to simulate the material's behavior, showing that the polyurea layer reduced concentrated stresses at the blast center and improved load distribution across the concrete surface. Additionally, the researchers noted that polyurea's performance is influenced by factors such as operating temperature and loading rate, with its stiffness and rubber-like behavior increasing at lower temperatures, thereby enhancing protection. Based on these findings, polyurea was recommended as a protective coating for structures exposed to explosive threats, including military buildings, critical infrastructure, and transportation systems, as it provides effective protection without significantly affecting the weight or dimensions of the concrete structure [62].

## 1.10 Physical and Chemical Properties

The effective utilization of polymers in across diverse fields of science and technology requires a thorough and comprehensive of their physical and chemical properties to ensure compatibility with the specific requirements of targeted applications. A clear understanding of the physical structure of polymers is particularly crucial, as it directly influences key characteristics such as transparency, flexibility, dye absorption, and resistance to harsh environmental conditions, including cracking induced by mechanical stress or interaction with certain organic solvents. Achieving the desired mechanical performance for various applications also necessitates examining the interrelationship between the physical properties and the chemical structure of the polymer. Structural limitations can be addressed, and overall performance enhanced, through and chemical modification techniques or technological development. Prominent functional additives incorporated into modern polymers include impermeability to liquids and gases, chemical resistance to solvents, and resistance to ultraviolet radiation. As a result of these features, polymers have gained widespread use in numerous industries, such as the production of impermeable clothing, packaging materials, preservative containers, laboratory flasks, electrical cable, and many other applications [63].

### 1.10.1 Optical Properties

The study of the optical properties of polymers aims to elucidate their optical behavior and the changes associated with it through spectral analysis of absorbance and transmittance across a wide range of wavelengths. These properties are governed by the nature and distribution of charges within the polymer. The absorbance spectrum, in particular, originates from the energy loss caused by the interaction between the incident light and the internal charges of the material. When a light beam strikes the surface of a polymer, several interactions may occur as a result of the coupling between the electromagnetic wave and the material. The total intensity of the incident electromagnetic radiation on the surface, denoted as ($I_o$), can then be distributed among three main processes, which may occur either independently or simultaneously: absorption of

the beam (Absorption - $I_A$), reflection from the surface (Reflection - $I_R$), and transmission through the material (Transmission - $I_T$) [63- 65].

$$\mathbf{I_o = I_A + I_R + I_T \quad \ldots\ldots\ldots\ldots \quad (1\text{-}3)}$$

Beam intensity is defined as the number of photons incident on a unit area per unit time. By normalizing equation (1-3) with respect to the incident beam intensity ($I_o$), a relative form of the relationship can be obtained, which expresses the intensity components in relative terms as follows:

$$\mathbf{A+R+T=1 \quad \ldots\ldots\ldots\ldots \quad (1\text{-}4)}$$

Where:
A: Absorbance ($I_A/I_o$), R: Reflectance ($I_R/I_o$), T: Transmittance ($I_T/I_o$).

It is not possible for the same material to have high values of absorbance, transmittance, and reflectance at the same time, due to the principle of energy conservation that governs the distribution of the intensity of the incident beam between these components [66].

## 1.10.2 Structural Properties

X-ray diffraction (XRD) is one of the most widely used techniques for studying the crystalline structure of solids. It is also regarded as one of the most exact and accurate techniques for figuring out where atoms are located in different kinds of materials. Since this method is non-destructive, it is perfect for gathering comprehensive structural data without compromising the integrity of the sample under study. When employed in diffraction analysis, X-rays are electromagnetic energy that resembles visible light but has a significantly shorter wavelength, usually between 0.5 and 2.5 Å. Because this range is similar to the interatomic spacing in solids, XRD can offer crucial details about crystalline materials, such as preferred orientation, crystal structure, and other structural factors, including crystallite size and the existence of crystal defects. XRD is also used to compute particle size, lattice constants, and the intensity of reflected radiation to precisely define the crystal structure [67]. When the particles constituting the sample powder are sufficiently small, the peaks in the XRD spectrum exhibit noticeable broadening. This broadening is inversely proportional to crystallite size. Therefore, it can be used as a reliable tool to estimate crystallite size through the Scherer equation, expressed as follows [68]:

$$\mathbf{D = K\lambda / \beta \cos\theta \quad \ldots\ldots\ldots\ldots \quad (1\text{-}5)}$$

Where:
β: represents the FWHM, which is the maximum width at mid-intensity. D: the size of the particles according to the Debye-Scherrer equation. λ: the wavelength of the X-rays used (1.504 Å). θ: the Braque angle. K: the Scherrer constant (a unitless number with a value of about (0.9)).

The actual value of the constant depends primarily on three fundamental factors. The first is the definition of width, that is, how the width of the signal or spectral band is determined or calculated. The second is the particle morphology, which refers to the geometric structure or external shape of the particles under investigation. The third factor is particle size distribution, namely the extent to which the particle sizes vary within the studied sample.

### 1.10.3 Transmittance

Transmittance (T) is defined as the ratio of the transmitted radiation intensity ($I_T$) through the membrane to the incident radiation intensity ($I_o$) on its surface. It provides a measure of the fraction of light or radiation that passes through the sample relative to the amount incident upon it. Transmittance is a dimensionless parameter, as it represents the quotient of two quantities with identical units [69]. The mathematical expression for transmittance is given as following [70]:

$$T = I_t / lo \quad \text{..... (1-6)}$$

Film thickness is one of the main factors influencing transmittance. An increase the thickness results in a significant decrease in transmittance due to the enhanced optical absorption within the material. As the film becomes thicker, the incident radiation undergoes greater absorption, causing a large portion of the radiation to be attenuated and, consequently, not transmitted through the film as required [71].

### 1.10.4 Absorbance

Absorbance(A) is defined as the ratio of the intensity of radiation absorbed ($I_A$) by a membrane to the original intensity of the incident radiation ($I_o$). This parameter represents the material's ability to absorb electromagnetic radiation. It is a dimensionless quantity, as it is obtained by dividing two quantities with identical units. The mathematical expression for absorbance is given as follows [72]:

$$A = I_A/I \quad \text{..... (1-7)}$$

### 1.10.5 Thermal Properties

The use of polymer based composite materials has become increasingly common in both traditional and modern engineering designs due to their superior thermal properties compared to other materials. The significance of these properties lies in their ability to withstand the elevated temperatures encountered under service conditions, thereby making them suitable for use as thermal barriers capable of resisting thermal stresses. Among the thermophysical properties that have attracted considerable attention from researchers are thermal conductivity (k), glass transition temperature ($T_g$), melting temperature ($T_m$), crystallization temperature ($T_c$), Thermogravimetric analysis (TGA). The primary purpose of investigating these thermal properties is to gain a comprehensive understanding of the thermal behavior of polymer

composites, which is essential for assessing their suitability and adaptation in a wide range of scientific and industrial applications [73].

### 1.10.5.1 Thermal Conductivity

Thermal conductivity is one of the fundamental phenomena of heat transfer in solids and represents a critical thermal property that directly influences performance in numerous industrial applications [74]. The thermal conductivity coefficient ($K_{th}$) reflects the ability of a material to transfer thermal energy through it. This transfer occurs via two primary mechanisms: the first involves the migration of free electrons in addition to vibrational waves within the crystal lattice (lattice vibrations or phonons). The second mechanism is associated with the acquisition of energy by valence electrons, which migrate from regions of higher temperature to regions of lower temperature, transferring their energy to neighboring atoms. The amount of energy transferred depends on the number of free electrons, which is influenced by the material type, the presence of defects within the crystal lattice, and the ambient temperature. Furthermore, atomic thermal vibrations play a significant role in energy transfer within the material. Figure (1-10) illustrates these detailed processes of heat transfer in solids [75].

$$q = -k\frac{dT}{dx} \quad \text{.....} \quad \textbf{(1-8)}$$

Where:

q: Heat flux or heat flow through a unit cross-sectional area of the material per unit time (J/sec), k: Thermal conductivity coefficient (W/M°C), dT / dx: Heat transfer rate per unit distance (M/°C).

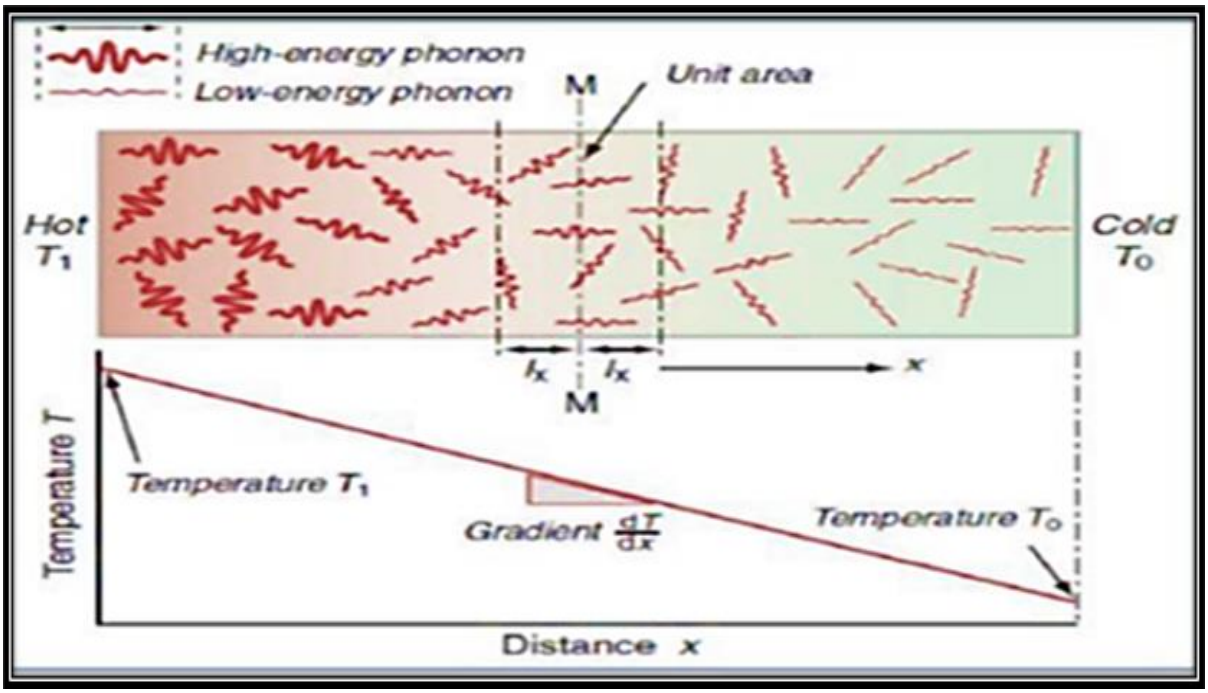


Figure (1-10): Heat transfer by the movement of phonons [75].

### 1.10.5.2 Thermal Degradation

Thermal degradation of polymers is a molecular decomposition process that occurs as a result of thermal stress. At elevated temperatures, structural changes take place within the components of the polymer chain. Under such conditions, molecular bonds may undergo cleavage, leading to reactions between the resulting products and causing significant alterations in the properties of polymer. Molecular degradability is considered part of a broader group of polymer degradation mechanisms that can be initiated by several factors [75, 76]. These include heat, involving pyrolysis and pyro-oxidative decomposition in the presence of oxygen; light, which induces photodegradation; and oxygen, which causes oxidative degradation. In addition, atmospheric factors such as exposure to ultraviolet radiation contribute to the degradation process. In general, the ability of plastics to withstand these degradation factors is known as thermal stability, which denotes their resistance to permanent changes in properties resulting from exposure to heat alone [[78]. The effect of temperature on the rate of chemical reactions leading to thermal dissociation can be expressed by the Arrhenius equation [75, 78].

$$k = A \exp(-Ea/RT) \quad \ldots\ldots\ldots\ldots \quad (1\text{-}9)$$

Where:
K: Time rate constant, A: Frequency factor, Ea: Activation energy, R: Gas constant (8.3 J/M. K), T: Thermodynamic temperature

### 1.10.5.3 Thermal Analysis Measurement

The term thermal stability is often used to describe changes in one or more physical properties resulting from exposure to different temperatures over specific periods of time. More broadly, thermal stability is defined as the ability of a polymer to resist thermal degradation [79, 80]. Thermogravimetric analysis (TGA) is one of the most prominent analytical methods for elevating thermal stability, and it is generally classified into two main types. The first is Isothermal TGA, in which the sample is held at a constant temperature while the weight loss is recorded over time. The second is Non-Isothermal TGA, where the sample temperature is increased at heating, and the mass change is recorded simultaneously with the temperature increase. This method is considered more informative, as it provides more accurate data regarding the upper limit of thermal stability (the thermal stability limit) [81]. Derivative thermogravimetry (DTG) can also be employed to determine the peak decomposition point. This technique is based on the continuous measurement of the sample mass during uniform temperature variation, with the results plotted on X–Y curves known as TGA curves [82]. TGA analysis measures the weight changes occurring as a function of temperature and provides essential information, including changes in sample composition, thermal stability, kinetic parameters of chemical reactions, determination of the onset of thermal decomposition (the thermal decomposition temperature), and estimation of the amount of mass lost at specific temperatures. Overall nature of the experimental results in thermogravimetric measurements are affected by multiple variables, which can be classified into two main groups:

Instrumental factors (thermometric balance): (a) Oven heating rate. (b) Geometric dimensions of the oven and the sample carrier or the sample itself. (c) Sensitivity of the recording devices. (d) Nature and composition of the sample carrier.

Sample properties: (a) Sample quantity. (b) Solubility of the gases released from the sample. (c) Sample particle size. (d) Heat of reaction. (e) Model layout. (f) Nature of the model. (g) Thermal conductivity of the model.

### 1.10.5.4 Glass Transition Temperature ($T_g$)

The glass transition temperature ($T_g$) represents the temperature at which a polymer undergoes a transition from a solid and brittle state to a more flexible state. This transition is defined as the point at which the mechanical and physical properties of polymer change, becoming elastic at temperatures above $T_g$ [83]. Polymeric materials experience several transformations when exposed to elevated temperatures. At temperatures below $T_g$, the material remains solid, hard, and brittle. Upon reaching $T_g$, it transforms into a flexible plastic material, which may subsequently enter a rubbery state in non-thermoplastic polymers, or a highly viscous liquid state in thermoplastics. The $T_g$ is determined by the mobility of atoms and molecules within the polymer chain and is influenced by several factors, including the complexity of the molecular structure, the strength of interchain bonding, and the molecular weight [82, 83].

## 1.11 Electrical Properties of Polymers

Electrical properties are among the most prominent characteristics that distinguish polymers. Previously, polymers were regarded solely as insulating materials; however, the discovery of high conductivity in some types of polymers has led to a qualitative breakthrough in this field [84, 85]. This property is of particular importance due to its wide-ranging potential for various technical applications. Polymers are classified according their electrical conductivity into three main categories: insulators, conductors, and semiconductors. Electrical conductivity in the semiconductor range is approximately between ($1\text{-}10^{-7}$ $S.cm^{-1}$), whereas conductors exhibit a conductivity greater than ($1$ $S.cm^{-1}$), and insulators have a conductivity less than ($10^{-7}$ $S\ cm^{-1}$) [86].

Insulator's polymers play a vital role in the electrical, thermal, and even acoustic insulation, since electrical and electronic applications typically require a combination of both conductive and insulating materials to achieve optimal performance. The development of highly conductive polymers with conductivities approaching those of metals represents a remarkable scientific achievement and has attracted widespread interest from researchers as well as commercial institutions. This interest stem from the unique combination of excellent electrical conductivity with other advantageous properties such as light weight, low cost, flexibility, high corrosion resistance, and the possibility of tailoring their chemical structure to enable them with biological molecules, thereby enhancing their compatibility with living tissues in medical applications [86, 87]. Polymers are also considered systems that deviate from conventional

Ohm's law and instead follow the principles of inorganic semiconductors. Electrical conduction in polymers is defined as the transport of charge carriers within the medium under the influence of an external electric field. The electrical conductivity depends primarily on the number, mobility, and type of charge carriers, whether electrons, holes, or ions, which can be generated either spontaneously or through doping. The electrical conductivity of polymers is expressed by the following relationship [88, 89]:

$$\sigma = n \mu q \quad \ldots\ldots\ldots\ldots \quad (1\text{-}10)$$

Where:

σ: Electrical conductivity is measured in units of (Siemens/m), n: Carrier concentration, measured in units of ($1/m^{-3}$), μ: Carrier mobility, measured in units of ($m^2/V.\ Sec$), q: Electrical charge (measured in coulombs).

Achieving good electrical conductivity in polymers requires both a large number of charge carriers and a high degree of carrier mobility. It is noteworthy that similar levels of conductivity can be observed under different physical conditions. For instance, identical conductivity may occur in two cases: one in which there is a large number of charge carriers with low mobility, and another in which there is a small number of carriers with high mobility. This balance between the number of carriers and their mobility illustrates that electrical conductivity depends not only on the total amount of charge transferred, but also on the efficiency and speed of charge transport within the material [90].

### 1.11.1 Electrically Conducting Polymers

Conjugated polymers have attracted increasing attention from researchers over the past five decades [91]. These polymers are characterized by molecular structures consisting of alternating single and double bonds along the polymer chain, which results in a state of electron delocalization. In this state, the π (pi) electrons are not confined between two specific atoms but are distributed along the chain, enabling their movement under the influence of an applied electric field. Due to this unique electronic structure, conjugated polymers exhibit semiconductor-like behavior even in the absence of doping, and are therefore classified as electrically conducting polymers. This class of polymers represents distinctive organic systems with unconventional electrical properties, as their conductivity span a wide range, from semiconductor levels to values comparable to metals [92]. Figure (1-11) illustrates the relationship between the composition of these polymers and the change in their electrical conductivity [93].

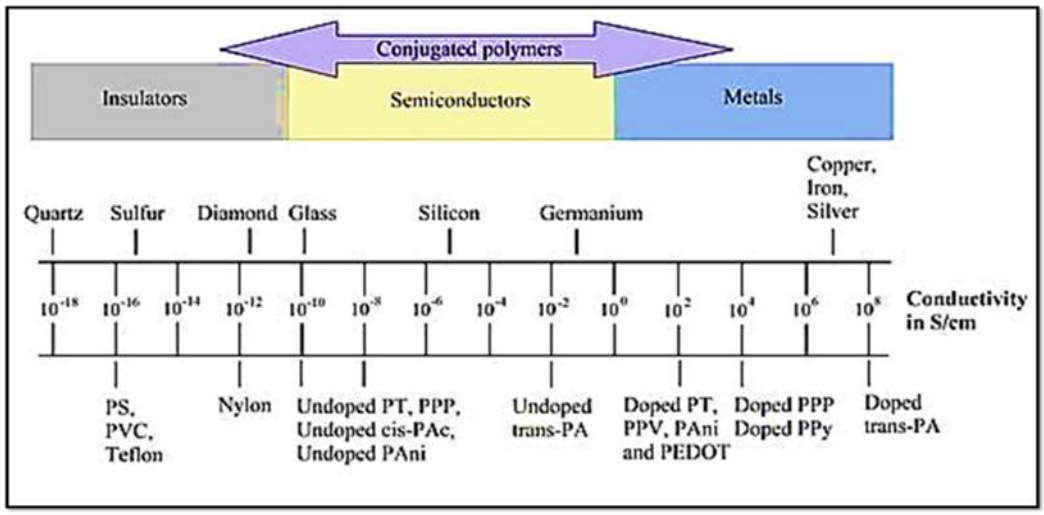


Figure (1-11): The relationship between the composition of these polymers and the change in their electrical conductivity [93].

In the context of electrically conductive polymers, it may be mistakenly assumed that these materials are simply conventional polymers filled with conductive molecules such as carbon or metal particles. However, scientific evidence demonstrates the existence of a class of organic polymers that possess intrinsic electrical conductivity without the incorporation of any conductive fillers. This unique property arises from the presence of a π–π conjugation system along the polymer chain, which results in electron delocalization and overlap of π electrons, thereby enabling their movement along the chain. These chains are typically composed of simple but heterogeneous atoms, such as sulfur (S) and nitrogen (N), which contribute to charge stability and distribution [94]. Although certain conductive polymers have been known for a long time, their electrical properties were not initially examined in depth. A major breakthrough in this field occurred serendipitously. During the preparation of polyacetylene, a student of the Japanese scientist Hideki Shirakawa added a catalyst at a concentration 1,000 times greater than required, resulting in the unexpected formation of a shiny, metal-like film. This incident marked the beginning of a groundbreaking discovery in collaboration with Alan Heeger and Alan MacDiarmid.

In 1977, they successfully synthesized conductive polyacetylene, which exhibited high electrical conductivity after exposure to iodine vapor, increasing its conductivity by more than ten millionfold. Their pioneering work was later recognized with the Nobel Prize in Chemistry in 2000, awarded for the discovery and development of polymers with high electrical conductivity. Conductive polymers are characterized by the unique combination of valuable electrical properties with advantageous mechanical and thermal features, including stiffness, strength, and remarkable resistance to corrosion [95]. It is noteworthy that most of the subsequently studied polymers, as shown in Figure (1-12), exhibit a regular alternation of single and double bonds. These polymers are distinguished from conventional polymers, which consist solely sigma (σ) bonds, by several important characteristics [96]. The small energy band gap, typically ranging from 1 to 4 electron volts (eV), leads to low-energy electronic excitations. This characteristic causes the material to function as a semiconductor. The polymer chains are readily oxidized or reduced, primarily through charge transfer processes involving

dopant molecules. When charge carriers are introduced through doping, their mobility increases, resulting in enhanced conductivity for the material. These charge carriers are quasi-free particles, or quasi-particles, that can move around in the material pretty freely, or at least along continuous polymer chains. They don't act like regular free electrons or holes [97].

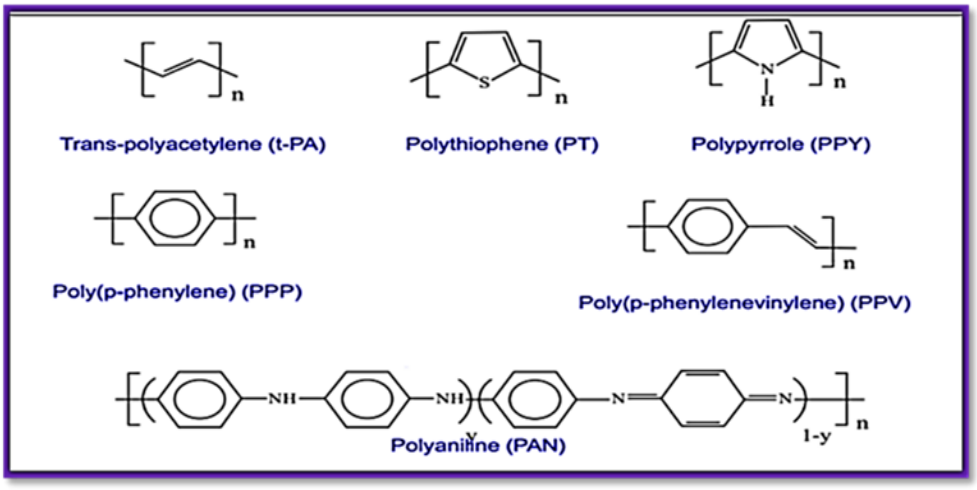


Figure (1-12): Structural formulas of some important successive polymers [96].

## 1.11.2 Polymers as Insulators

A widely recognized fact is that most polymers function as electrical insulators, a principle that has become a scientific axiom [98]. This is property underlies their extensive application in various types of electrical wire insulation. The insulating behavior of polymers attributed to the nature of their chemical bonds, which predominantly consist of sigma (σ) covalent bonds, thereby preventing the free transfer of electrons and impeding the flow of electrical current. In addition to electrical insulation, many polymers are utilized in thermal insulation applications, even under conditions of high temperatures. Some polymer types are also employed in sound insulation, particularly in the form of foams, due to their capacity to absorb acoustic waves. A limited subset of polymers exhibits exceptional chemical properties that allow them to transform into stably charged particles, thereby functioning as semiconductors or, in some cases, as electrically conductive materials. In contemporary industrial and electronic applications, the reliance on insulating polymers continues to grow. The selection of an appropriate polymer insulator is determined by several factors, notably the insulation intensity, intrinsic physical properties, temperature sensitivity, and resistance to electric fields. Among the fundamental properties considered when evaluating the performance of polymers as electrical insulators are the following [99].

### 1.11.2.1 Electrical conductivity

Electrical conductivity is defined as the opposite of electrical resistivity and depends on the number, type, and mobility of charge carriers whether electrons or ions. In insulating materials, the density of these free charges is very low, with almost no mobility, which results in extremely poor conductivity. As the temperature increases, the mobility of these charges also increases, leading to a corresponding rise in conductivity. To improve insulation efficiency, it is preferable to purify the polymer from ionic impurities that may arise as a result oxidation or reduction processes [99].

As the electric field strength applied to an insulator increase, its conductivity begins to rise until the potential difference reaches a critical threshold. Beyond this limit, a sharp increase in the flowing current occurs, resulting in insulation breakdown, whereby the material loses its insulating properties and behaves as a conductor. The voltage at which this breakdown takes place represents a measure of the material's dielectric strength. Experiments studies have demonstrated that polymers free of polar impurities exhibit high electrical insulation capacity. At room temperature, the electrical breakdown voltage typically ranges between $10^7$-$10^6$ (V/cm). However, this value decreases significantly in the presence of moisture or air bubbles, due to the possibility of ionization within the electric field [99].

The relative permittivity, also known as the dielectric constant, represents the ratio of the electrical capacitance of a capacitor filled with a polymer material to that of the same capacitance when filled with a vacuum. This property is dependent on the frequency of the electric field applied during the measurement [99].

Dielectric loss is defined as the amount of electrical energy converted into heat when an electric current passes through the dielectric material. This loss is influenced by the chemical composition of the polymer, particularly the strength of its molecular bonds and the mobility of both the repeating units and the side groups. Stronger intermolecular interactions reduce the mobility of polymer chains, thereby increasing the temperature at which dielectric loss begins. The incorporation of polar groups enhances these intermolecular forces, whereas the introduction of hydrocarbon groups as side branches reduces weakens them, which may consequently lead to an increase in dielectric loss [99].

## 1.11.3 Classification of Conducting Polymers

Electrically conducting polymers were generally classified into two main categories, depending on the conduction mechanism and the nature of the molecular structure. One of these categories is intrinsically conducting polymers, which exhibit electrical conductivity as a direct consequence of their fundamental molecular structure, without the need for additional conduction-inducing materials. Their conductivity arises from the presence of regular and continuous π-conjugated double bonds along the polymer chain, which enable electron

delocalization. In such systems, the π electrons are not confided to a single carbon atom but are instead delocalized across the entire molecular chain in the form of an "electron umbrella", allowing them to move relatively freely and thereby impart significant conductivity. Most polymers in this category display conductivity within the semiconductor range, although higher conductivity values can be achieved through doping. In contrast, the second category is extrinsically conducting polymers, which include polymers that are inherently insulating or very low conductivity, but whose electrical properties can be substantially enhanced through the incorporation of external materials (dopants) that modify their electronic structure. These polymers can be improved by filling them with conductive particles such as carbon or metals, which form conductive network within the polymer matrix, or by doping them with salts and acids, as in the case of polyaniline doped with strong acids, which results in a remarkable increase in conductivity. Furthermore, the addition of ionic additives or inorganic compounds also contributes to enhancing charge transport within the polymer network [100]. Figure (1-13) illustrates this classification, highlighting the distinct conduction mechanisms associated with each category [101].

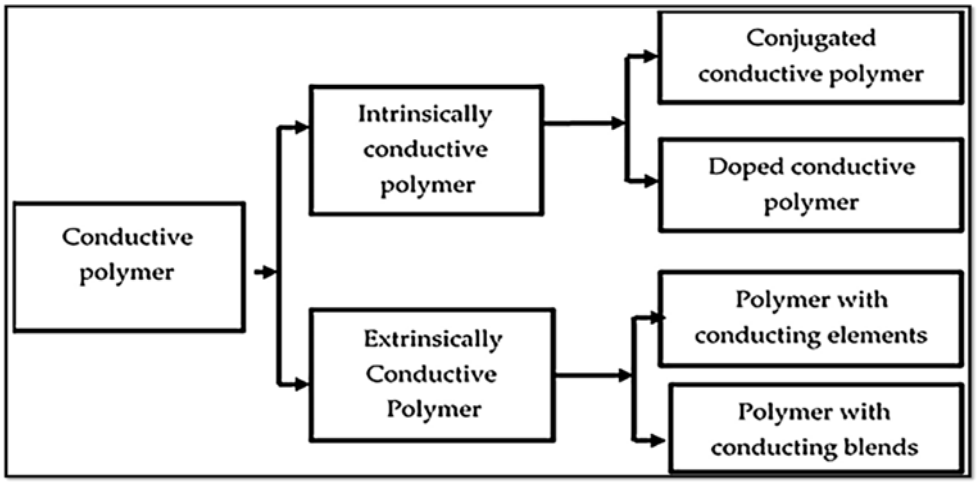


Figure (1-13) presents representative structures of such polymers [101].

## 1.11.4 Doping Techniques

Doping represents one of the primary approaches for enhancing the electrical conductivity of polymers, particularly sequential ones. Its purpose is to introduce charge carriers into the polymer system through controlled modifications in oxidation or reduction states. Several doping techniques have been developed, among which the most significant are the following. First, chemical doping: in this method, the polymer undergoes oxidation or reduction using appropriate oxidizing or reducing agents. This can be achieved through various procedures, such as exposing the polymer to the vapor of the doping agent under low pressure or immersing the polymer disc in a doping solution [102]. Second, photochemical doping: this technique

involves exposing the polymer to ultraviolet (UV) irradiation, resulting in electronic excitation and, consequently, enhanced electrical conductivity [103]. Third, electrochemical doping: in this approach, the polymer functions as an electrode immersed in an electrolyte solution (either organic or aqueous). Doping is achieved by applying a specific voltage to the electrode, which facilitates the incorporation of dopant ions into the polymer matrix. This method is often preferred because the oxidation or reduction level can be precisely controlled by tuning the applied voltage, thereby enabling effective regulation of charge transfer [104].

## 1.11.5 Doping of Conjugated Polymers

Polymers have traditionally been employed as insulating materials due to their very high electrical resistance. Until the mid-20th century, the concept that polymers could serve as conductive materials was not scientifically recognized [105]. However, subsequent years witnessed significant developments, highlighted by the discovery of organic conjugated polymers capable of exhibiting electrical conductivity when doped with strong electron acceptors or donors. The field was inaugurated in the mid-1970s, when Hideki Shirakawa successfully prepared electrically conductive polyacetylene [106]. Later, Alan Heeger and Alan MacDiarmid observed that the conductivity of polyacetylene increased dramatically upon doping with strong oxidizing or reducing agents. When polyacetylene was doped with compounds such as iodine ($I_2$), bromine ($Br_2$), arsenic pentafluoride ($AsF_5$), or sodium naphthalide (Na-naphthalide), its conductivity increased from an initial value not exceeding ($10^{-9}$ $ohm^{-1}.cm^{-1}$) to approximately ($5x10^2$ $ohm^{-1}.cm^{-1}$), representing a qualitative leap in the field of conductive organic polymers [106, 107]. Doping is defined as a process that modifies the oxidation or reduction state of sequential polymers, resulting in fundamental changes in the electronic properties of the material [109]. The origin of electrical conductivity in these materials lies in the presence of doping-induced charge carriers that move along the polymer chain. Sequential polymers are effective conductors for the following reasons [110]: (a) Doping introduces effective charge carriers into the polymer's electronic system. (b) The attraction of electrons in the repeating units leads to the diffusion of charge carriers along the chain, while their three-dimensional transport is achieved through interchain interactions. Doping can be accomplished either by: Oxidation: electrons transfer from the polymer to the dopant, resulting in partial depletion of previously filled bands. Reduction: electrons transfer from the dopant to the polymer, resulting in partial filling of empty bands. These two cases give rise to two types of semiconductors: P-type semiconductors: resulting from the loss of electrons (oxidation). N-type semiconductors: resulting from the gain of electrons (reduction) [111]. The oxidation reaction with halogens (P-type) can be represented as follows:

$$(\pi\text{-polymer})_n + 3/2\ ny\ I_2 \longrightarrow [(\pi\text{-polymer})^{+y}\ (I_3^-)_y]_n \quad \text{..... (1-11)}$$

While the reduction reaction with the alkali metal (n-type):

$$(\pi\text{-polymer})_n + [Na^+(C_{10}H_8)^-]_y \longrightarrow [(Na^+)_y\ (\pi\text{-polymer})^{-y}]_n + (C_{10}H_8)^o \quad \text{..... (1-12)}$$

## 1.11.6 Mechanism of Electrical Conductance in Polymers

Successive polymers undergo a fundamental transformation in their electrical properties following doping. This transformation has been elucidated through various physical theories and perspectives. Upon doping, charged species are generated within the polymer structure, which are directly responsible for carrying electrical current when an external voltage is applied. One of the most prominent theoretical frameworks used to explain electrical conduction in polymers is the band theory. According to this theory, the removal or addition of electrons to a polymer leads to the formation of charged defects within the polymer chain. In the case of trans-polyacetylene, these defects manifest as unpaired electrons, resulting from the alternation of bond types (double and single) in opposite directions along the same chain. This electronic imbalance gives rise to solitons, which act as effective charge carriers along the polymer chain [112]. Figure (1-14) illustrates the resulting structure of this type of defect [113]. The presence of these charged entities, such as solitons, polarons, and bipolarons, facilitates the movement charge along the polymer chain and, throughout the material. This mechanism leads to a significant increase in electrical conductivity after doping, compared to the original insulating state of the polymer [114].

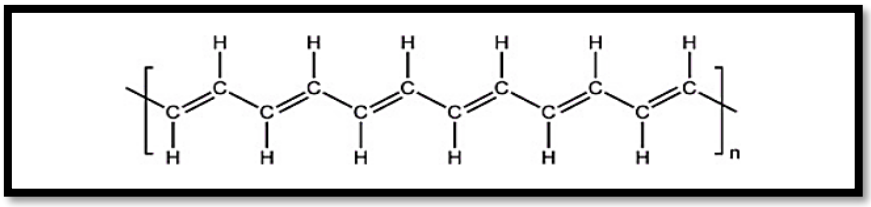

Figure (1-14): Shows the structure of the trans-polyacetylene chain [113].

This type of electronic defect in the polymer chain is referred to as a soliton [113]. The formation of a soliton generates a new energy level within the energy bandgap of the polymer chain, representing a transitional state that enables charge movement along the chain. The electrical character of a soliton depends on the number of electrons it contains: it can carry one electron, in which case it is electrically neutral; it can carry two electrons, making it negatively charged; or it can be devoid of electrons, making it positively charged. When two neutral solitons meet on the same polymer chain, they tend to combine to form a double bond, stabilizing the chain. When a neutral soliton interacts with a charged soliton, the result is a polaron [114], a charged particle with a local deformation in the chain. When two charged solitons meet, they form a bipolaron [115], this characterizes a more stable double-charge state inside the polymer structure. The movement of electricity across various polymers is explained by the transport of electrons from the highest occupied molecular orbital (HOMO) to the lowest unoccupied molecular orbital (LUMO).

The energy differential between the valence and conduction bands is where this transfer takes place. Consequently, as the energy gap between the HOMO and LUMO narrows, electrical

conductivity increases [116]. Studies have demonstrated that increasing conjugation along the polymer chain directly contributes to reducing the energy gap, thereby enhances electrical conductivity. The doping process further contributes by creating an additional energy level between the HOMO and LUMO, which facilitates electron transfer to the conduction band, thus improving conductivity. Recent research has also indicated that the conduction mechanism involves electron transfer from the LUMO level back to the HOMO. Consequently, the higher the LUMO energy and the lower the HOMO energy, the greater the probability of electron transfer, resulting in higher conductivity [117]. Additionally, another explanation for the mechanism of electrical current transfer within polymers involves the formation of charge transfer complexes (CTCs) [118], which arise from partial charge transfer between the polymer and the dopant [119]. These charged complexes act as the active agents in electric current transfer, capable of moving along the polymer chain, as in polyacetylene, or between chains, as in polyisoprene [120].

## 1.12 Nano Materials

The world is experiencing an increasing demand for a new and promising class of materials known as nanomaterials, owing to their versatility in practical applications. The nanometer scale can be illustrated by aligning five silicon atoms or ten hydrogen atoms, each measuring about one nanometer in length. When the size of a material, or one of its dimensions, falls within the range of 1 to 100 nanometers, it is classified as a nanomaterial [115]. These materials are significantly smaller than their bulk counterparts and are characterized by a high surface/volume ratios [116]. As particle size decreases, the proportion of atoms on the surface increases, leading to highly reactive particles with unique chemical, optical, physical, and electronic properties. Nanotechnology is a rapidly evolving field with broad applications in the chemical, pharmaceutical, engineering, and food industries [116], [117]. The term "nanometer" was first introduced in 1914 by Richard Adolf Zsigmondy. In 1959, during the annual meeting of the American Physical Society, American physicist and Nobel laureate Richard Feynman presented a specific concept of nanotechnology; this lecture is regarded as the first official academic presentation of the concept [119].

## 1.13 Synthesis of nanomaterials

Physical methods were employed to produce nanoparticles through a variety of processes that modify materials at the nanoscale. These techniques enable precise control over particle properties, including size, shape, and composition [120]. The most prominent physical methods include the melting mixing method, laser pyrolysis method, pulsed wire discharge method, and high-energy ball milling method. Chemical methods represent some of the most common, effective, and efficient approaches for producing metallic nanoparticles. They are simple, rapid, and cost-effective, and do not require complex equipment, making them suitable for large-scale production. Nanoparticles (NPs) obtained via these methods also demonstrate high stability during long-term storage [121]. The most important chemical methods are the chemical reduction of metal salts, the sol-gel method, the microemulsion method, and the son chemical

method. The top-down approach and the bottom-up approach are the two main ways that nanomaterials are made, as shown in Figure (1-15).

### 1.13.1 Top-down approach

Top-down approaches employ techniques to reduce the size of bulk materials, transforming them into fine nanostructures. These methods include processes such as mechanical milling, laser ablation, micro-drilling, sputtering, electro-explosion, and micro-optical processing. In these approaches, the original bulk materials are broken down into nanoparticles to achieve the desired nanoscale dimensions.

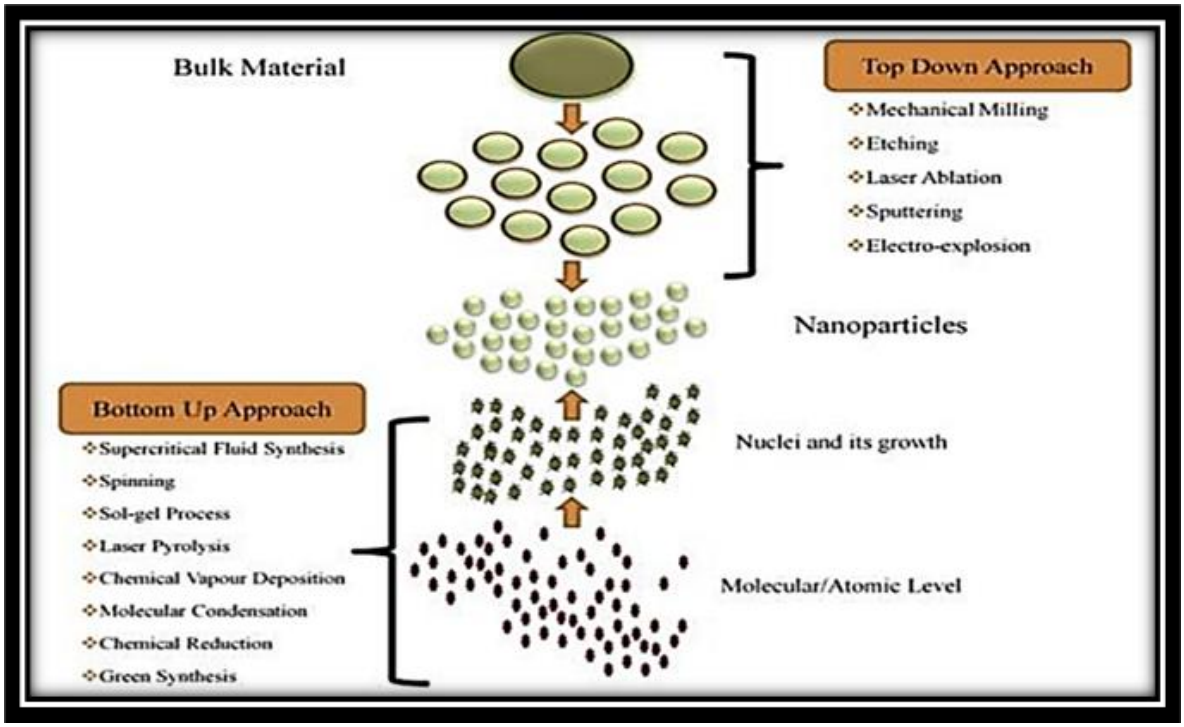


Figure (1-15): The synthesis of nanomaterials via top-down and bottom-up approaches [122].

Nanomaterials employed in reinforcement processes demonstrate numerous beneficial characteristics, such as elevated strength, reduced weight, efficient chemical reactivity, diminutive size, extensive surface area, and superior stability [123]. These materials enhance the properties of the base polymer matrix. Reinforcement materials may be composed of metals, ceramics, or polymers, and are characterized by high resistance and ductility, with variations depending on the material type and intended application. They can take various forms, including particles, flakes, fillers, or fibers. Their sources also vary, ranging from natural minerals to synthetic organic and inorganic compounds [124].

### 1.13.1.1 Electrospinning method

To understand the basic idea behind electrospinning, think of a droplet with a spherical charge made of a conductive, low-molecular-weight liquid in a vacuum. There are two forces acting on the droplet: surface tension, which keeps it in a spherical shape, and an electrostatic repulsive force that breaks it apart. During the electrospinning process, a polymer melt or solution is introduced into the spinneret tip under the influence of a high-voltage electric field. As the voltage increases, the droplet transforms into a conical shape, referred to as the "Taylor cone." This shape arises when the electrostatic repulsive force exceeds the surface tension. After the Taylor cone forms, the charged liquid jet is pushed towards a grounded metal collector. The liquid could be a polymer solution, an emulsion, or a polymer melt. As the jet travels from the Taylor cone to the collector, it either evaporates the solvent or solidifies the melt, resulting in solid nanofibers. Finally, a mat composed of non-woven fibers is placed over the collector [124-126].

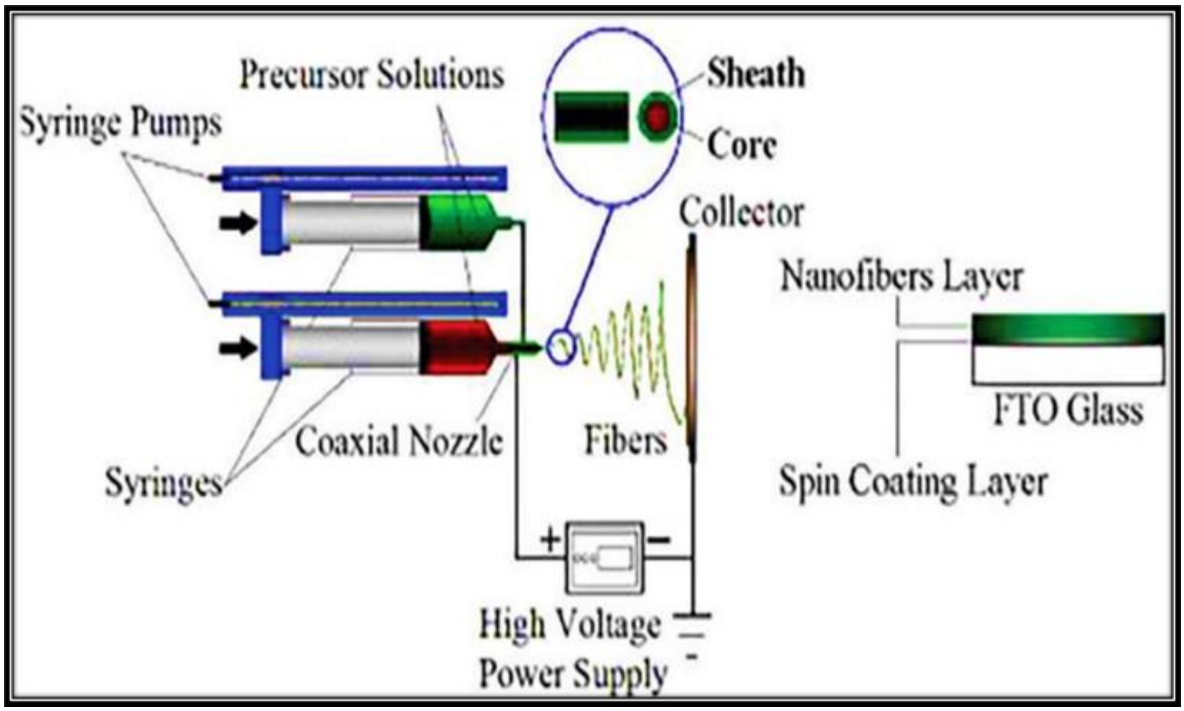


Figure (1-16): A schematic diagram of the coaxial electrospinning technique [127].

### 1.13.2 Bottom-up approach

This methodology involves arranging atoms and molecules in a regular and precise manner to construct structures at the nanoscale, producing materials with well-defined nanoscale dimensions and inherently small size.

### 1.13.2.1 Soft and hard templating methods

The manufacturing of porous nanoparticles heavily depends on both hard and soft template techniques. Among these, the soft template method is a conventional and simple way to create nanomaterials. Its benefits come from producing materials with various morphologies, being simple to use, and having comparatively gentle processing conditions [128]. This method uses various soft templates to create porous nanostructures, including flexible organic molecules, block copolymers, and anionic, cationic, and nonionic surfactants [129]. The fundamental interactions between soft templates and starting materials include electrostatic forces, van der Waals interactions, and hydrogen bonding [130].

In general, the soft template strategy operates via two principal mechanisms for creating ordered mesoporous materials: cooperative self-assembly and "true" liquid crystal templates [129]. Several factors influence the resulting mesoporous structures, including surfactant and feedstocks concentrations, their ratio, surfactants structures, and the environmental conditions during synthesis [128]. Using well-structured solid materials as templates, the rigid template method also referred to as nano casting creates nanostructures for specific uses. Precursor particles fill the rigid template's pores, as seen in Figure (1-17) [130]. The template process generally comprises three main steps: first, selecting or fabricating a suitable original template; second, filling the mesoporous template pores with a specific precursor material, which is subsequently converted into an inorganic solid; and third, removing the template to produce the mesoporous version [131]. Numerous nanomaterials with distinctive structures, including nanowires, nanorods, three-dimensional nanostructures, nanoscale metal oxides, and other nanoparticles, can be synthesized using this technique [132]. This discussion underscores the versatility and effectiveness of both soft and hard template methods in producing diverse nanomaterials.

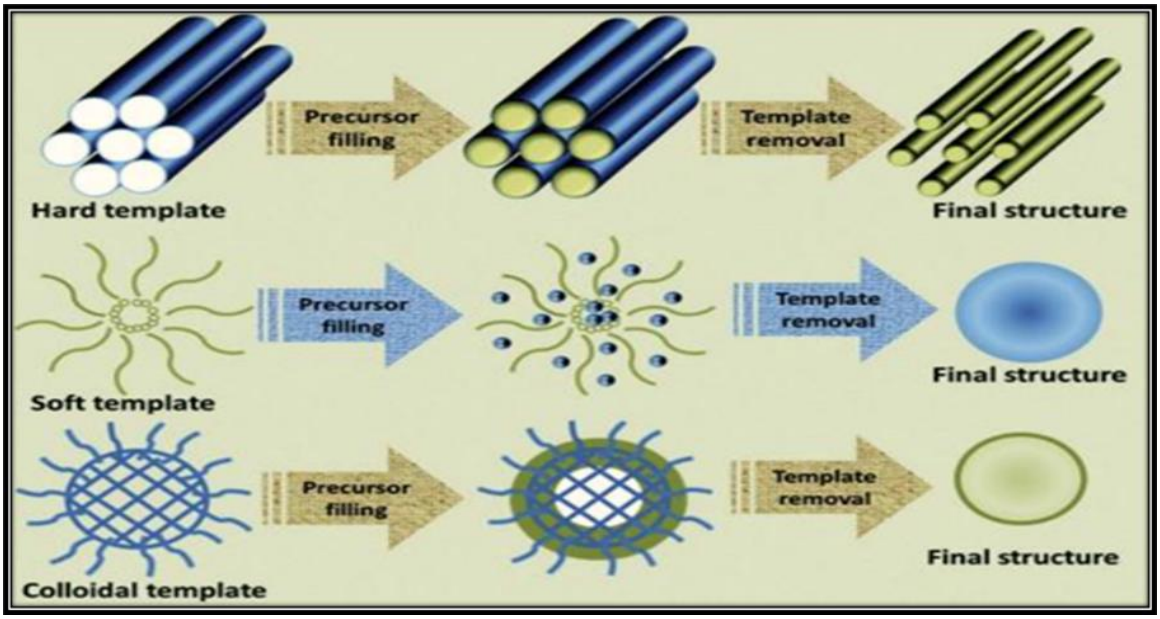


Figure (1-17): A schematic representation of the synthesis of materials using different types of templates [130].

## 1.14 Classification of Nanomaterials based on the Structural Configuration/Composition

Nanomaterials can be classified according to their structural composition into four main categories: organic, inorganic, carbon-based, and composite nanomaterials [133].

### 1.14.1 Organic Nanomaterials

These materials are derived from organic molecules that have been modified at the nanoscale. Common examples include micelles, ferritins, dendrimers, and liposomes, all of which are forms of organic or polymeric nanoparticles [133].

### 1.14.2 Inorganic Nanomaterials

Since these substances don't include carbon hydrogen bonds, they are considered inorganic nanoparticles. Usually, metals or metal oxides make them up [133].

### 1.14.3 Carbon Nanomaterials

Carbon nanotubes, carbon nanofibers, graphene, fullerenes, and carbon black are the five primary varieties that fall under this category. Fullerenes are a notable example in which carbon atoms are arranged in spherical or elliptical structures, commonly referred as "Buckey spheres "[133].

### 1.14.4 Composite Nanomaterials

These materials are formed by integrating nanoparticles with other materials. They include three main types of compositions: nanoparticles integrated with bulk materials, nanoparticles integrated with larger materials, and nanoparticles integrated with other nanoparticles [133].

Nanoscience focuses on study of the fundamental principles of governing molecules and compounds with sizes are less than 100 nanometers, emphasizing the determining of their physical and chemical properties, as well as understanding the phenomena associated with nanoscale dimensions. This discipline also aims to achieve precise control over material fabrication at the atomic level, as altering the number of atoms comprising a particle leads to significant changes in the properties of the resulting material [133, 134]. Nanocomposites (NCs) are multiphase solids in which one of the phases has dimensions of less than 100 nm, or all three have dimensions of less than 100 nm [135- 137]. There are also ceramic-polymer nanocomposites, polymer matrix nanocomposites, polymer-layered silicate nanocomposites, inorganic-organic polymer nanocomposites, and inorganic-organic hybrid polymer nanocomposites [138].

Materials known as polymer matrix nanocomposites require the dispersion of inorganic nanoparticles with one dimension within the 10-100 $A^{o}$ range. When compared to ordinary polymer composites or pure polymers, these composites significantly improve the mechanical and physical properties [138]. In this context, researchers aim to develop safe and efficient

methods for synthesizing silver nanoparticles. Utilizing plant extracts, including leaves and seeds, has emerged as one of the most promising methodologies regarding safety and efficiency. Kantha and Arunachalam demonstrated that the preparation silver and gold nanoparticles using aqueous plant extracts is an environmentally friendly option, which also accelerates the nanoparticle production process [138, 139]. Their results indicated that the particle size can be controlled by adjusting the amount of extract used [140, 141]. The subsequent chapters will detail the methods employed to obtain these nanoparticles using plant extracts. Conversely, copper nanoparticles are recognized for their excellent catalytic activity, electrical and thermal conductivity, and biological properties. In addition to their low cost compared with silver and gold nanoparticles, they present challenges such as rapid oxidation and agglomeration, necessitating the use of encapsulating agents like polymers and organic ligands [143]. Chemical synthesis methods encompass various techniques, including wet reduction with reductants such as $NaBH_4$ and hydrazine, accompanied by antioxidants such as ascorbic acid as an encapsulating agent, thermal decomposition of copper compounds using organic materials, microwave-assisted synthesis and microemulsion technology, wherein aqueous nanodroplets act as microreactors to yield homogeneous particles [144].

Copper nanoparticles are utilized in numerous applications, including the catalysis of organic reactions, such as click chemistry, and the breakdown of industrial dyes like methylene blue when exposed to light. They possess antimicrobial properties, as they generate reactive oxygen species that can damage bacterial DNA. Additionally, these nanoparticles promote wound healing by encouraging angiogenesis. Additionally, they improve the thermal conductivity of various liquids. The substantial surface area of copper nanoparticles, combined with Brownian motion, has the potential to enhance the thermal conductivity efficiency of ethylene glycol by as much as 35%. Consequently, they may prove highly beneficial in applications such as electronics, sensors, and coolants [144].

## 1.15 Aims of This Study

1) Synthesize two monomers and incorporate them into eight polyurea polymers with aliphatic and aromatic segments.
2) Synthesis and characterize silver and copper nanoparticles and their using.
3) Investigate the structural, morphological and compositional features of the synthesized materials using FTIR, NMR, XRD, FESEM, EDX, TEM, and zeta potential analysis.
4) Investigate the electrical conductivity of the prepared polyurea nanocomposite.
5) Evaluate the thermal properties of the pristine polyurea polymers

# *Chapter Two*

## *EXPERIMENTAL*

## 2.1 Instruments and Chemicals

The instruments used in the present study and their models, companies and origin are listed in Table (2-1), the chemicals listed in Table (2-2).

**Table (2-1): Instruments used in study, models, companies and origin**

| Ser. | Device | Company | Origin | Laboratory |
|---|---|---|---|---|
| 1 | FT-IR Spectrophotometer, FT-IR-1800 | Shimadzu | Japan | BPC Analysis Center Adhamiya / Baghdad |
| 2 | Nuclear Magnetic Resonance Spectrometer (NMR), 400MHz | Bruker 400MHz | Germany | College of Education / University of Basra |
| 3 | Thermogravimetric (TGA) SDT Q600 V20.9 Build 20 | TA Instruments | USA | International University of Kashan / Iran |
| 4 | X-Ray Diffraction (XRD), PW3064 | Malvern Panalytical | Netherlands | College of Science / University of Basra |
| 5 | Four-Point Probe System (T2001A3) | Ossila | UK | College of Science / University of Misan Chemistry Dept. |
| 6 | Field Emission Scanning Electronic Microscope (FESEM), 5 KV | Zeiss | Germany | Tehran University/ Advanced Materials Characterization Institute |
| 7 | Transmission Electron Microscopy (TEM), (Tec nail $^{TM}$ G2F20) | FEI | UK | International University of Kashan / Iran |
| 8 | Energy Dispersive X-ray Spectroscopy (EDX), | Instruments Oxford | UK | International University of Kashan / Iran |
| 9 | Zeta Potential | GFR | Germany | International University of Kashan / Iran |
| 10 | Ultrasonic Bath Sonicator, WHC-A10H | Daihan Scientific | China | University of Misan / College of Science/ Chemistry Dept. |
| 11 | Melting Point Apparatus | Stuart (Cole-Parmer) | UK | University of Misan / College of Science/ Chemistry Dept. |

**Table (2-2): Chemicals used, chemical formula, company and origin**

| Ser. | Chemicals | Chemical Formula | Company | Origin | Purity |
|---|---|---|---|---|---|
| 1 | Ammonium Hydroxide | $NH_4OH$ | Avonchem | UK | 25% W/W |
| 2 | Ethanol Absolute | $C_2H_5OH$ | Fluka | Germany | 99.9% |
| 3 | Hexamethylene Diisocyante (HDI) | $C_8H_{12}N_2O_2$ | Sigma-Aldrich | Germany | 97% |
| 4 | 1,4-phenylene Disocyanate(PDI) | $C_8H_4N_2O_2$ | Sigma-Aldrich | USA | 99% |
| 5 | Silver nitrate | $AgNO_3$ | Hunan Sincere chemicals | China | 99% |
| 6 | Sodium Citrate | $Na_3C_6H_5O_7$ | Fluka | Germany | 98% |
| 7 | Sulphuric acid | $H_2SO_4$ | Chem Lab | UK | 97% |
| 8 | Terephthalaldehyde (TPAL) | $C_8H_6O_2$ | Bidepharm | China | 99.5% |
| 9 | Terephthalic Acid (TPA) | $C_8H_6O_4$ | Sigma-Aldrich | USA | 99% |
| 10 | Thiosemicarbazide (TSC) | $CH_5N_3S$ | Loba Chemie PVT. LTD | India | 98% |
| 11 | Tolylene Diisocyanate (TDI) | $C_9H_6N_2O_2$ | Sigma-Aldrich | Germany | 80% |
| 12 | Methylenediphenyl Diisocyanate (MDI) | $C_{15}H_{10}N_2O_2$ | Industry Engineering | UAE | 99.5% |

## 2.2 Synthesis of Monomers

### 2.2.1 Synthesis of Terephthaldehyde Bis(thiosemicarbazone) (TBT)

Terephthalaldehyde (1 mmol, 1.341 gm) was mixed with ethanol (50 mL) under continuous stirring for 10 min. A solution of thiosemicarbazide (2 mmol, 1.823 gm) in 50 mL water-ethanol mixture was added to a solution (1:1 V/V) and reflux for 3 hours. After completion of the reaction, the mixture was allowed to cool for 1 hour and then filtered. The obtained precipitate was washed with distilled water. The precipitate was then dried and purified using a cooled ethanol-water mixture. Finally, the product was dried in a vacuum oven for 2 hours. (TLC eluent; MeOH/DCM at a ratio of 1:2). The Table (2-3) shows the physical properties of monomer (2) [145].

## 2.2.2 Synthesis of 5,5'[(1,4-phenelene) bis(1,3,4-thiadiazol-2-amine)] (TDA)

Terephthalic acid (1mmol, 1.661 gm) was mixed with thiosemicarbazide (2mmol, 3.646 gm) in round-bottom flask equipped with a condenser. Then, 15 mL of concentrated sulfuric acid was added dropwise under cold conditions (0 °C, ice bath). The reaction mixture was refluxed for three days, after which it was poured over crushed ice. Ammonia solution was then added until the mixture was neutralized (pH = 7). The resulting yellow precipitate was collected by filtration, washed with a saturated sodium bicarbonate solution, and subsequently rinsed with distilled water. After drying, it was recrystallized in ethanol. Finally, the product was dried in a vacuum oven for 5 hours. (TLC eluent; MeOH:DCM at a ratio of 1:3). The table (2-3) shows the physical properties of the prepared monomer (3) [146].

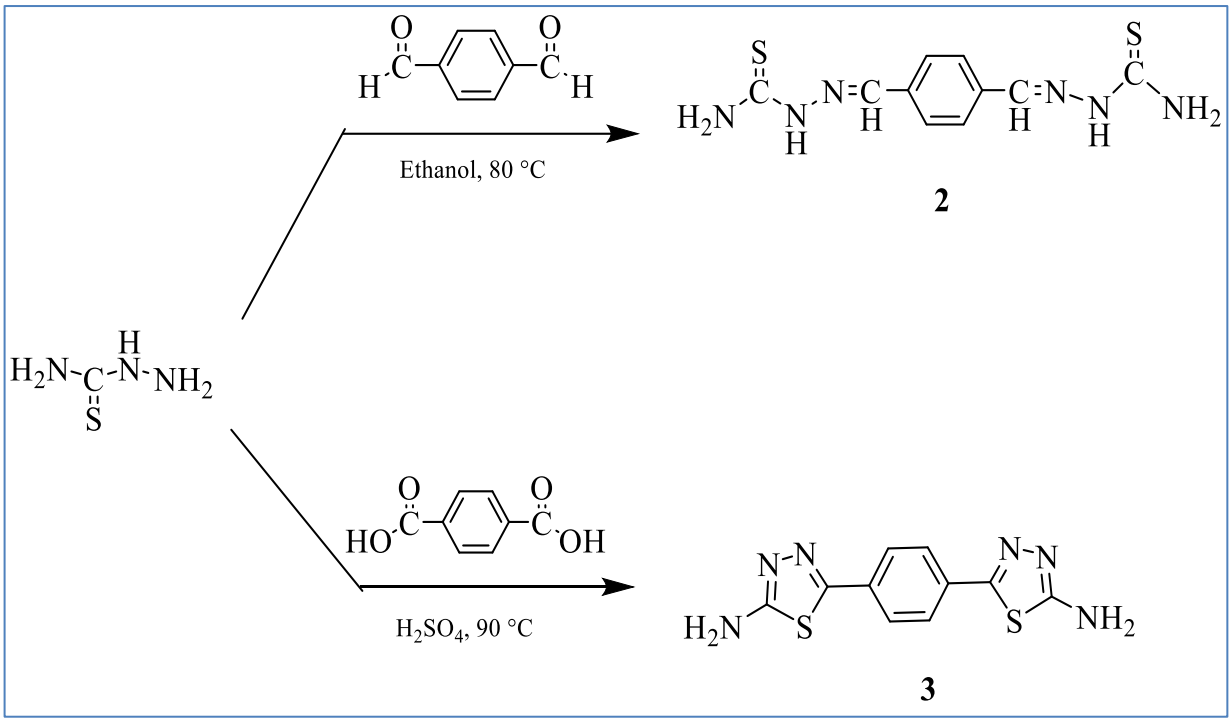


Figure (2-1): Synthesis pathways of Schiff-base diamine monomers: (2) terephthaldehyde bis(thiosemicarbazone) (TBT) and (3) 5,5′[(1,4-phenylene) bis(1,3,4-thiadiazol-2-amine)] (TDA).

**Table (2-3) shows the physical properties of monomers.**

| Monomers | Structural Formula | Molecular Weight (gm/mol) | Melting Point °C | Color | Yield % |
|---|---|---|---|---|---|
| **2** | 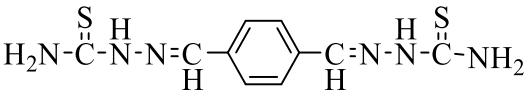 Terephthaldehyde bis(thiosemicarbazone) | 280.37 | 275-277 | Yellow crystals | 96.70 |
| **3** | 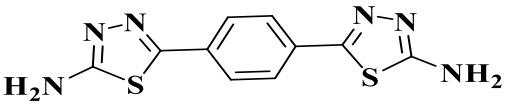 5,5'-(1,4-phenylene) bis(1,3,4-thiadiazol-2-amine) | 276.34 | 240-242 | Yellow acicular crystals | 31.72 |

# 2.3 Synthesis of polyurea polymers

## 2.3.1 Synthesis Polyurea Polymers based on TBT (Group (1))

Into a 100-mL, two-necked round-bottom flask equipped with an $N_2$ inlet tube, a condenser, a magnetic stirrer, an oil bath, and a thermometer were placed the synthesized diamine, (2 mmol, 0.5607 gm in 10 mL dry NMP). Prior to use, NMP was purified using 3Å molecular sieves. The sieves were first activated by heating them under reduced pressure (about 200 mbar) for 4 hours. The reaction mixture was stirred at room temperature for a few minutes. The reaction mixture was stirred at room temperature for a few minutes. Subsequently, a solution containing the selected diisocyanate (TDI, MDI, PDI and HDI; 2mmol in 10 mL of dry NMP) was added in one portion. The mixture was stirred for 3 hours at 60 °C, and then it was precipitated in 50 mL of water. The polymer was filtered and washed with hot water, purified using a cold ethanol/acetone mixture, and finally vacuum-dried at 50 °C for 6 hours. (TLC eluent; EtOAc /Pet.ether at a ratio of 1:2). Table (2-4) shows the physical properties of the polymers [147].

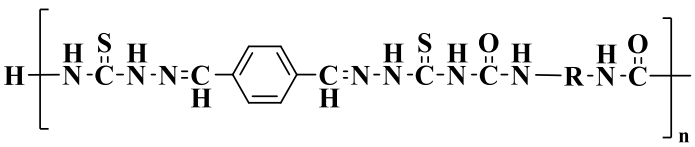

Figure (2-2): Aromatic polyurea containing hydrazone linkages.

**Table (2-4) shows the physical properties of the polymers.**

| Monomer TBT | Type of Isocyanate (R) | **Melting Point °C** | **Color** | **Yield %** |
|---|---|---|---|---|
| **2a** | OCN-($CH_3$) $C_6H_3$-NCO | 142-144 | Yellow | 46.83 |
| **2b** | OCN-$C_6H_4$-($CH_2$)-$C_6H_4$-NCO | 241-243 | Yellow | 93.80 |
| **2c** | OCN-$(CH_2)_6$-NCO | 229-231 | Yellow | 55.94 |
| **2d** | OCN-$C_6H_4$-NCO | 252-254 | Dark brown | 62.24 |

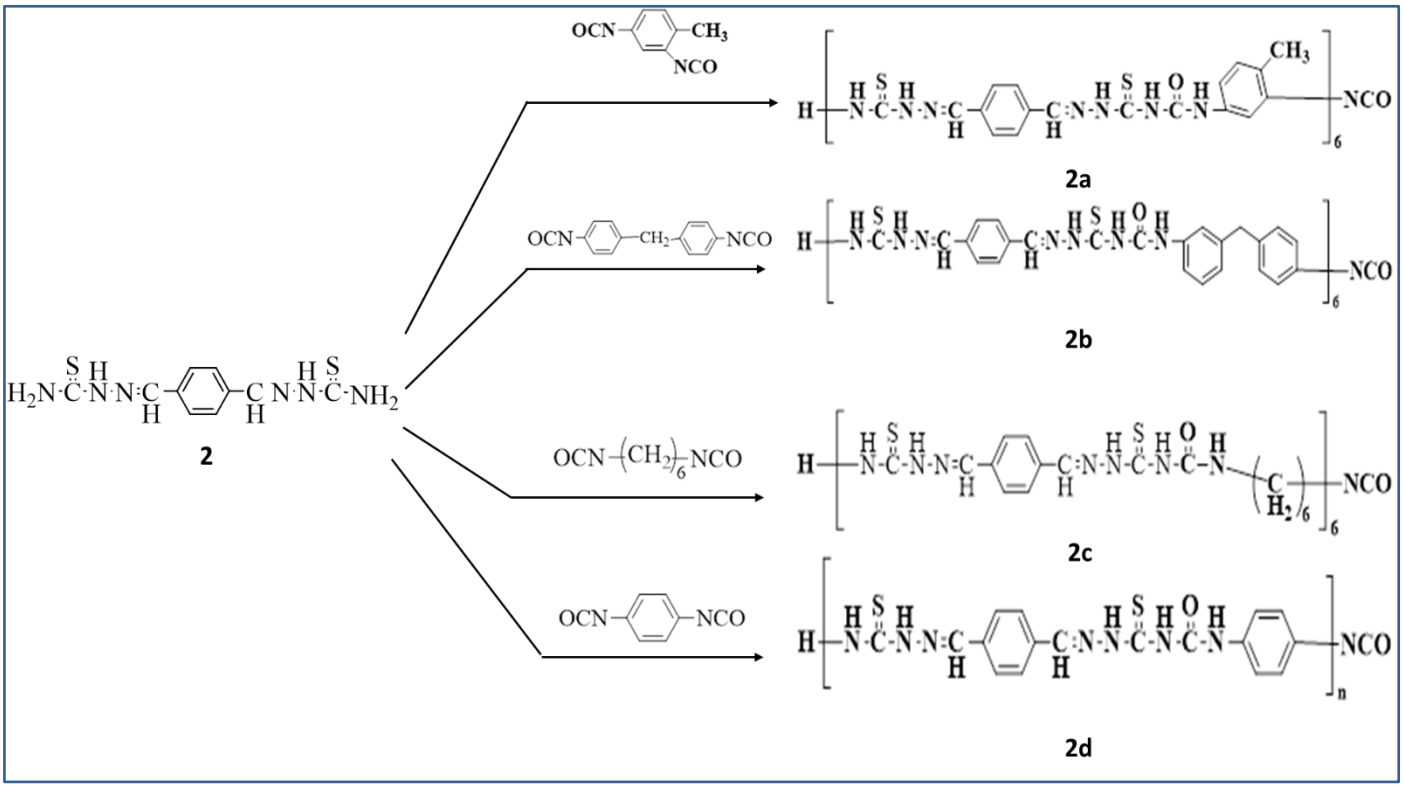


Figure (2-3): Polycondensation route for polyurea polymers derived from monomer 2.

## 2.3.2 Synthesis Polyurea Polymers Based on TDA (Group (2))

Into a 100-mL, two-necked round-bottom flask equipped with an $N_2$ inlet tube, a condenser, a magnetic stirrer, an oil bath and a thermometer were placed the synthesized diamine, (2 mmol, 0.5527 gm in 10 mL of dry N-Methyl-2-pyrrolidone (NMP)). Prior to use, NMP was purified using 3Å molecular sieves. The sieves were first activated by heating them under reduced pressure (about 200 mbar) for 4 hours. The reaction mixture was stirred at room temperature for a few minutes. Subsequently, a solution containing the selected diisocyanate (TDI, MDI, PDI and HDI; 2mmol in 10 mL of dry NMP) was added in one portion. The mixture was stirred for 3 hours at 60 °C, and then it was precipitated in 50 mL of water. The polymer was filtered and washed with hot water, purified using a cold ethanol/acetone mixture, and finally vacuum-dried at 50 °C for 6 hours. (TLC eluent; EtOAc/Pet.ether at a ratio of 1:2). Table (2-5) shows the physical properties of the polymers [147].

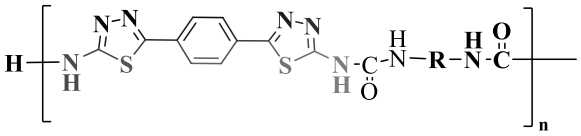

Figure (2-4): Aromatic polyurea containing thiadiazol linkages.

**Table (2-5) shows the physical properties of the polymers.**

| Monomer TDA | Type of Isocyanate (R) | **Melting Point °C** | **Color** | **Yield %** |
|---|---|---|---|---|
| **3a** | OCN-($CH_3$) $C_6H_3$-NCO | 121-123 | Off-white | 83.92 |
| **3b** | OCN-$C_6H_4$-($CH_2$)-$C_6H_4$-NCO | 286-288 | Black | 70.23 |
| **3c** | OCN-$(CH_2)_6$-NCO | 118-120 | Black | 49.97 |
| **3d** | OCN-$C_6H_4$-NCO | 298-300 | Dark Red | 46.53 |

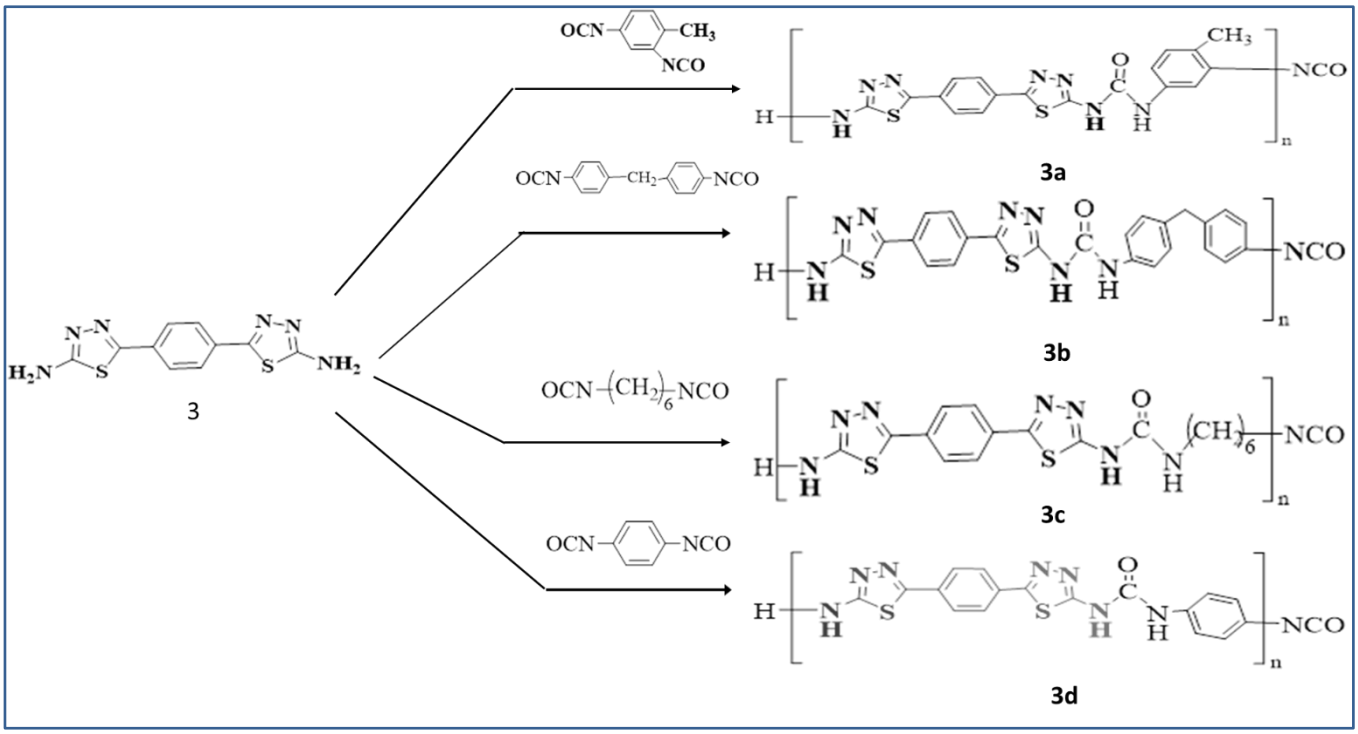


Figure (2-5): Polycondensation route for polyurea polymers derived from monomer 3.

## 2.4 Synthesis of Nanoparticles

### 2.4.1 Synthesis of Silver Nanoparticles

In a 500-mL beaker, silver nitrate (0.98 g dissolved in 50 ml of distilled water), and the mixture was maintained at 60°C for 30 minutes. Then, a sodium citrate solution (2 g dissolved in 50 ml of distilled water) was added, and the reaction was allowed to proceed for 1 hour. This was followed by the addition of a previously prepared green tea extract (obtained by dissolving 1 gm of green tea leaves in 100 mL of distilled water). The reaction mixture was then left for 2 hours until silver crystals precipitated on beaker surface. The product was separated by centrifugation (6000 rpm) for 15 minutes, washing twice with distilled water and once with ethanol. The precipitate was dried at 45°C and stored away from light. Finally, the product exhibited a gray color, weigh 0.58 g [148].

### 2.4.2 Synthesis of Copper Nanoparticles

In a 500-mL beaker, copper (II) sulfate (2mmol, 0.5 g dissolved in 30 mL of distilled water), and the mixture was maintained at 60 °C for 15 min. Subsequently, a solution containing polyvinyl alcohol (PVA) (0.065 g dissolved in 10 mL of distilled water) was then added, and the reaction was allowed to proceed for 30 min. Thereafter, approximately 33 mL of sodium hydroxide solution (0.99 g, 50% w/v distilled water) was gradually added dropwise over 1 hours. This was followed by the addition of 2.4 ml of hydrazine hydrate, and the reaction

mixture was kept for an additional 2 hours. The product was separated by centrifugation at (6000 rpm) for 15 minutes, washing twice with distilled water and once with ethanol. The precipitate was then dried at 45°C, yielding a dark red powder, weight of 0.0962 g [149].

## 2.5 Preparation of Conductive Polyurea Polymers Nanocomposite

To prepare the conducting samples 0.05 g of the previously synthesized polyurea polymers mixture was then dissolved with a few drops of dimethylformamide (DMF) and subjected to ultrasonic bath sonicator for 2 minutes to obtain a homogeneous solution, hereafter referred to as conductive ink. Several drops of the prepared mixture were cast onto a glass slide and left to allow the solvent to evaporate, thereby yielding a sample ready for electrical measurements, as illustrated in (Figure 2-6) [150].

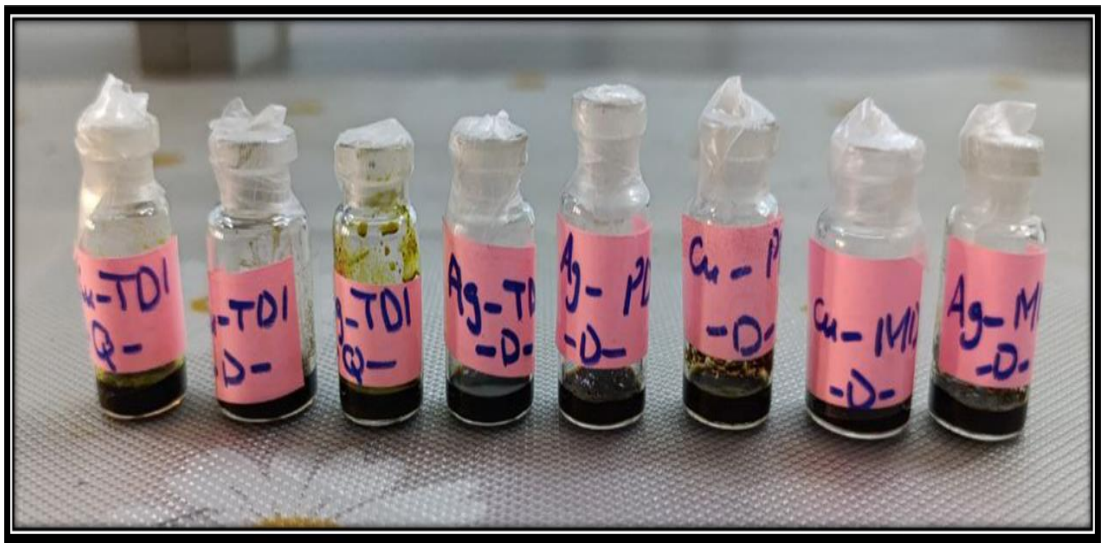

Figure (2-6): Laboratory photograph of conductive ink prepared by doping of polyurea polymers.

# *Chapter Three*

## *Results and Discussion*

## 3.1 Spectral characterization of Prepared Monomers

### 3.1.1 Fourier Transform Infrared Spectrophotometry (FT-IR)

The FTIR spectra of the free thiosemicarbazone, recorded using the KBr pellet method, exhibited the characteristic peaks summarized in Table (3-1) based on the reference [145]. These spectral features are further illustrated in the FTIR spectrum presented in Figure (3-1).

**Table (3-1): The major peak bands of monomer 2**

| Functional Group | Vibration/ Mode | Literature Range ($cm^{-1}$) | Observed ($cm^{-1}$) | Band Shape & Intensity |
|---|---|---|---|---|
| $-NH_2$ (Primary amine) | N-H stretching (asym, sym) | 3395-3265 | 3471-3267 | Broad, Strong |
| -NH- (Secondary thioamide) | N-H stretching | 3192 | 3197 | Broad, Medium |
| C-H (aromatic) | C-H stretching | | 2993 | Medium |
| C-H (aliphatic) | C-H stretching | | 2924 | |
| C=N (imine/azomethine) | C=N stretching | 1593 | 1593 | Medium-strong, sharp |
| C=C (aromatic ring) | Stretching | – | 1519-1463 | Medium-strong, sharp |
| C-N | Stretching | 1465 | 1411 | Medium, sharp |
| C=S (thioamide) | Stretching | 1358 | 1357 | Medium, sharp |
| C-H (aromatic) | Out-of-plane bending | – | 1008-804 | Variable, sharp |

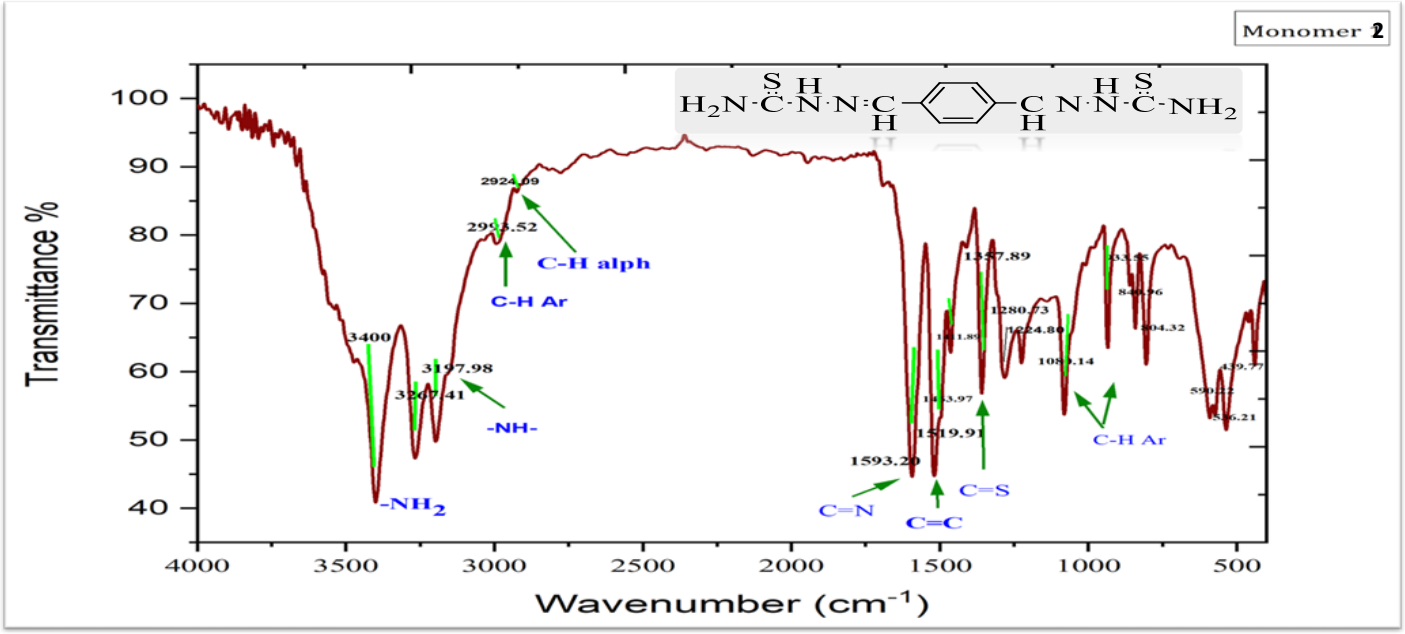


Figure (3-1): FT-IR Spectrum of Monomer 2.

The FTIR spectra of TDA, obtained through the KBr pellet method, revealed the characteristic absorption bands in Table (3-2) according to reference [146]. These results are further depicted in the FTIR spectrum shown in Figure (3-2).

**Table (3-2): The major peak bands of monomer 3**

| Functional Group | Vibration/ Mode | Literature Range ($cm^{-1}$) | Observed ($cm^{-1}$) | Band Shape & Intensity |
|---|---|---|---|---|
| $-NH_2$ (primary amine) | N-H stretching (asym, sym) | 3282-3097 | 3296-3113 | Broad, strong |
| C-H (aromatic) | C-H stretching | 3000 | 2995 | Broad, weak |
| C=N (imine/ Het-cyclic) | C=N stretching | 1620 | 1678 | Strong, sharp |
| C=C (aromatic ring) | C=C Stretching (asym,sym) | 1541-1410 | 1571-1421 | Medium, sharp |
| N-N | Stretching | 1041 | 1037 | Medium |
| C-N aromatic | Stretching | 1332 | 1388 | Medium |
| C-S Het-Cyclic | Stretching | 688 | 682 | Medium |

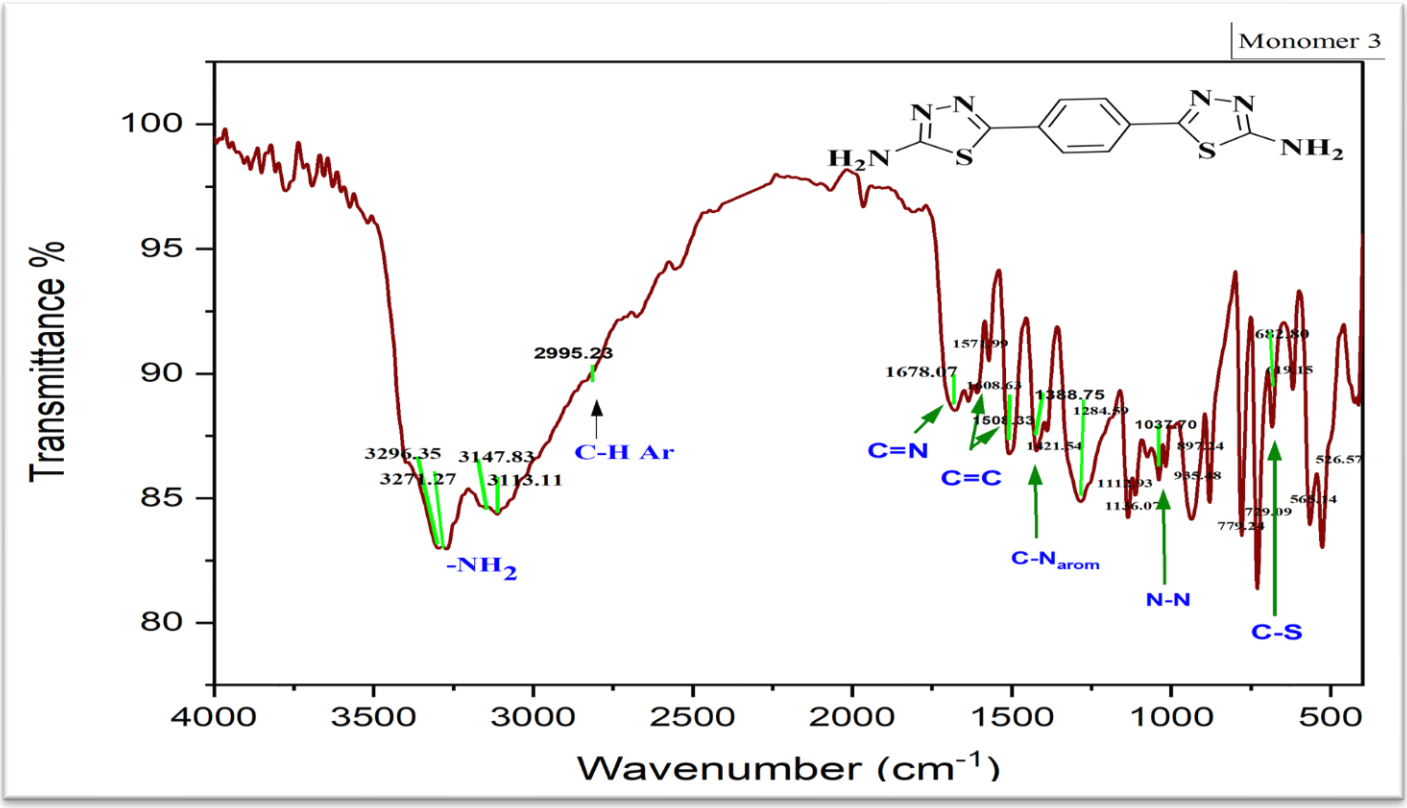


Figure (3-2): FT-IR Spectrum of Monomer 3.

### 3.1.2 Hydrogen Nuclear Magnetic Resonance ($^1$H-NMR Spectra of TBT and TDA)

All hydrogen nuclear magnetic resonance (**$^1$**H-NMR) spectra of the prepared monomers exhibited two signals corresponding to the solvent DMSO-$d_6$ at room temperature. The first signal appeared at δ = 2.50 ppm and was attributed to the solvent protons, while the second signal at δ = 3.36 ppm was assigned to residual water present in the solvent.

The proton nuclear magnetic resonance spectrum ($^1$H-NMR, 400 MHz, DMSO-$d_6$) of the synthesized monomer TBT exhibited four characteristic regions of resonances in full agreement with the proposed structure. A broad singlet at δ 11.50 ppm was assigned to the thioamide NH protons [–NH–C(=S)], strongly deshielded due to the electron-withdrawing thione group and the possible involvement in intra-/intermolecular hydrogen bonding. In the experimental spectrum, the para-substituted aromatic protons resonated at δ 8.04 ppm as a broad singlet rather than the expected multiplet. This behavior is attributed to the very close chemical shifts of the aromatic protons, leading to coalescence of signals under the employed conditions. A sharp singlet at δ 8.26 ppm corresponded to the vinylic protons of the imine (–CH=N–), while another resonance at δ 7.82 ppm was assigned to the terminal –$NH_2$ protons, typically broadened due to exchange effects. The relative integrations of all signals were consistent with the expected number of protons in the molecular structure (4H aromatic, 2H imine, 2H thioamide NH, and 4H amino $NH_2$). These results confirm the proposed molecular structure and support the high purity of the compound, as illustrated in Figure (3-3) and summarized in Table (3-3).

**Table (3-3): Chemical shifts of protons in monomer 2**

| δ (ppm) | Multiplicity | Integration | Assignment |
|---|---|---|---|
| 11.50 | br, s | 2H | Thioamide NH |
| 8.26 | s | 2H | Vinylic CH=N |
| 8.04 | br, s | 4H | Aromatic protons |
| 7.82 | br, s-m | 4H | Terminal -$NH_2$ |
| 3.36 | s | - | HDO |
| 2.50 | sep. | - | Residual DMSO-$d_6$ |

**br= broad, s= singlet, m= multiplet*

The proton nuclear magnetic resonance spectrum ($^1$H-NMR, 400 MHz, DMSO-$d_6$) of the synthesized para-disubstituted bis(thiadiazol-2-amine) derivative monomer 3 was recorded at room temperature. The aromatic protons of the para-disubstituted benzene ring were expected to appear as doublets due to ortho coupling (J ≈ 7–9 Hz). However, in the experimental spectrum the resonance was observed as an apparent singlet, which can be explained by the high molecular symmetry and partial overlap with the broad $NH_2$ signal. A broad signal integrating for approximately four protons appeared at δ = 7.21 ppm, corresponding to the two terminal –$NH_2$ groups. The broadness and slight downfield shift of this signal can be attributed to hydrogen bonding and proton exchange in the strongly polar DMSO-$d_6$ medium. Notably, this broad resonance partially overlaps with the second expected aromatic doublet, which explains the reduced resolution of the ortho-coupling pattern (J = 8.2 Hz) [147]. Overall, the

spectral features are fully consistent with the proposed molecular structure, as illustrated in figure (3-4) and summarized in table (3-4).

**Table (3-4): Chemical shifts of protons in monomer 3**

| δ (ppm) | Multiplicity | Integration | Assignment |
|---|---|---|---|
| 7.78 | s | 4H | Aromatic protons |
| 7.21 | br, s | 4H | Terminal -$NH_2$ |

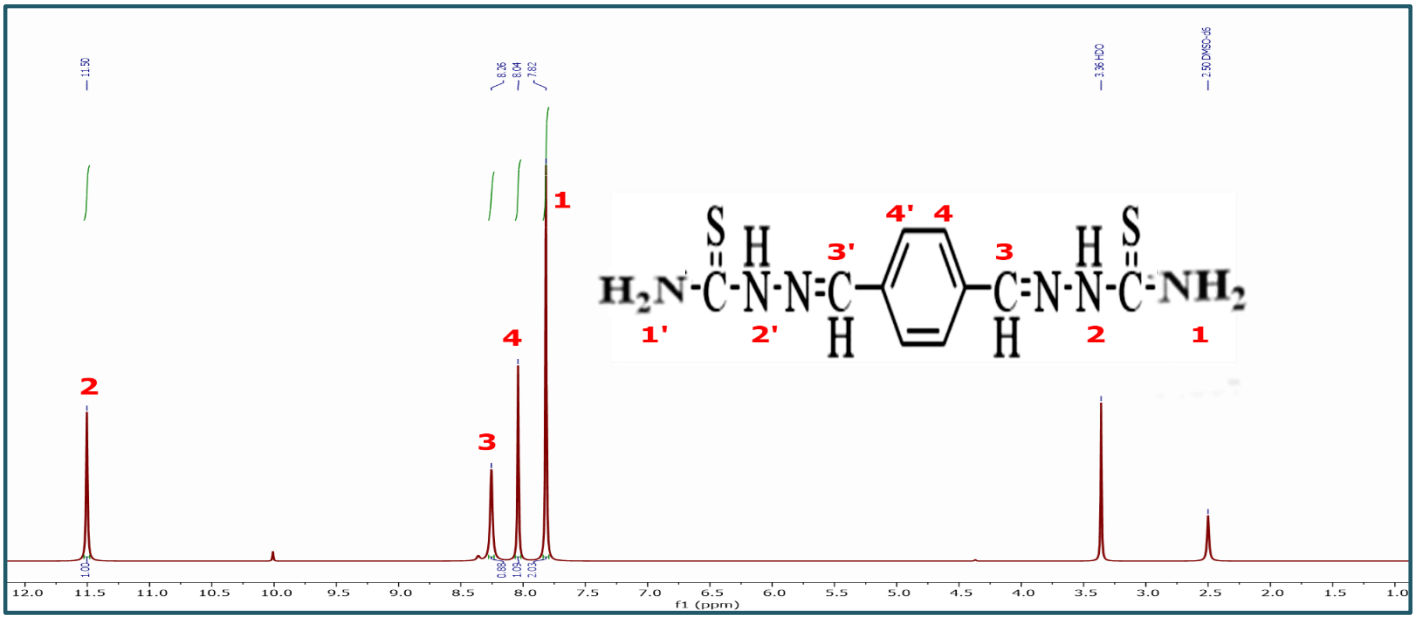


Figure (3-3): $^{1}$H-NMR of Monomer 2

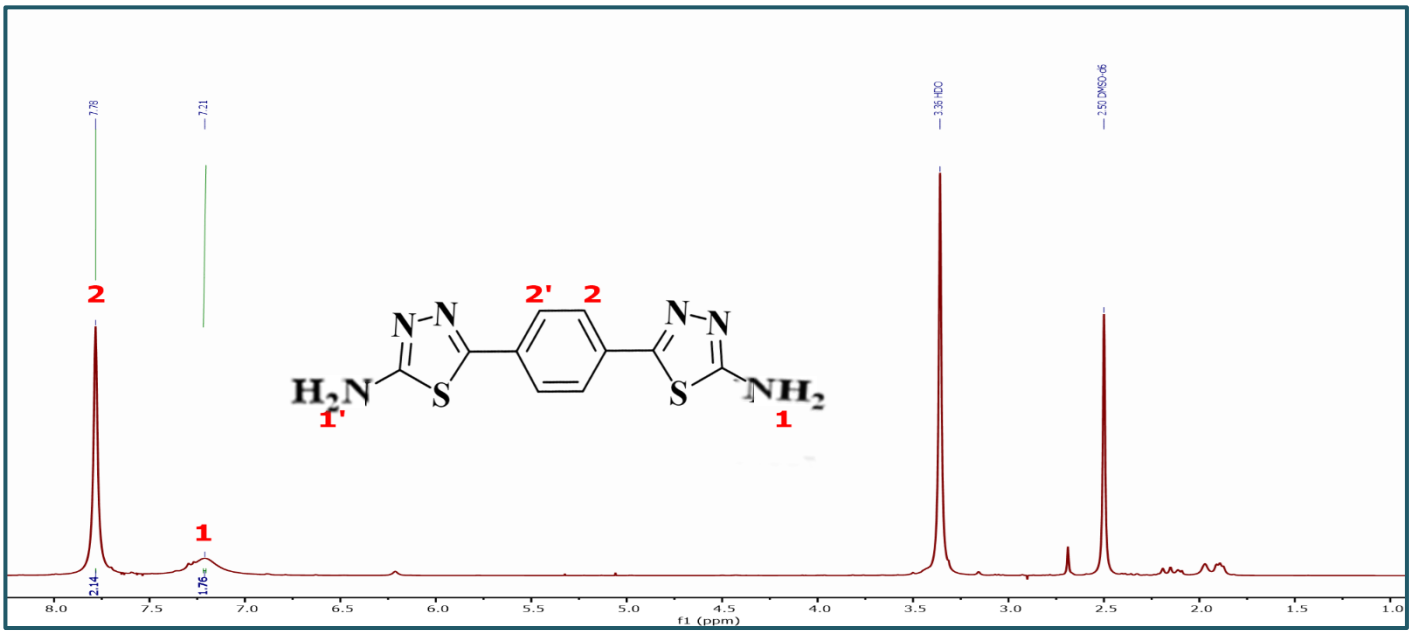


Figure (3-4): $^{1}$H-NMR of Monomer 3

### 3.1.3 Carbon Nuclear Magnetic Resonance ($^{13}$C-NMR Spectra of TBT and TDA)

The carbon nuclear magnetic resonance spectrum ($^{13}$C-NMR) was recorded at 100.62 MHz for $^{13}$C. Measurements were carried out at room temperature (≈ 292.5 K) using DMSO-$d_6$ as solvent and tetramethylsilane (TMS) as internal reference (δ = 0.00 ppm). The spectrum was acquired with 2048 scans and a relaxation delay of 2.0 s.

The $^{13}$C-NMR spectrum of Monomer 2 exhibited a characteristic resonance at δ 178.43 ppm, assigned to the thioamide carbon (C=S). This represents the most deshielded signal in the spectrum, as the carbon is strongly electron-deficient due to the high electronegativity of the adjacent sulfur and nitrogen atoms. The ipso carbon directly bonded to the imine functionality (–C=N–) appeared at δ 142.09 ppm. The deshielding of this carbon arises from the electron-withdrawing nature of the imine nitrogen, which exerts both an inductive effect, thereby shifting the resonance downfield. The para carbon was observed at δ 135.86 ppm with relatively low intensity, consistent with a quaternary aromatic carbon. The aromatic CH carbons (C2, C3, C5, C6) resonated at δ 128.24 ppm, where the signals overlapped due to the high symmetry of the para-disubstituted benzene ring. Overall, these spectral features are fully consistent with the proposed molecular structure and confirm the successful synthesis of the target monomer, as illustrated in figure (3-5) and summarized in table (3-5).

**Table (3-5): Chemical shifts of carbons in monomer 2**

| δ (ppm) | Carbon type | Structural assignment |
|---|---|---|
| 178.43 | C1 | Thioamide carbon (C=S) |
| 142.09 | C2 | C (directly bonded to C=N) |
| 135.86 | C3 | C-para (aromatic quaternary) |
| 128.24 | C4 | Aromatic carbons |

**Cq= quaternary carbon.*

The $^{13}$C-NMR spectrum of the synthesized monomer TDA exhibited four well-resolved signals that are fully consistent with the proposed molecular structure. The resonances at δ 173.48 and 163.43 ppm are attributed to the imine-type carbons (C=N) of the thiadiazole rings. Their strong deshielding effects from the nearby electronegative nitrogen and sulphur atoms cause pronounced downfield chemical shifts. These effects lower the electron density around these carbons and make them more sensitive to the external magnetic field. The signal at δ 143.69 ppm comes from the ipso carbons of the central benzene ring that are directly connected to the electron-withdrawing thiadiazole substituents. This connection causes more deshielding than unsubstituted aromatic carbons. The aromatic carbons are responsible for the resonance at δ 129.92 ppm. This effect is because the para-disubstituted benzene ring has a very high degree of symmetry, which makes the peaks look like they are all in one place. The peaks between δ 39 and 41 ppm are the leftover signal from the DMSO-$d_6$ solvent [147], as illustrated in figure (3-6) and summarized in table (3-6).

**Table (3-6): Chemical shifts of carbons in monomer 3**

| δ (ppm) | Carbon type | Structural assignment |
|---|---|---|
| 173.46 | C1 | Imine carbon of thiadiazole ring |
| 163.43 | C2 | Second imine carbon of thiadiazole ring (C=N) |
| 143.69 | C3 | C (aromatic quaternary) |
| 129.92 | C4 | Aromatic carbons |

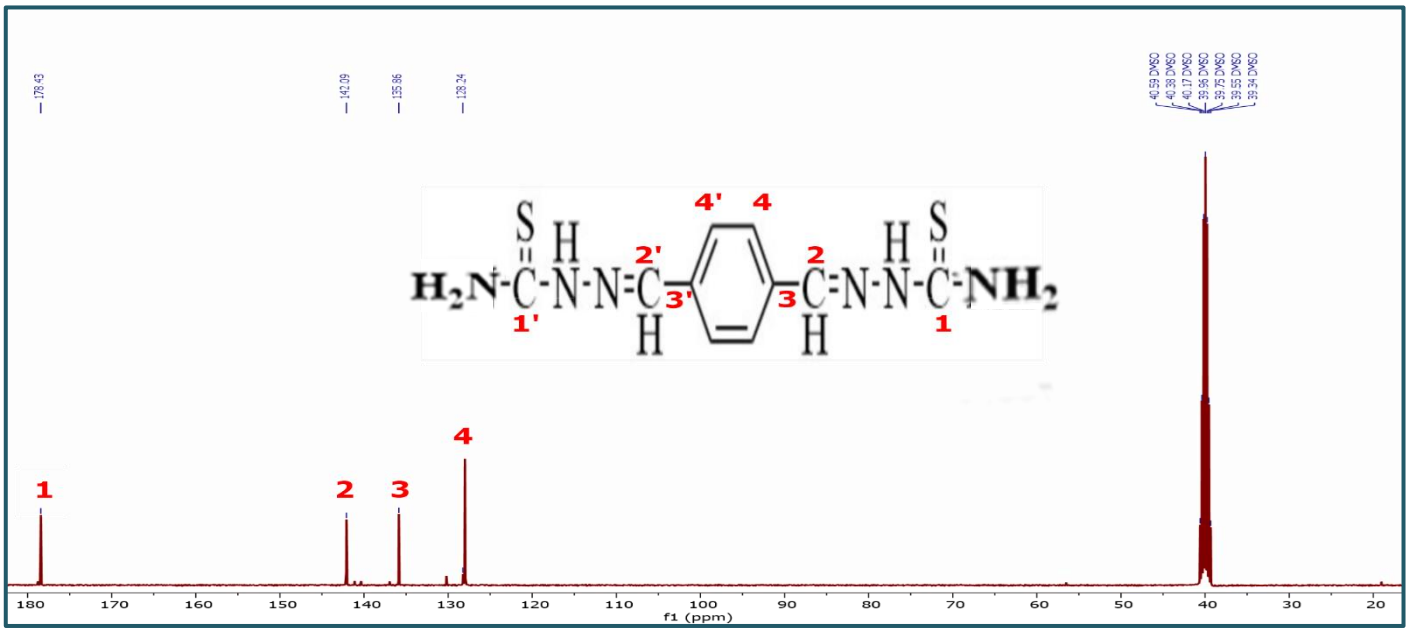


Figure (3-5): $^{13}$C-NMR for Monomer 2

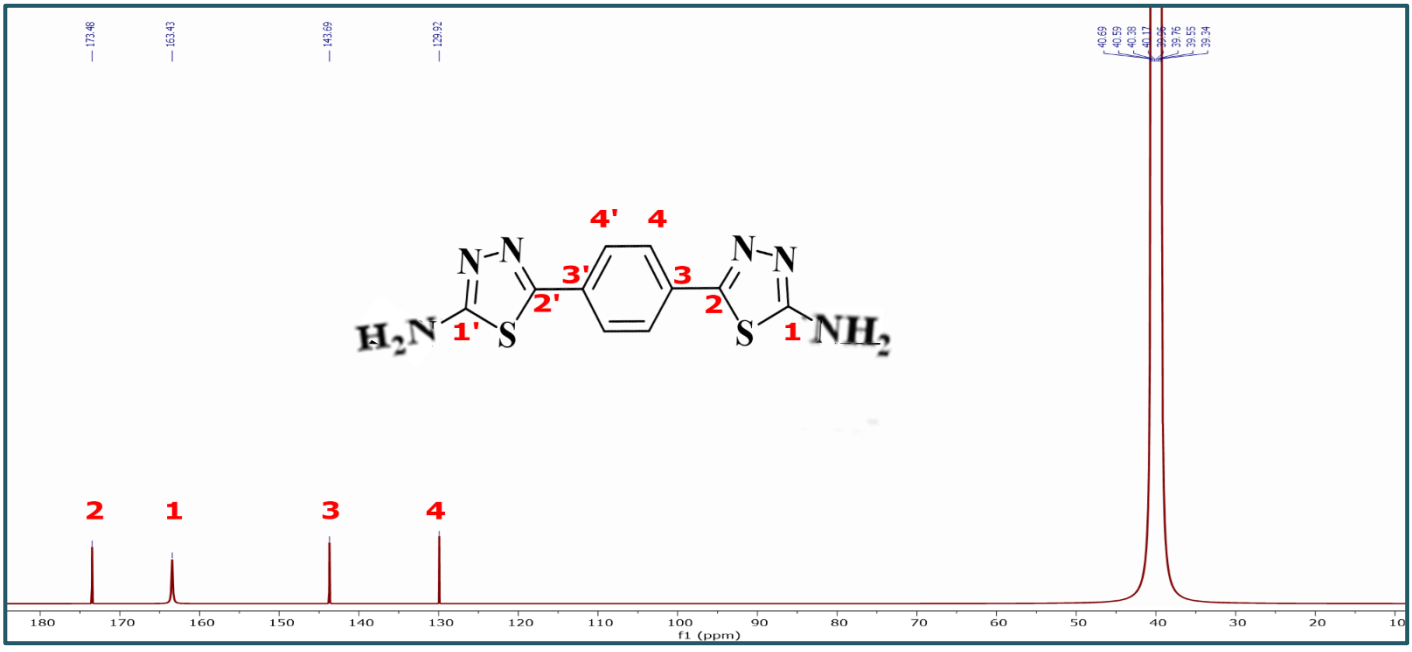


Figure (3-6): $^{13}$C-NMR for Monomer 3

## 3.2 Spectral characterization of Polyurea Polymers

### 3.2.1 Fourier Transform Infrared Spectrophotometry (FT-IR) for Polyurea Polymers of Monomer TBT (Group 1)

The FT-IR spectra of the synthesized polyurea-based polymers Group 1 exhibited well-defined absorption bands attributable to the principal functional groups within their molecular framework. The stretching vibrations of primary amine groups (–$NH_2$) were observed in the range of 3500–3300 $cm^{-1}$, typically appearing as two broad absorptions due to extensive hydrogen-bonding interactions. In contrast, the stretching vibrations of secondary amine groups (–NH–) were detected in the range of 3350–3220 $cm^{-1}$ with moderate to weak intensity. Aromatic C–H stretching modes were recorded between 3100 and 3000 $cm^{-1}$, whereas aliphatic C–H stretching vibrations appeared at 2975–2850 $cm^{-1}$, accompanied by their characteristic bending absorptions at 1465–1370 $cm^{-1}$. Most significantly, the complete consumption of both precursors during the polymerization process is indicated by the disappearance of the stretching absorption bands of isocyanate groups (2270–2280 $cm^{-1}$) and primary diamine (3392-3261 $cm^{-1}$), verifying the effective establishment of the polyurea polymer network [148]. The carbonyl (C=O) stretching vibrations of urea linkages were clearly distinguished: non-hydrogen-bonded (“free”) carbonyls appeared at 1695–1685 $cm^{-1}$, whereas strongly hydrogen-bonded carbonyls were identified in the range of 1655–1625 $cm^{-1}$. The imine (C=N) stretching vibrations were also recorded between 1660 and 1620 $cm^{-1}$, frequently overlapping with the urea carbonyl bands. Moreover, characteristic Ar–C–N stretching absorptions were detected in the region of 1360–1250 $cm^{-1}$, while the range 1280–960 $cm^{-1}$ was assigned to C–N–N and N–N stretching modes. Additionally, medium-intensity absorptions at 1180–1050 $cm^{-1}$ corresponded to C=S stretching vibrations, confirming the incorporation of thioamide functionalities. These spectral assignments are in agreement with previously reported literature [149].

**Table (3-7): The major peak bands of polyurea polymers of group 1**

| Code | -$NH_2$ | -NH- | N=C=O | Ar-C-H | Alpha-C-H | C=O | C=N | C=C | Ar-C-N | C-N-N | C=S |
|---|---|---|---|---|---|---|---|---|---|---|---|
| 2a | 3377 | 3174 | – | 2989 | 2968-2929 | 1666 | 1595 | 1531-1400 | 1361-1276 | 1224 | 1093 |
| 2b | 3392-3261 | 3155 | – | 3024 | 2924 | 1662 | 1597 | 1535-1409 | 1359-1280 | 1230 | 1089 |
| 2c | 3388-3269 | 3157 | – | – | 2989-2854 | 1683 | 1587 | 1523-1409 | 1359-1280 | 1257 | 1083 |
| 2d | 3392-3273 | 3201 | – | 3039 | 2997-2926 | 1660 | 1595 | 1514-1404 | 1359-1300 | 1220 | 1083 |

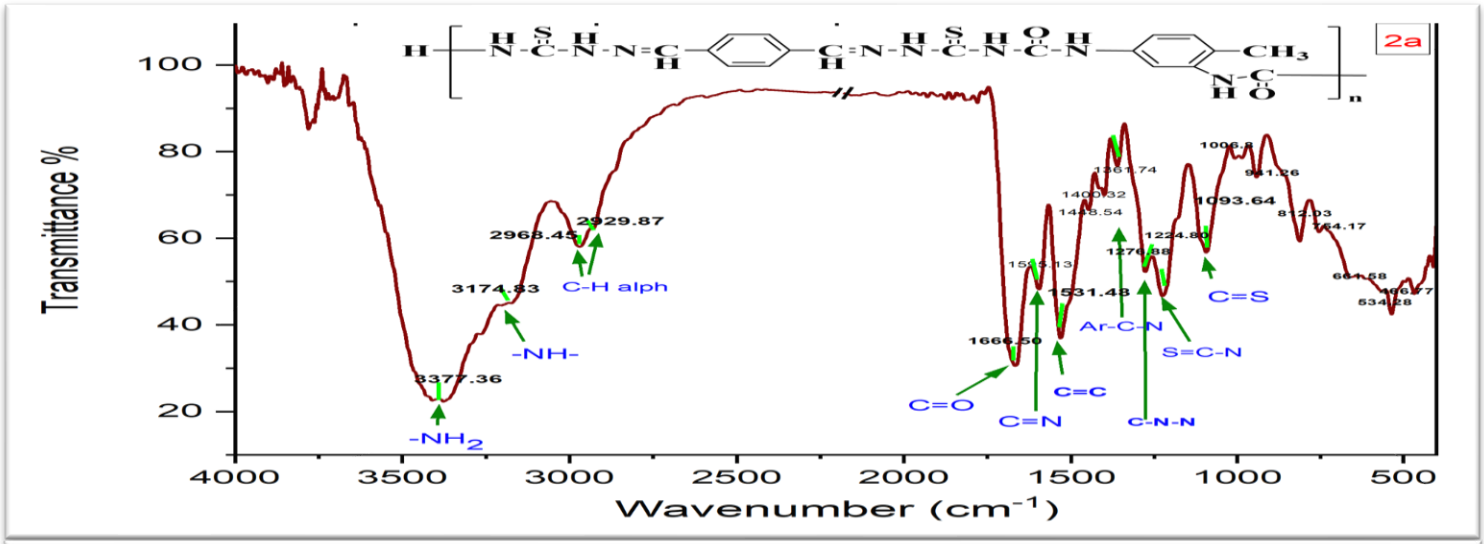
2a
Transmittance %
Wavenumber (cm⁻¹)
3377.36
-NH2
3174.53
-NH-
2968.45
2929.87
C-H alph
1666.50
C=O
1531.43
C=N
Ar-C-N
C=C
1276.88
C-N-N
1224.84
S=C-N
1093.64
C=S

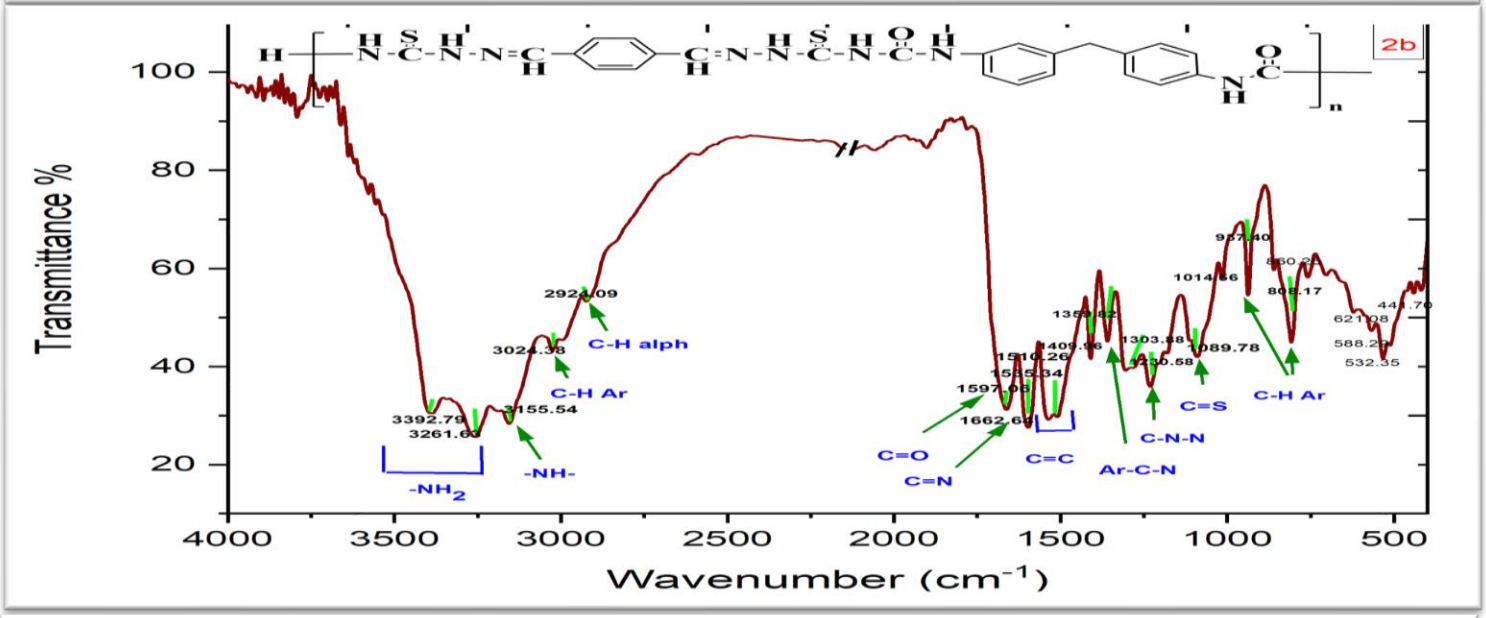
2b
Transmittance %
Wavenumber (cm⁻¹)
3392.79
3261.60
-NH2
3155.54
-NH-
3024.38
2924.09
C-H alph
C-H Ar
1662.62
C=O
C=N
C=C
Ar-C-N
C-N-N
1303.88
1089.78
C=S
C-H Ar

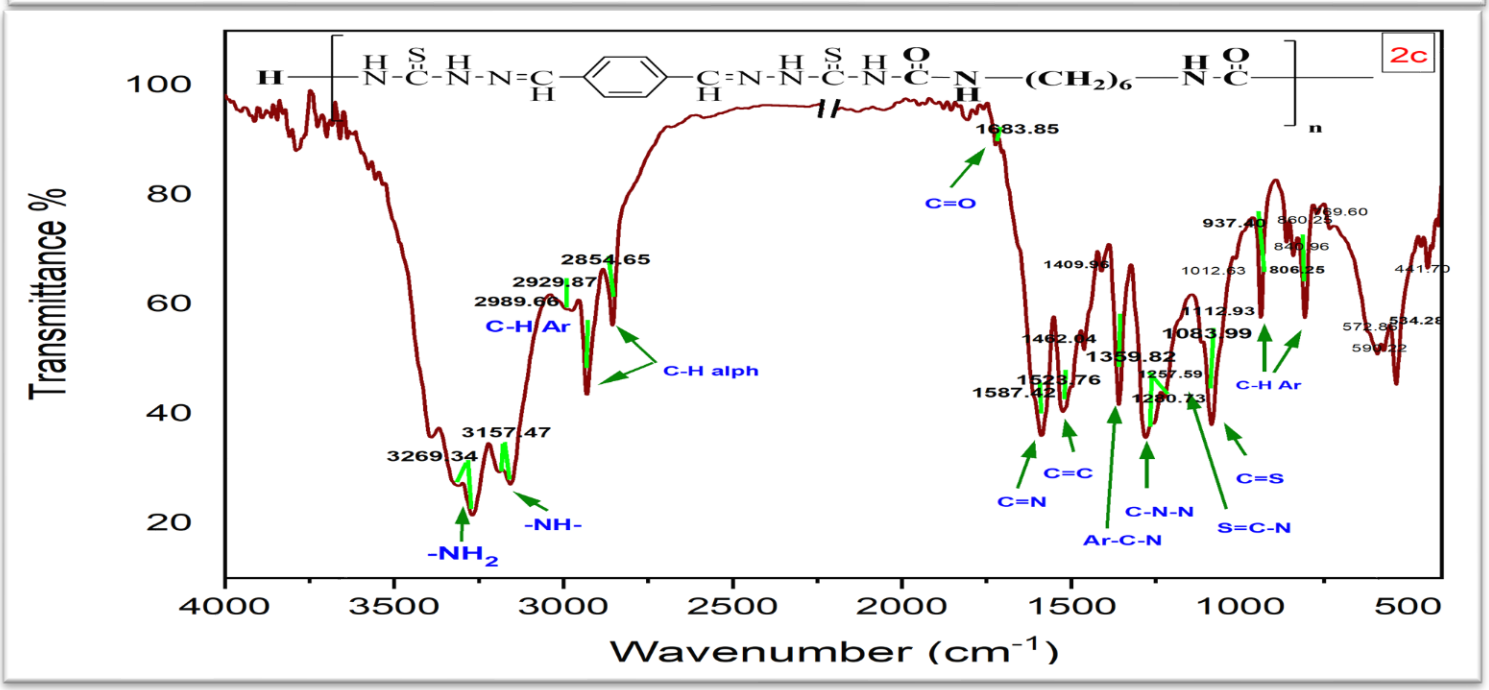
2c
Transmittance %
Wavenumber (cm⁻¹)
1683.85
C=O
3269.34
3157.47
-NH-
-NH2
2989.66
2929.87
2854.65
C-H Ar
C-H alph
1587.42
C=N
C=C
Ar-C-N
C-N-N
S=C-N
C=S
1083.99
C-H Ar

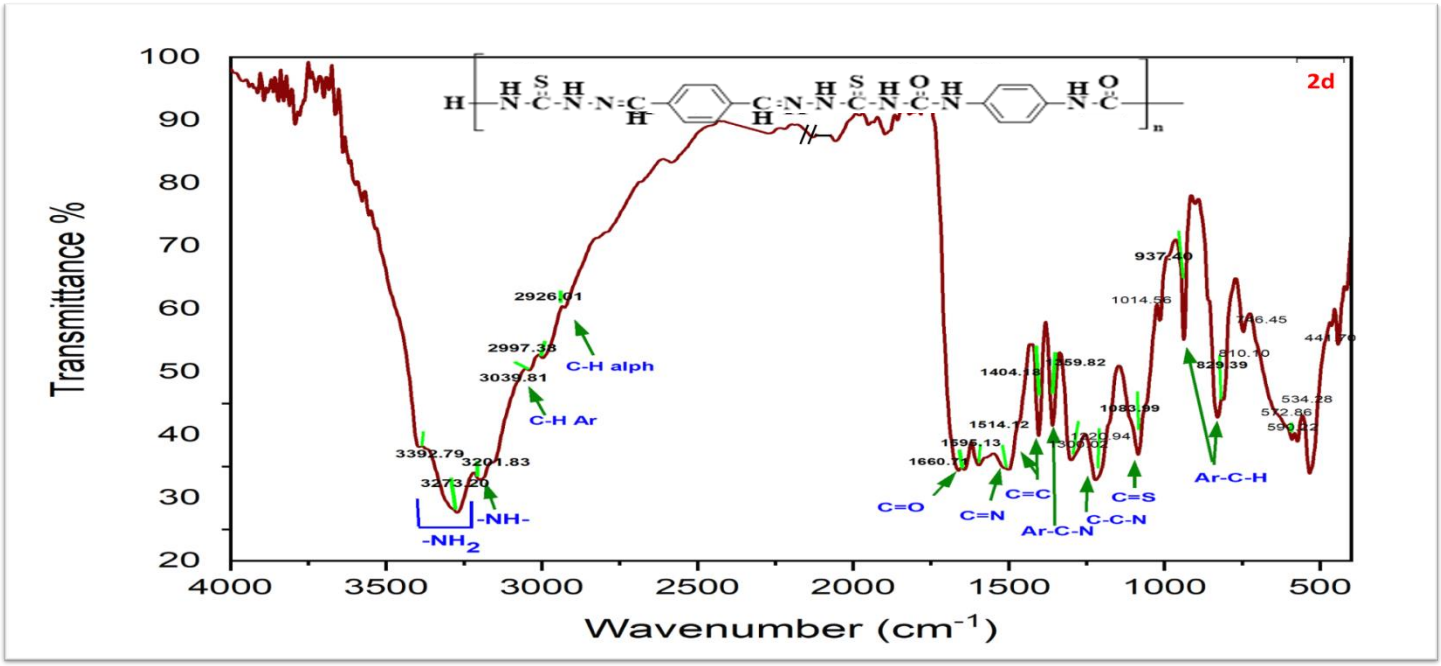


Figure (3-7): FT-IR Spectra for Polyurea Polymers Prepared from Monomer 2 (Group 1).

### 3.2.1 Fourier Transform Infrared Spectrophotometry (FT-IR) for Polyurea Polymers of Monomer TDA (Group 2)

The successful creation of urea linkages within the polymer backbone was confirmed by the distinctive absorption bands seen in the FT-IR spectra of the produced polyurea polymers (3a–3d). The stretching vibrations of N–H groups cause a big absorption band at 3300 $cm^{-1}$, increasing in size due to strong hydrogen bonding interactions between and within molecules. The stretching vibration of the C=N bond is responsible for a strong band at 1627 $cm^{-1}$. This indication means that Schiff-base couplings are present in the polymer chain. The absorption band at 1608 $cm^{-1}$ shows that urea groups and aromatic molecules have been added to the polymer structure. This conclusion is because the C=C bonds in the aromatic ring have expanded. The stretching vibrations of C–N–N at the absorption band of 1112 $cm^{-1}$ show that the thiadiazole unit is present in the polymer structure. The C–S stretching vibrations at 682 $cm^{-1}$ show that there are bonds in the polymer framework that contain sulphur [149], and the unique absorption bands of the main amines (3600–3400 $cm^{-1}$) and isocyanate groups (2270–2280 $cm^{-1}$) show that both reactants were completely used up during polymerisation, which means that the polyurea polymer network was successfully made [148].

**Table (3-8): The major peak bands of IR spectra polyurea polymers of group 2**

| Code | -$NH_2$ | -NH- | N=C=O | Ar-C-H | Alpha-C-H | C=O | C=N | C=C | Ar-C-N | C-N-N | C−S |
|---|---|---|---|---|---|---|---|---|---|---|---|
| 3a | 3439-3269 | 3155 | – | 3010-3050 | 2924-2872 | 1712 | 1618 | 1548 | 1408-1300 | 1298 | 661 |
| 3b | 3493 | 3307 | – | 3041 | 2908 | 1716 | 1604-1558 | 1433 | 1408-1301 | 1236 | 655 |
| 3c | 3331-3400 | 3165 | – | 2929 | 2854 | 1707 | 1566 | 1431-1402 | 1566 | 1381-1226 | 634 |
| 3d | 3296 | 3188 | – | 3041 | 2997 | 1701 | 1627 | 1508-1602 | 1301 | 1217 | 648 |

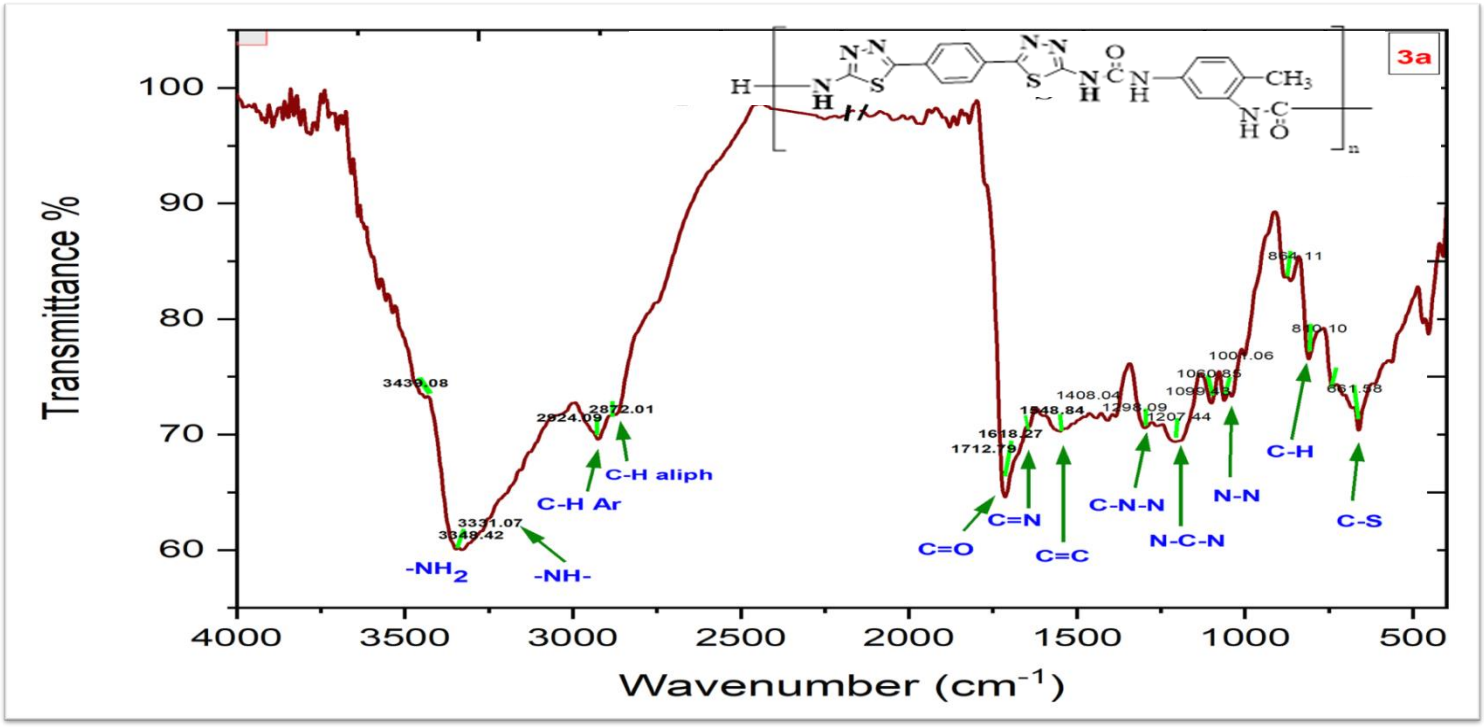

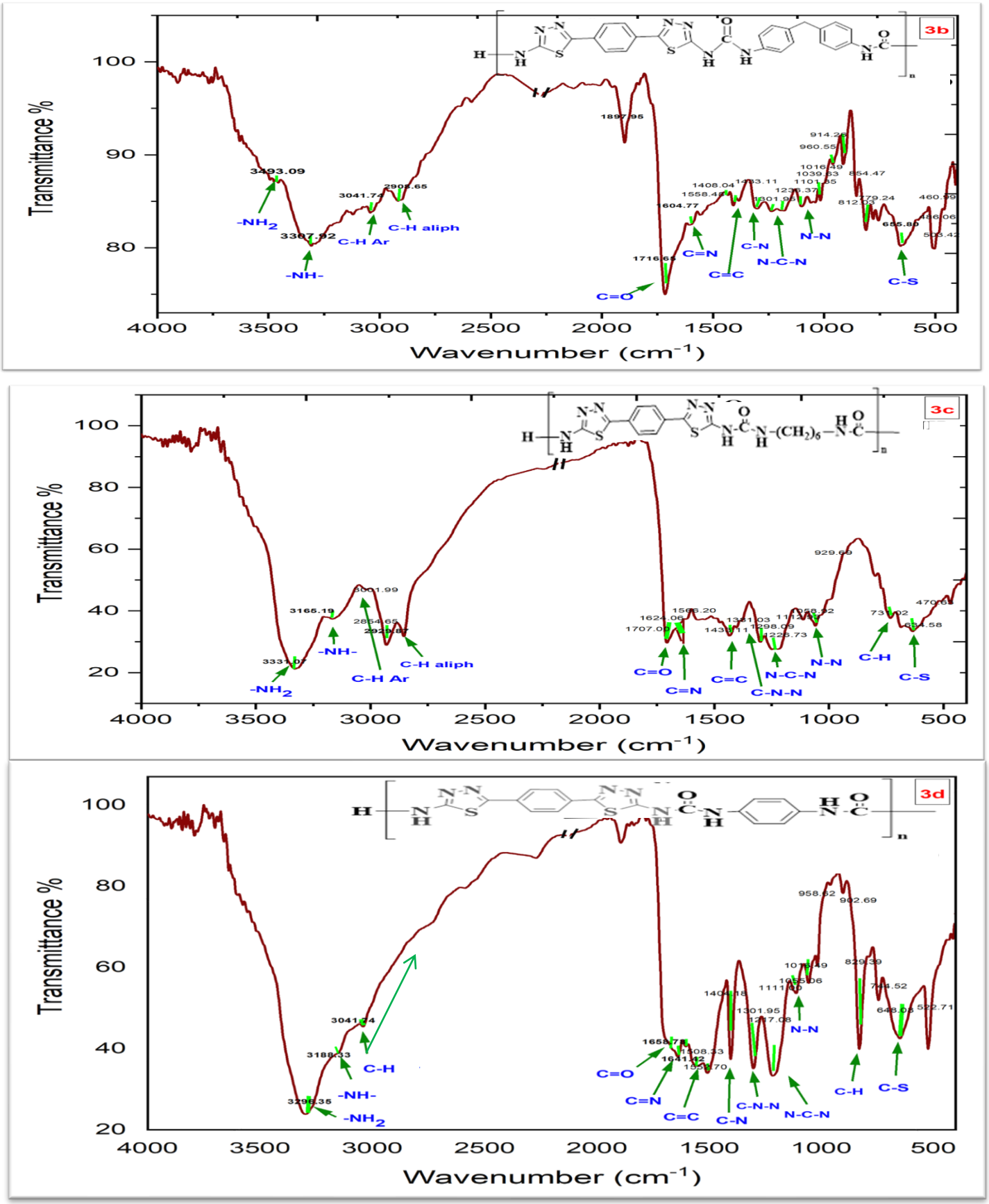


Figure (3-8): FT-IR Spectra for Polyurea Polymers Prepared from Monomer 3 (Group 2).

## 3.3 Characterization of Nanoparticles (AgNPs and CuNPs)

The synthesis of nanoparticles was characterized by X-ray diffraction (XRD) and Fourier transform infrared (FT-IR) spectroscopy.

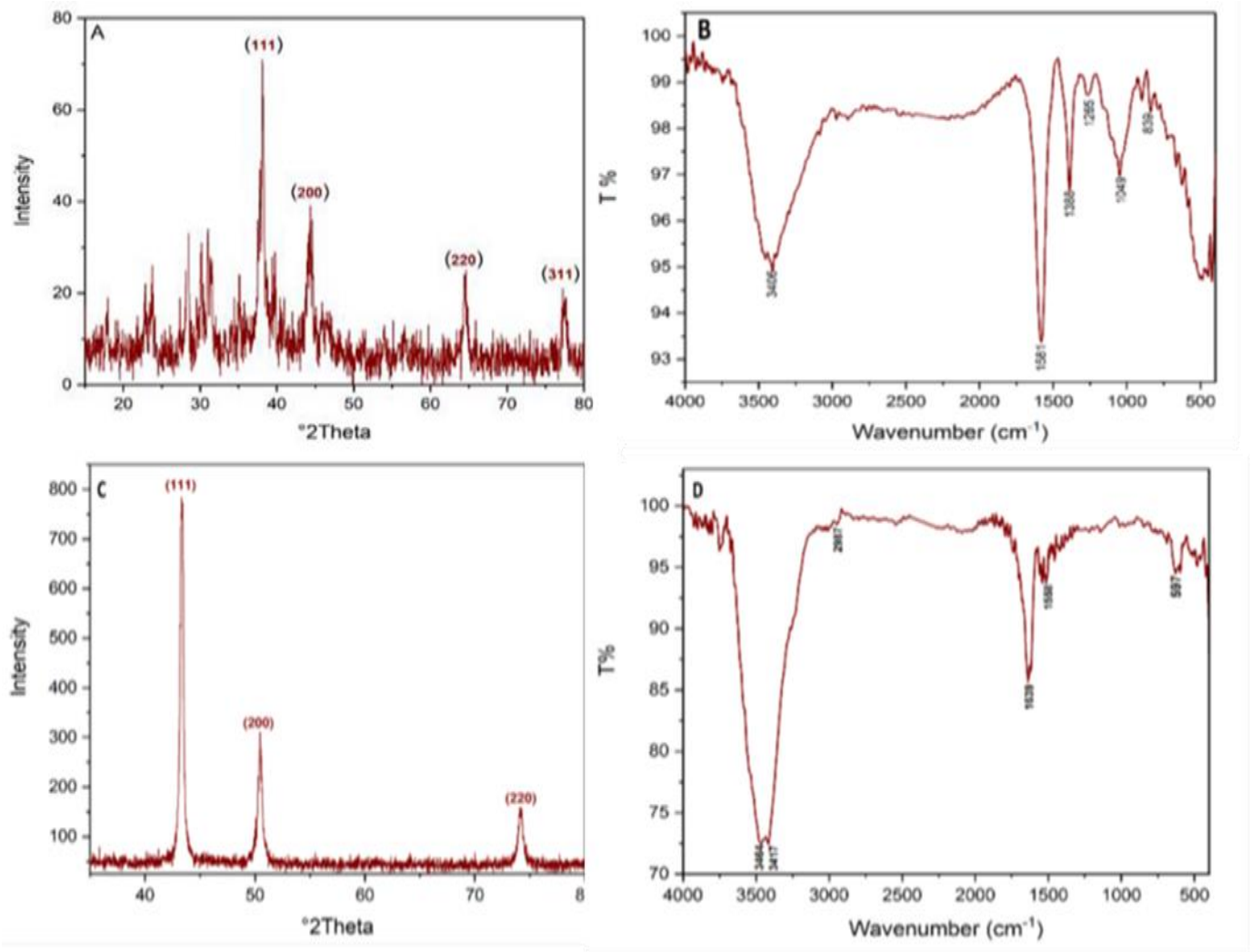


Figure (3-9): Characterization of biosynthesized nanoparticles: (A) XRD pattern of AgNPs; (B) FT-IR spectrum of AgNPs; (C) XRD pattern of CuNPs; (D) FT-IR spectrum of CuNPs.

Figure (3-9) shows the X-ray diffraction (XRD) patterns of silver and copper nanoparticles. The X-ray diffraction (XRD) pattern of silver nanoparticles (AgNPs) displayed four distinct diffraction peaks with 2θ values of 38°, 44°, 64°, and 77°, as referenced by JCPDS card No. 04-0783. These peaks correspond to the (111), (200), (220), and (311) crystal planes of face-center cubic (FCC) silver. The lack of additional impurity peaks indicates that the synthesized AgNPs possess a high degree of crystallinity and phase purity. Furthermore, the pronounced intensity of the (111) diffraction peak also demonstrates a preferred crystallographic orientation, which is a typical feature of silver nanoparticles synthesized using plant extracts

[150]. The XRD pattern of copper nanoparticles (CuNPs) showed three different diffraction peaks with 2θ values of 43.4°, 50.4°, and 74.1°. These peaks correspond to the (111), (200), and (220) crystal planes of metallic copper, according to JCPDS card No. 04-0836. The produced nanoparticles consist solely of pure metallic copper ($Cu^0$) and are protected from oxidation by the surrounding organic capping agents [151]. Using the Debye-Scherrer equation, the average crystallite sizes of silver and copper nanoparticles were calculated [68].

$$\mathbf{D = \frac{K\lambda}{\beta \cos\theta} \ldots\ldots\ldots\ldots (1-5)}$$

Where (D) represents the crystallite size, (K) is the shape factor (0.9), (λ) is the X-ray wavelength (0.15406 nm for Cu Kα radiation), (β) is the full width at half maximum (FWHM) of the diffraction peak in radians, and (θ) is the Bragg diffraction angle. The calculated crystallite size is summarized in Table (3-9).

**Table (3-9): Particle size by Debye- Scherrer equation**

| Element | 2Theta (2θ) | FWHM(β) | Theta (θ) (radians) | β (radians) | D(nm) | $D_{average}$ (nm) |
|---|---|---|---|---|---|---|
| Ag | 38.1431 | 0.2362 | 0.3330 | 0.004122 | 37.2 | 34.43 |
| | 44.6225 | 0.1574 | 0.3893 | 0.002746 | 57.1 | |
| | 64.4912 | 0.3936 | 0.5627 | 0.00687 | 24.9 | |
| | 77.4349 | 0.5760 | 0.6760 | 0.01005 | 18.5 | |
| Cu | 43.2721 | 0.1440 | 0.378 | 0.00251 | 61.99 | 61.3 |
| | 50.4687 | 0.1181 | 0.4404 | 0.00206 | 77.67 | |
| | 74.1266 | 0.2362 | 0.6471 | 0.004122 | 44.1 | |

Figure (3-9) displays the Fourier transform infrared (FT-IR) spectra of the produced copper and silver nanoparticles. Using sodium citrate and green tea extract to reduce silver nitrate, the FT-IR spectrum of AgNPs revealed multiple unique absorption bands that represented the functional groups involved in the synthesis process. O–H stretching vibrations produced a broad absorption band with a core at 3406 $cm^{-1}$, suggesting that the plant extract included hydroxyl groups derived from polyphenolic chemicals. Aromatic C=C stretching vibrations were identified as the source of the absorption band at 1581 $cm^{-1}$, with additional contributions from asymmetric stretching of carboxyl groups ($COO^-$). The symmetric stretching vibrations of the carboxyl groups produced by the citrate ions were represented by another unique peak at 1388 $cm^{-1}$. A symmetrical interaction between the citrate molecules and the nanoparticle surface is indicated by the predicted spacing between the symmetric and asymmetric $COO^-$ stretching bands (Δv = 193 $cm^{-1}$). Additionally, the stretching vibrations of the C–O bond in alcohols and ethers were attributed to the absorption bands at 1265 and 1049 $cm^{-1}$, whilst the out-of-plane bending vibrations of the C–H bond in aromatic rings were linked to the band at 839 $cm^{-1}$. All of these findings support the idea that the phenolic and citrate chemicals in the green tea extract work in concert to reduce and stabilize silver nanoparticles.

Similar to this, the FT-IR spectra of CuNPs, which were made from copper sulfate using hydrazine hydrate and sodium hydroxide in the presence of polyvinyl alcohol (PVA) as a

stabilizer, displayed multiple unique absorption bands that represented the functional groups used in the synthesis. The O–H stretching vibrations of hydroxyl groups from PVA and adsorbed water molecules on the nanoparticle surface are responsible for the broad bands at 3464 and 3417 $cm^{-1}$. The C–H stretching of aliphatic groups inside the PVA backbone was identified as the cause of the band at 2987 $cm^{-1}$. N–H bond stretching vibrations from hydrazine residues may have contributed somewhat to the two bands centered at 1639 and 1622 $cm^{-1}$, which were mainly attributed to the bending vibrations of adsorbed water (H–O–H). The N–H or C=C vibrations linked to the peaks at 1558 and 1541 $cm^{-1}$ suggest either a shift in the hydrogen bonding environment inside PVA or partial interactions between hydrazine and the polymer matrix. Out-of-plane bending vibrations of the polymer's C–H were discovered to be responsible for a faint band at 688 $cm^{-1}$, which corresponded to the copper oxides (CuO or $Cu_2O$). This finding is consistent with earlier research that found the vibrational range of copper oxides to be between 400 and 620 $cm^{-1}$. Overall, the stability of the resultant nanoparticles and the effectiveness of the copper reduction process are confirmed by the FT-IR spectra. The development of stable nanostructures shielded by organic capping layers is confirmed by the observed vibrational bands, which show efficient interaction between the nanoparticles and the organic functional groups created by the reducing and stabilizing agents [152].

## 3.4 Thermal stability (TGA) of pure polyurea polymers for Group 1 and Group 2

Thermogravimetric analysis (TGA) in a nitrogen environment was used to assess the thermal stability of the produced polyurea polymers (Figure 3-8).

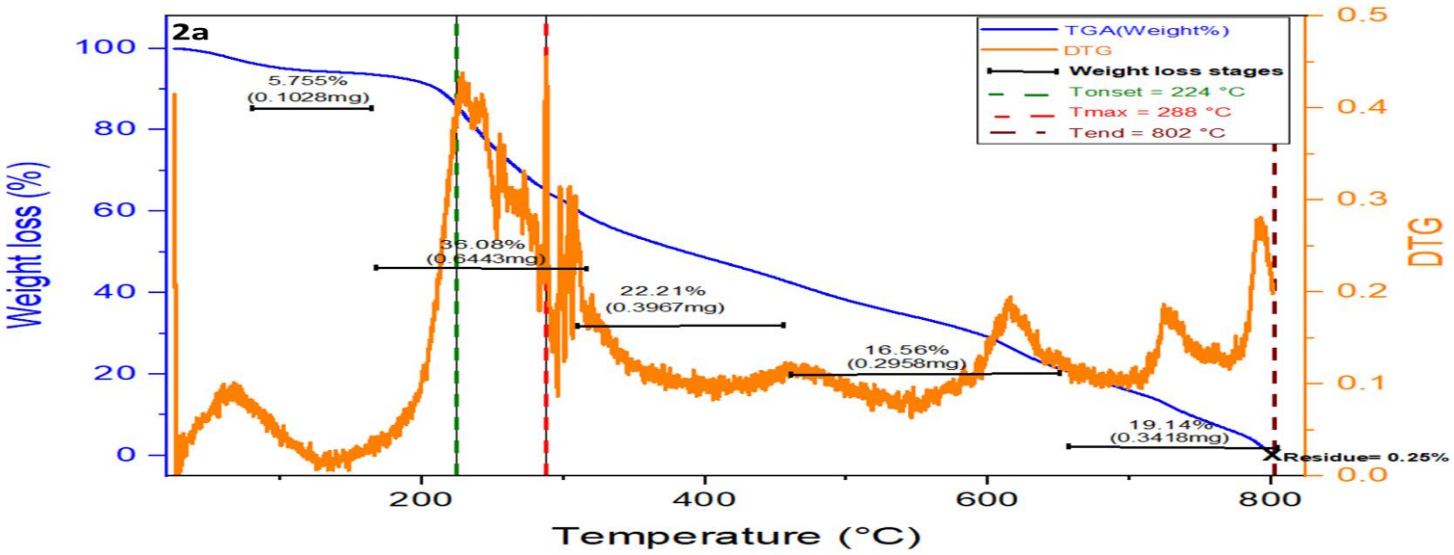

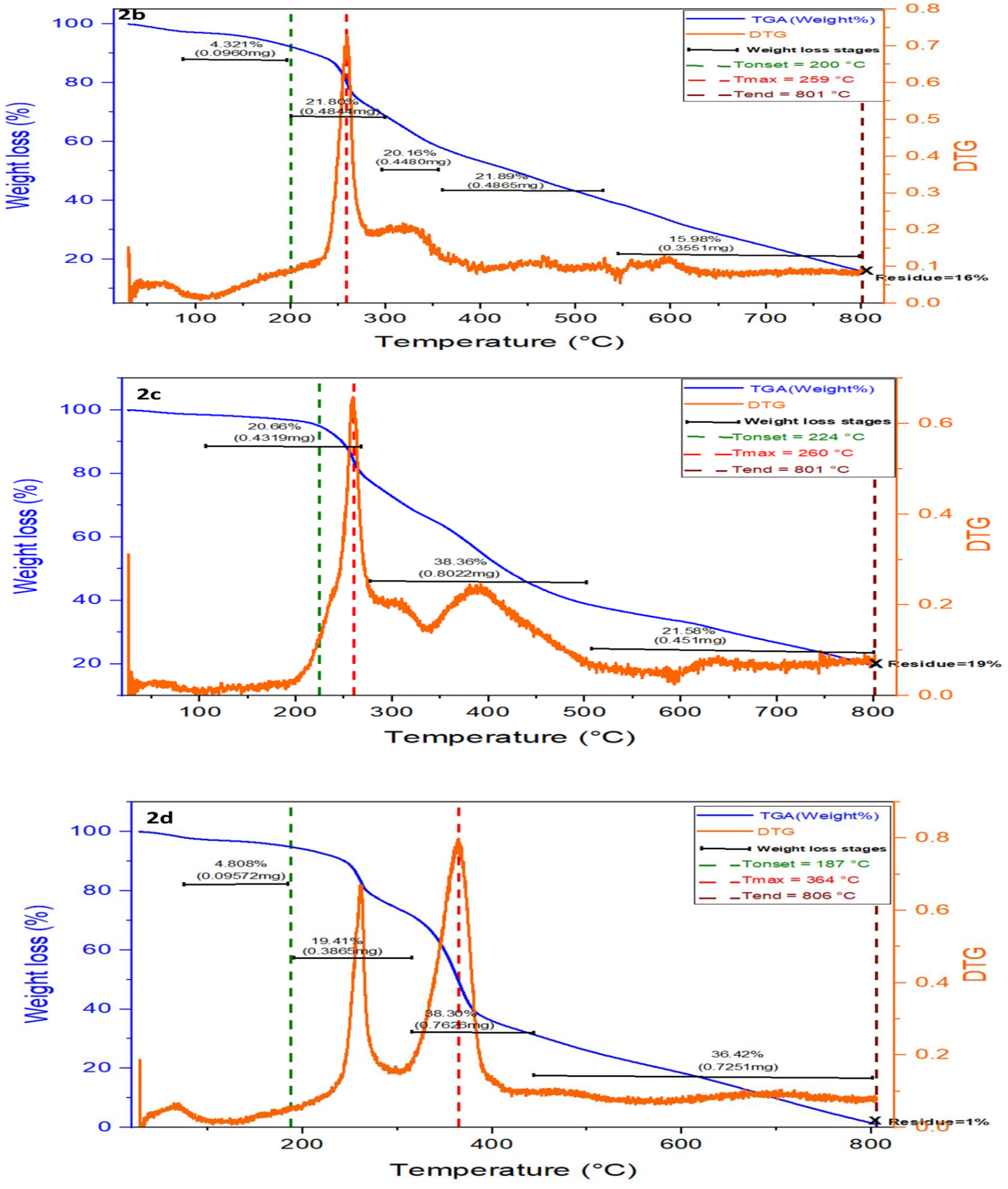


Figure (3-10): TGA thermogravimetric of pure polyurea polymers (Group 1).

Table (3-10) provides a summary of the thermogravimetric analysis (TGA) and derivative thermogravimetric analysis (DTG) used to assess the thermal behavior of the pure polyurea sample shown in Figure (3-10). The findings showed that the onset varied from 187 to 224°C, and the maximum decomposition temperatures ($T_{max}$), which corresponded to the primary stages of polymer chain breakdown, occurred between 259 and 364°C. The DTG curves were utilized to determine the $T_{max}$ values and to further elucidate the principal thermal degradation stages. These results indicate that the studied polyurea polymers have moderate to good thermal stability within this temperature range. The total weight loss ranged from 80.6% to 99.75%, signifying nearly complete decomposition of the polymer structure at elevated temperatures. The remaining residues (0.25–19%) are attributed to relatively stable carbonaceous species persisting after the breakdown of the polymer matrix. Overall, these finding demonstrate a typical thermal degradation pattern for pristine polyurea polymers, confirming the purity of the polymeric matrix and the absence of inorganic phases affecting the degradation process.

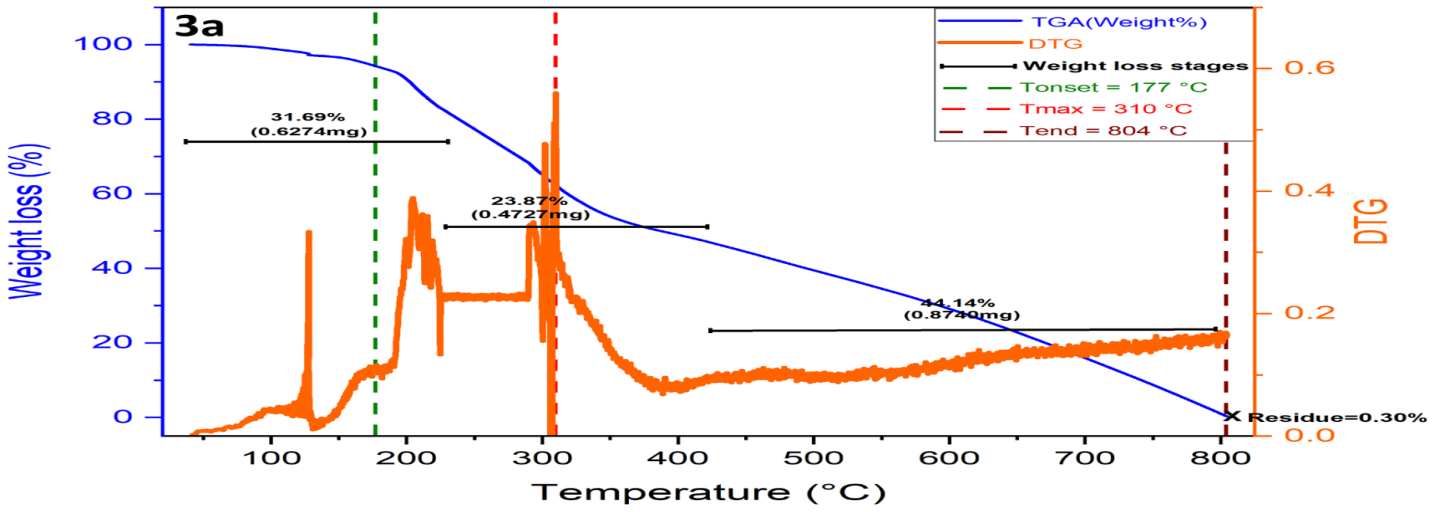


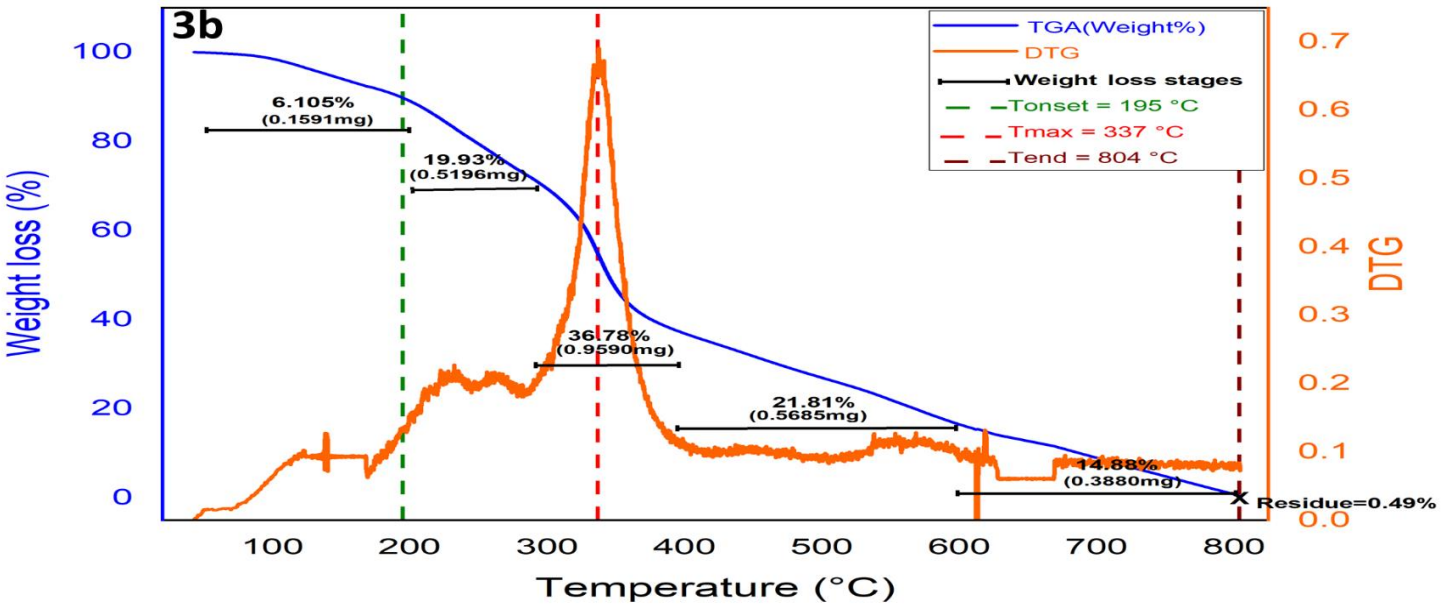

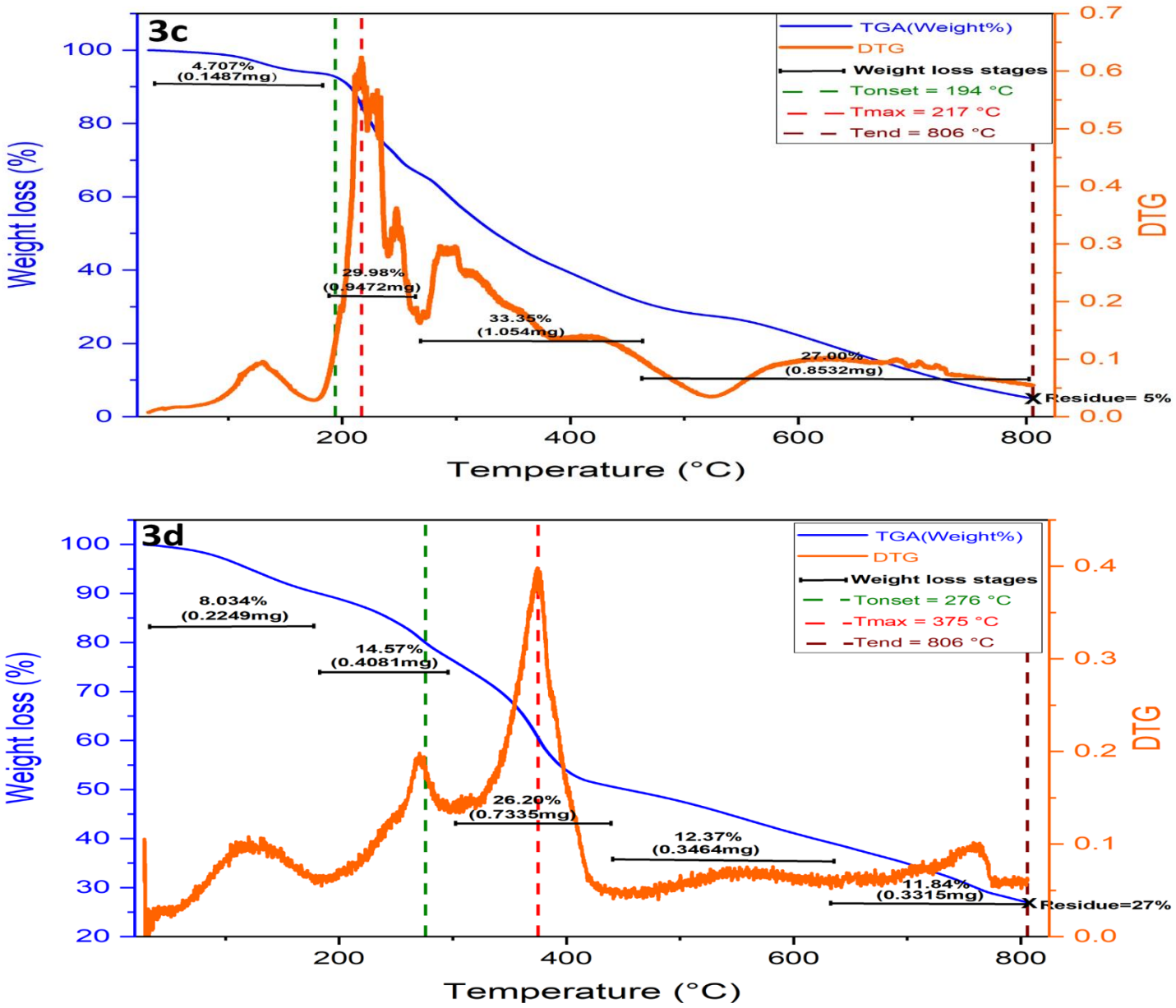


Figure (3-11): TGA thermogravimetric of pure polyurea polymers (Group 2).

Thermogravimetric analysis (TGA) and derivative thermogravimetric analysis (DTG) were used to analyze the thermal behavior of the pure polyurea samples in group 2, as shown in Figure (3-11) and Table (3-10). The results showed that the initial decomposition temperatures ($T_{onset}$) ranged between 177 and 276 °C, whereas the maximum decomposition temperatures ($T_{max}$) occurred within the range of 217–375 °C, corresponding to the principal degradation stages of the polymer chains. The DTG curves were employed to determine the $T_{max}$ values more accurately and to clarify the main stages of thermal degradation. These findings indicate that the synthesized polyurea polymers exhibit moderate to high thermal stability across this temperature range. The total weight loss was found to range between 73% and 95%, reflecting

the nearly complete decomposition of the polymeric structure at elevated temperatures. The remaining residues (0.3–27%) are attributed to thermally stable carbonaceous materials or minor inorganic traces that persist after the breakdown of the polymer matrix.

In general, the synthesized polyurea polymers incorporate aromatic rings, conjugated systems, and Schiff base moieties. As a result, upon thermal treatment, these polymers tend to form a char residue rather than undergoing complete volatilization. Accordingly, samples 2c and 3d demonstrate a pronounced ability to generate char, reflecting enhanced thermal stability and a highly aromatic, complex structure. In contrast, samples 2a and 3a undergo nearly complete decomposition, indicating comparatively lower structural stability. Among all samples, 3d exhibits the highest thermal stability, which can be attributed to its molecular architecture characterized by a higher degree of aromaticity and conjugation, improved resistance to thermal degradation, and the formation of a protective char layer.

**Table (3-10): Thermal decomposition parameters obtained from TGA and DTG curves of polyurea polymer.**

| Polymer code | $T_{onset}$ (°C) | $T_{max}$ (°C) | $T_{end}$ (°C) | Total weight change (%) | Residue (%) |
|---|---|---|---|---|---|
| Group 1 | | | | | |
| 2a | 224 | 288 | 802 | 99.75 | 0.25 |
| 2b | 200 | 259 | 801 | 84.16 | 16.00 |
| 2c | 244 | 260 | 801 | 80.60 | 19.00 |
| 2d | 187 | 364 | 806 | 98.30 | 1.00 |
| Group 2 | | | | | |
| 3a | 177 | 310 | 804 | 99.70 | 0.30 |
| 3b | 195 | 337 | 804 | 99.51 | 0.49 |
| 3c | 194 | 217 | 806 | 95.03 | 5.00 |
| 3d | 276 | 375 | 806 | 73.02 | 27.00 |

## 3.5 Morphological and Compositional Analysis

The morphology and elemental composition of the polyurea/silver and copper nanocomposites were examined using FESEM, EDX, TEM, Zeta analysis.

### 3.5.1 Morphological analysis based on FESEM and EDX micrographs

As seen in Figure (3-12), the metal-containing polyurea nanocomposites' surface shape and elemental composition were examined using FESEM and EDX. The FESEM images revealed distinct morphological variations depending on the type of metal added (Ag or Cu) as well as on the nature of the polymer backbone (samples 2b and 2d). For the silver-based nanocomposites (Ag-2b and Ag-2d), the FESEM micrographs showed a uniform distribution of AgNPs throughout the polyurea matrix, confirming their in-situ formation during synthesis. Sample Ag-2b exhibited nearly spherical particles with diameters ranging from 62–26 nm, whereas Ag-2d exhibited smaller, more compact nanoparticles within the range of 43–25 nm.

This variation illustrates how the polymer chain structure affects the nanoparticles' nucleation and growth characteristics. Strong interfacial contact between the metal and the polymer is facilitated by the uniform and evenly distributed AgNPs, which form effective electron transport in excellent. In contrast, the copper-based nanocomposites (Cu-2b and Cu-2d) displayed markedly different surface morphologies. The Cu-2b sample was observed to contain clustered spherical particles with diameters ranging from 45–28 nm, while the Cu-2d exhibited a bimodal particle morphology composed of both spherical and rod-like structures, with sizes ranging from 84–22 nm. This indicates a non-uniform crystallization process of the CuNPs due to the influence of the polyurea environment during the reduction process. It is worth noting that the rod-like copper structure in Cu-2d sample contributes to the creation of interconnected metal pathways that improve charge transport efficiency within the matrix.

The EDX spectra confirmed the presence of the target metal elements (Ag or Cu) along with C, N, and S signals associated with the organic structure of the polyurea and the thiosemicarbazide moieties. Quantitative EDX analysis Table (3-11) confirmed the high metal loading in all nanocomposites, with silver-based systems showing greater incorporation efficiency than their copper-based counterparts. This confirms that metallic nanoparticles are effectively embedded without any observable contaminants. The polyurea backbone's structural stability and coordination with the embedded metallic domains are further supported by the presence of carbon, nitrogen, and sulfur.

Overall, the FESEM and EDX analyses confirm the successful preparation of polyurea-metal nanocomposites with a homogeneous particle distribution and strong interactions between the organic and metal components. The tightly packed and fine-grained structure of the nanoparticles especially in Ag-2d and Cu-2d contributes to the formation of an electron conductive nanocomposite network, thereby contributing directly to the observed enhancement in electrical conductivity.

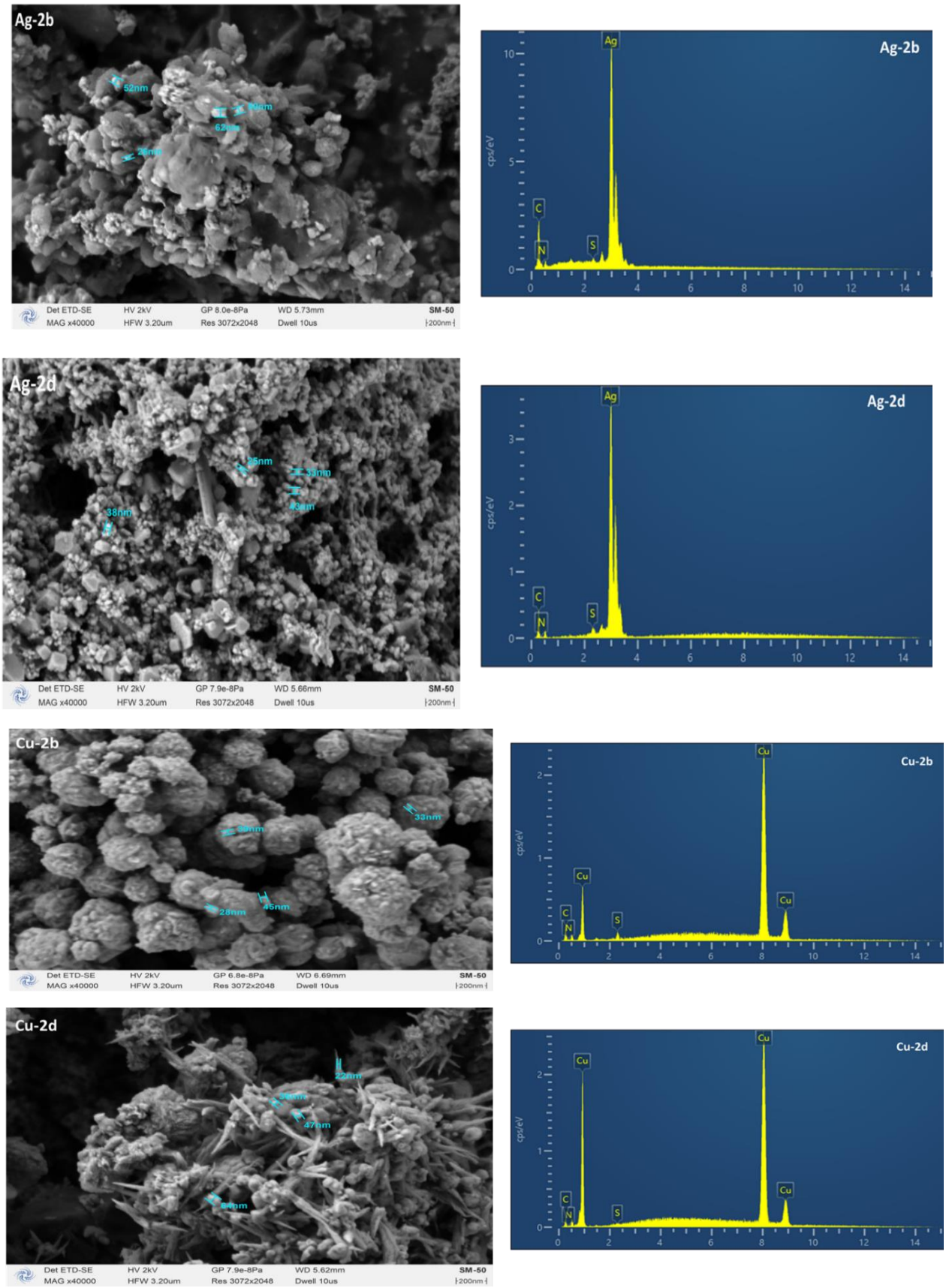


Figure (3-12): FESEM micrograph and corresponding EDX analysis of polyurea/silver and copper nanocomposite (Group 1).

Field emission scanning electron microscopy (FESEM) and energy-dispersive X-ray spectroscopy (EDX) were used to analyze the surface morphology and elemental composition of the metal-containing polyurea nanocomposites, as shown in Figure (3-13). The micrographs showed that the polymeric backbone structure of samples (3b and 3d) and the type of metal (Ag or Cu) included caused significant differences in surface morphology. The FESEM images of the silver-based nanocomposites (Ag-3b and Ag-3d) demonstrated a uniform dispersion of silver nanoparticles within the polyurea matrix, verifying their in-situ production. Nearly spherical AgNPs with sizes between 48-34 nm were visible in sample Ag-3b, indicating a small particle clustering along the polymer chains. Ag-3d, on the other hand, showed more homogeneous and compact nanoparticles with diameters ranging from 58-38 nm. This difference suggests that the nucleation and growth behavior of AgNPs are largely controlled by the polymer chain structure. Ag-3d compact packing and even dispersion of nanoparticles improves the metal-polymer matrix interfacial adhesion, which facilitates electron transport and significantly raises electrical conductivity.

In the case of copper-based nanocomposites (Cu-3b and Cu-3d), the FESEM images revealed rougher and more aggregated surface structures. The Cu-3b sample exhibited clusters of quasi-spherical nanoparticles with diameters ranging from 177-37 nm, indicating partial particle coalescence. On the other hand, Cu-3d showed a mixture of small spherical and irregularly shaped particles with diameters between 85-30 nm, suggesting a heterogeneous crystallization process influenced by the polyurea environment during $Cu^{2+}$ reduction. In contrast to the pure polymer, Cu-3d interconnected copper domains help to create conductive pathways throughout the matrix, which improves electrical conductivity and charge transfer.

The EDX spectra confirmed the successful incorporation of the target metallic elements (Ag or Cu) in all nanocomposites, accompanied by the characteristic signals of C, N, and S, which are attributed to the organic framework of the polyurea and the thiosemicarbazide moieties. The spectra's strong, sharp metal peaks show that the metal nanoparticles were well embedded in the polymer matrix without any discernible contaminants.

Overall, the FESEM and EDX analyses confirm the successful preparation of polyurea–Ag and polyurea–Cu nanocomposites with uniformly distributed nanoparticles and strong interactions between the organic and metallic components. The increased electrical conductivity of these composites in comparison to pure polymers can be explained by the compact and fine-grained morphology shown, especially in Ag-3b and Cu-3d, which help establish an interconnected electron-conductive network inside the polymer matrix.

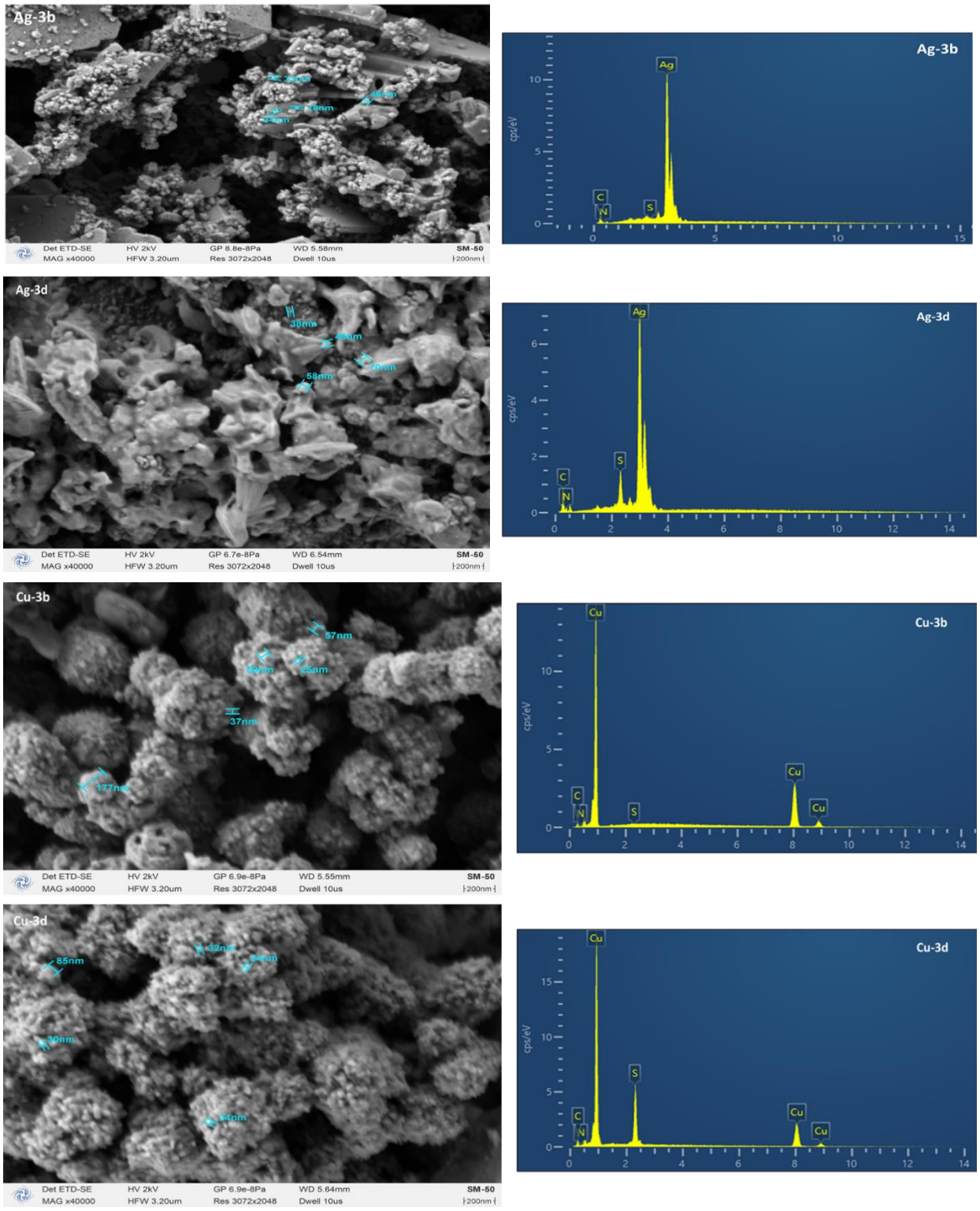


Figure (3-13): FESEM micrograph and corresponding EDX analysis of polyurea/silver and copper nanocomposite (Group 2).

**Table (3-11): Comparative EDX elemental composition of polyurea/metal nanocomposite**

| Sample | Metal | Particle size (nm) | Metal (wt%) | C (wt%) | N (wt%) | S (wt%) |
|---|---|---|---|---|---|---|
| TBT Polymers | | | | | | |
| Ag-2a | Ag | 62-26 | 75.2 | 18.7 | 5.78 | 0.36 |
| Ag-2b | Ag | 43-25 | 83.7 | 13.5 | 2.19 | 0.62 |
| Cu-2b | Cu | 45-28 | 34.8 | 53.8 | 8.89 | 2.49 |
| Cu-2d | Cu | 84-22 | 65.4 | 30.4 | 3.83 | 0.36 |
| TDA Polymers | | | | | | |
| Ag-3b | Ag | 48-34 | 91.48 | 7.41 | 1.05 | 0.07 |
| Ag-3d | Ag | 58-38 | 73.09 | 15.79 | 7.52 | 3.60 |
| Cu-3b | Cu | 177-37 | 85.78 | 14.05 | 0.16 | 0.00 |
| Cu-3d | Cu | 85-30 | 65.85 | 20.98 | 1.64 | 11.53 |

## 3.5.2 Morphological analysis based on TEM micrographs

TEM image analyses of TBT-based polyurea composites containing silver and copper nanoparticles (samples Ag-2b, Ag-2d, Cu-2b, and Cu-2d) provide a comprehensive explanation of the influence of metal type and polymer chain arrangement on nanoparticle formation and distribution within the matrix.

In the silver-containing systems, the images showed the successful formation of quasi-spherical silver particles homogeneously distributed within the polyurea matrix, confirming the effectiveness of the in-situ formation process. In the Ag-2b sample, moderate agglomeration was evident with a wider size range 10-50 nm, while the Ag-2d sample exhibited smaller 5-25 nm, more uniformly distributed particles. The distribution plots also revealed a narrow Gaussian distribution in Ag-2d, indicating better control over nucleation processes and particle stability. In the copper-containing samples (Cu-2b and Cu-2d), the particles also appeared quasi-spherical, but with a different agglomerative character due to the copper reduction dynamics. Cu-2b exhibited moderate agglomeration 10-100 nm and a broader Gaussian distribution, while Cu-2d observed highly homogeneous 5-100 nm and fine particles with a more controlled size distribution.

These findings show that the size and distribution pattern of the nanoparticles within the matrix are significantly influenced by both the type of metal and the polymer structure. Greater nucleation and entrainment efficiency inside the polymer network were shown by the smaller sizes and more homogeneous nanostructures of the Ag-2d and Cu-2d samples. It is anticipated that these uniform and fine structures will enhance charge transfer and improve the electrical and thermal properties of the composites by improving the interfacial contact between the metal domains and the polymer chains.

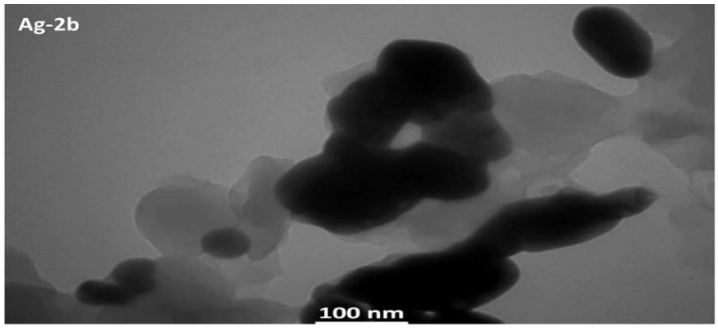
Ag-2b
100 nm

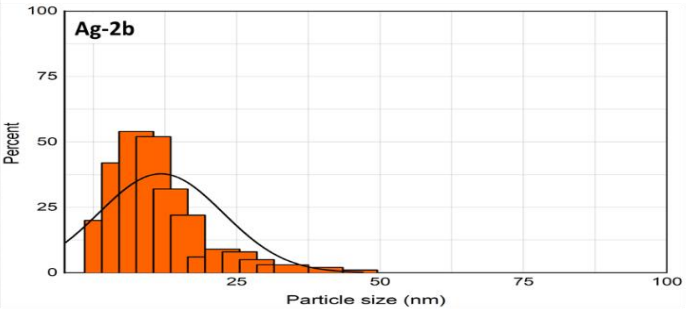
Ag-2b
Percent
Particle size (nm)
0
25
50
75
100

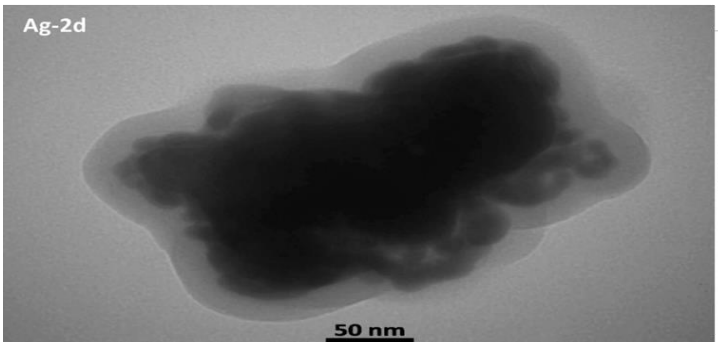
Ag-2d
50 nm

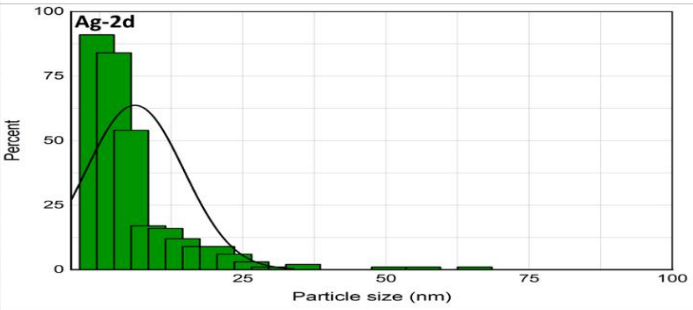
Ag-2d
Percent
Particle size (nm)
0
25
50
75
100

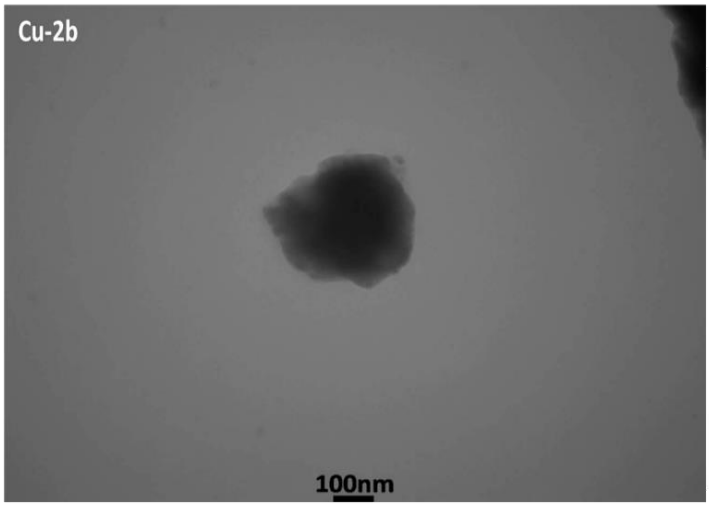
Cu-2b
100nm

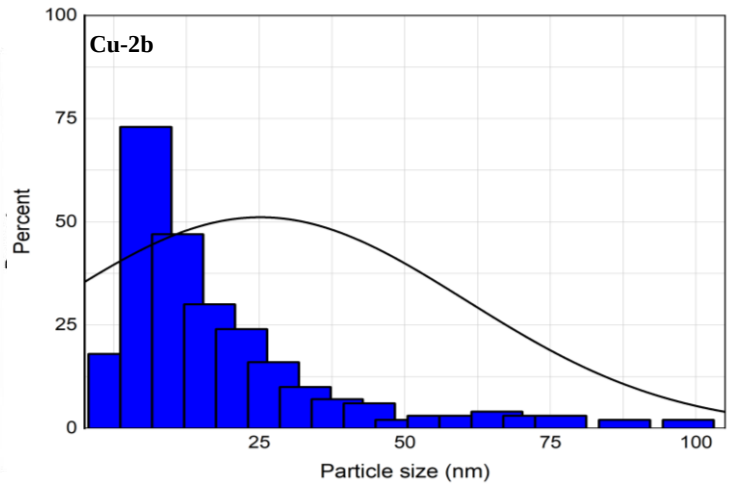
Cu-2b
Percent
Particle size (nm)
0
25
50
75
100

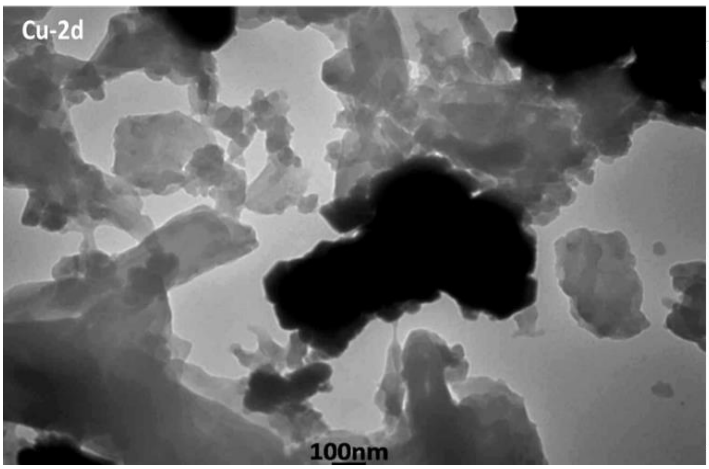
Cu-2d
100nm

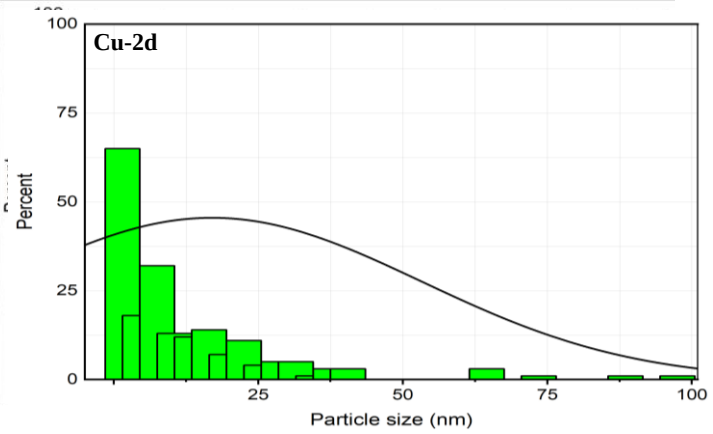
Cu-2d
Percent
Particle size (nm)
0
25
50
75
100

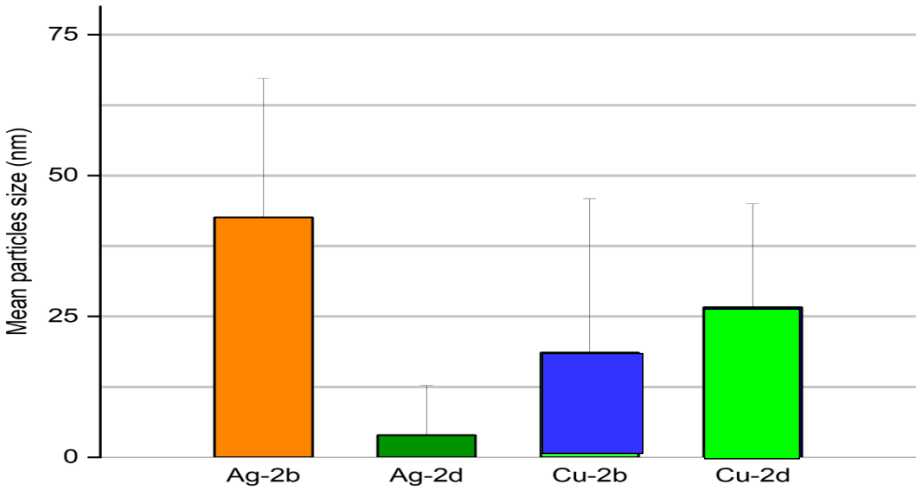


Figure (3-14): TEM images of polyurea/silver and copper nanocomposite showing particle size analysis (Group 1).

Comparative analysis of TEM images and particle size distribution plots for the four systems (Ag-3b, Ag-3d, Cu-3b, and Cu-3d) highlights the clear influence of both the metal type and the nature of the polymer chain in determining the mechanism of nanoparticle formation and their distribution within the polyurea matrix.

In the silver-containing systems, the Ag-3b sample exhibits relatively irregular nanoparticle distribution with limited partial agglomeration 5- 100 nm, indicating a balance between the nucleation and growth phases during the in-situ formation process. The Ag-3d sample, on the other hand, is characterized by a fine nanostructure 10-20 nm and a homogeneous narrow Gaussian distribution of small, discrete silver particles with high morphological regularity. This reflects the polymer matrix's ability to stabilize the nanoparticle nuclei and precisely control their growth, reducing the likelihood of their coalescence and maintaining their structural homogeneity. In copper containing systems, the Cu-3b sample exhibited quasi-spherical and polyhedral particles with moderate agglomeration 10-100 nm, attributed to the partial crystalline ordering that occurs during the reduction of copper ions. A balanced relationship between the rate of reduction and the polymer's capacity to limit growth and stabilize nanostructures within the matrix was demonstrated by Cu-3d 10-73 nm with narrow Gaussian distribution, which displayed a distinct pattern with partially connected nanoparticles dispersed as branched nanoscale networks or chains within the polymer matrix.

These findings confirm that both metal type and polymer structure fundamentally regulate the nucleation, growth, and morphological stability of nanoparticles. While copper systems typically create localized nanoscale networks and interconnected structures, silver systems, especially Ag-3d, show a high degree of structural homogeneity and uniform nanoscale dispersion. The functional characteristics of the nanocomposites amply demonstrate these

morphological variations. While the interconnected Cu-3d copper networks offer effective channels for electron transport and heat dissipation, the regular silver structures improve charge transfer and electrical current distribution, ultimately improving the final nanocomposites' electrical conductivity and thermal stability.

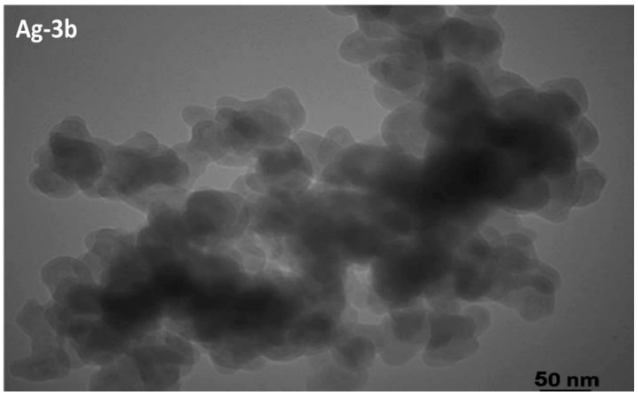


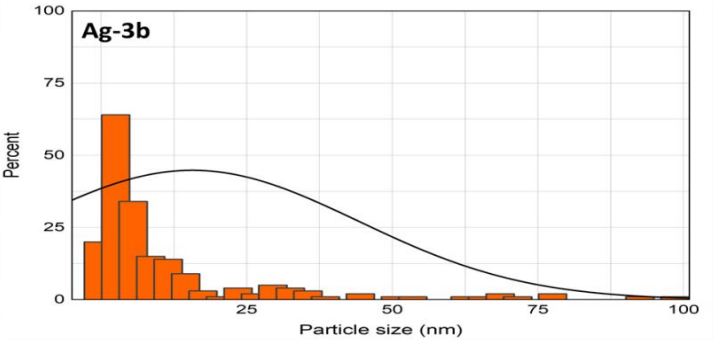


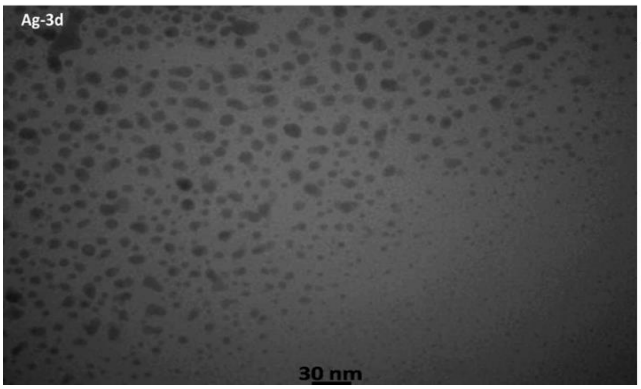


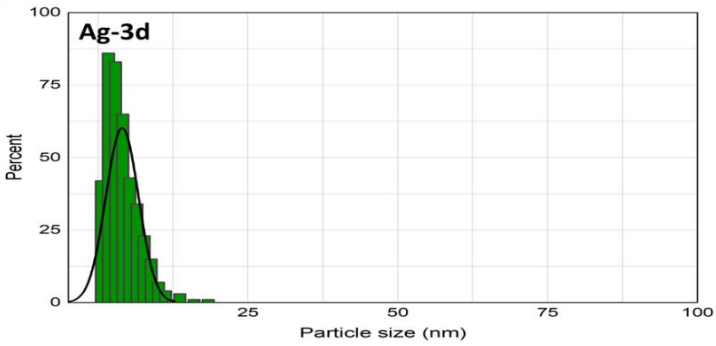


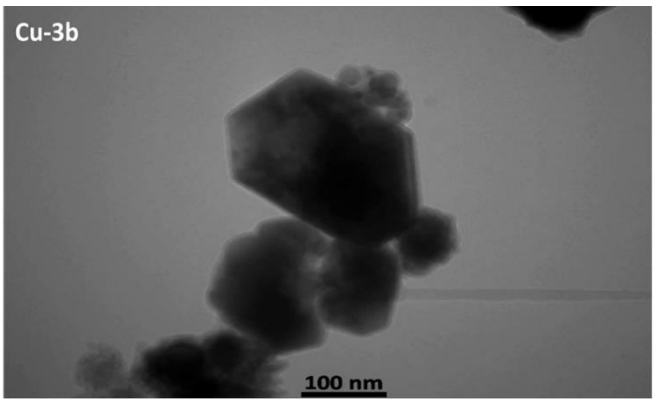


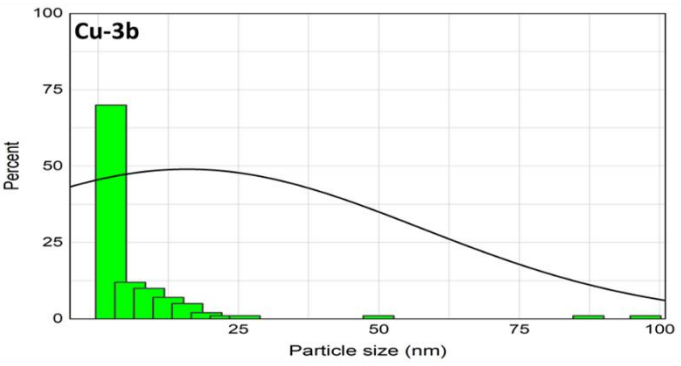


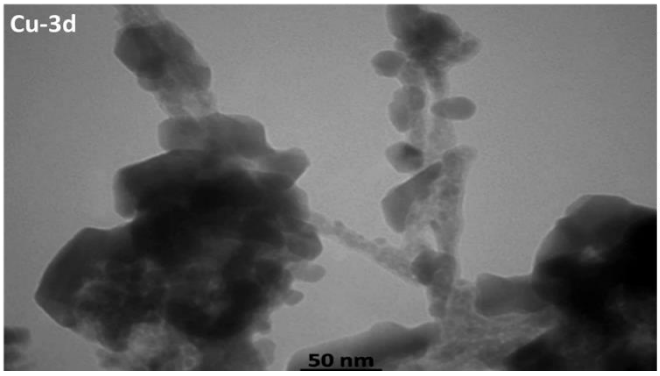


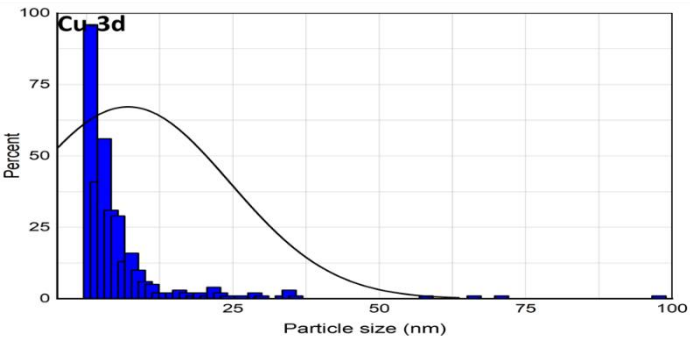

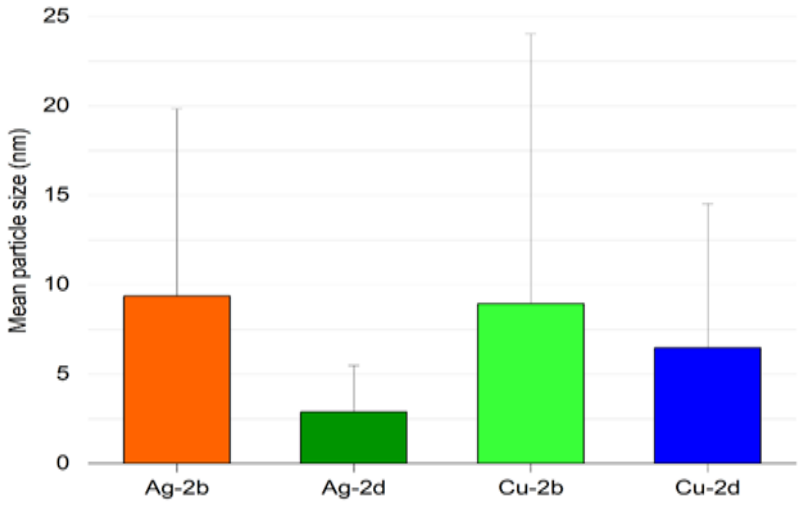


Figure (3-15): TEM image of polyurea/silver and copper nanocomposite showing particle size analysis (Group 2).

### 3.5.3 Zeta potential

A basic electrical characteristic found in suspended particles, polymers, and surfactants, the zeta potential (ζ-potential) provides a direct measure of the stability of colloidal systems [153], [154]. When copper and silver nanoparticles are mixed with polyurea polymers, the ζ-potential value reflects the uniformity and dispersion of the particles inside the polymer matrix. Strong electrostatic stability, which prevents particle aggregation and promotes uniform dispersion, is indicated by a high absolute value ($|\zeta| > 30$ mV), whereas a low value indicates the possibility of aggregation or weak bonding between the particles and the polymer, which would adversely affect the composite's electrical conductivity and thermal properties. To assess the effectiveness of the integration process between nanoparticles and polyurea chains and to comprehend the connection between surface charge and the system's electrical and physical stability, the ζ-potential is measured [155].

Nano polymer stability is directly impacted by the zeta potential. The repulsive forces between the particles increase with the distance of the zeta potential from zero (positive or negative), which keeps the particles from clumping together and helps them stay suspended and stable in the medium for longer. High stability and no chance of particle aggregation or precipitation are indicated by zeta potential values larger than ±30 mV. Nanoparticle aggregation and a quick loss of stability result from weak repulsive forces when the zeta potential is near zero (between -30 and +30 mV). A significant negative zeta potential value is seen in copper-doped polyurea compounds (particularly Cu-2b in the Figure (3-16)), which leads to improved particle stability compared with other metals or formulations carrying a lower charge. Increasing the charge (and its distance from zero) in polyurea doped with metallic nanoparticles therefore increases

stability and prevents particle agglomeration, which is essential in industrial and medical applications where the particles must be dispersed throughout the medium and not settle rapidly [156].

Figure (3-17) the Ag-3b spectrum (black): Shows a value near zero (about -5 to +10 mV), indicating extremely poor particle stability and fast aggregation over time. This makes it unsuitable for applications that need long-term stability and homogeneous nanoscale distribution. Ag-3d (red) and Cu-3b (blue) spectra: Their values are concentrated between -35 and -10 mV, indicating moderate stability where particle aggregation is generally prevented by strong repulsive forces; nevertheless, in saltwater or low pH settings, some aggregation may occur. Cu-3d (green): This compound has the biggest negative charge and a more noticeable peak at about -45 mV. It has the best colloidal stability of all the compounds and is very successful at preventing aggregation in the majority of chemical environments [157].

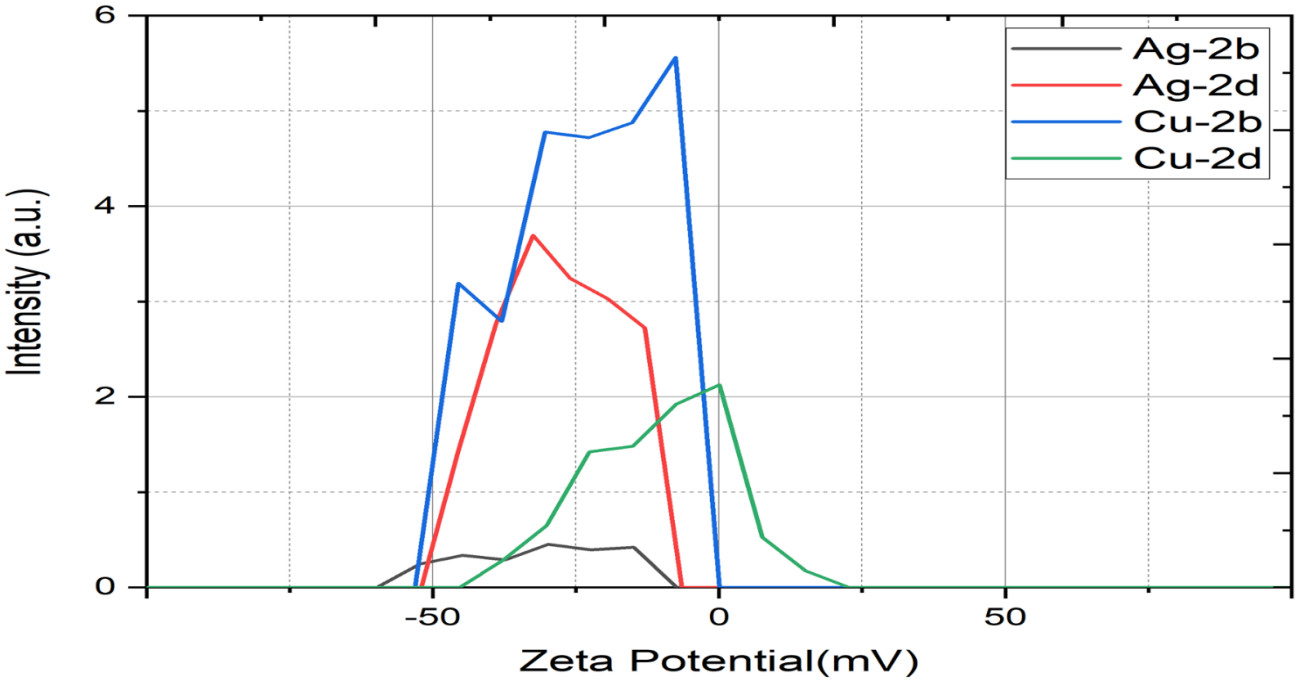


Figure (3-16): Zeta potential of polyurea/silver and copper nanocomposite (Group 1).

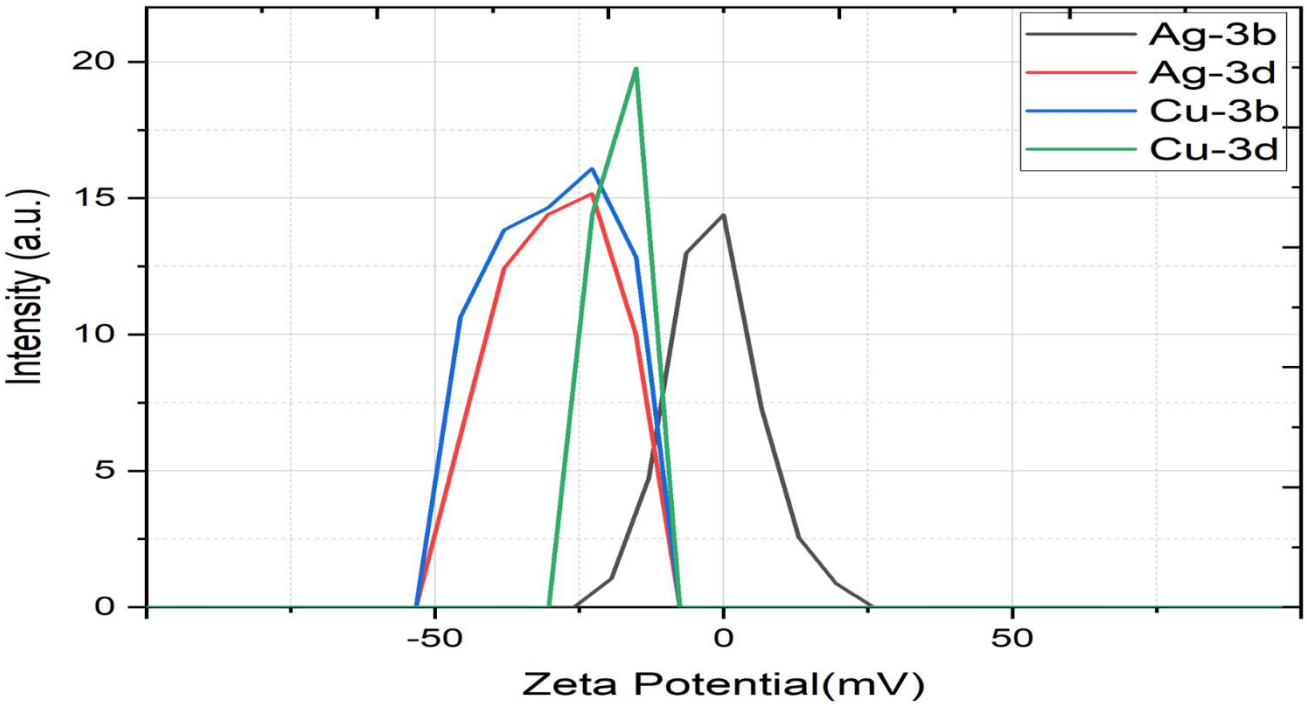


Figure (3-17): Zeta potential of polyurea/silver and copper nanocomposite (Group 2).

**Table (3-12): Zeta Potential Values and Stability Classification of Nanocomposite Samples.**

| Sample | Zeta Potential (mV) | Stability Classification |
|---|---|---|
| **TBT Polymers** | | |
| Ag-2b | -35.1 | Good stability, strong electrostatic repulsion, well dispersed system with low aggregation. |
| Ag-2d | -28.3 | Moderate stability, sufficient repulsion, relatively stable dispersion. |
| Cu-2b | -27.1 | Moderate stability, moderate repulsion, possible slow aggregation over time. |
| Cu-2d | -7.5 | Poor stability, weak repulsion, high tendency toward aggregation. |
| **TDA Polymers** | | |
| Ag-3b | -2.8 | Poor stability, weak repulsion, high tendency toward aggregation. |
| Ag-3d | -29.4 | Moderate stability, adequate repulsion, relatively stable dispersion |
| Cu-3b | -20.1 | Moderate stability, moderate repulsion, possible slow aggregation over time. |
| Cu-3d | -31.1 | Good stability, strong electrostatic repulsion, well dispersed system with low aggregation. |

Among the investigated samples, Ag-2b from the first group exhibited the highest colloidal stability, with a zeta potential value of −35.1 mV, indicating strong electrostatic repulsion between nanoparticles and excellent resistance to aggregation. In contrast, within the second group, Cu-3d demonstrated the best stability, with a zeta potential of −31.1 mV, which also reflects a highly stable dispersion system. The superior stability of these samples is attributed to their high absolute zeta potential values ($|\zeta| > 30$ mV), which enhance interparticle repulsion and prevent agglomeration. Therefore, Ag-2b and Cu-3d can be considered the most stable formulations in their respective groups, making them promising candidates for applications requiring well-dispersed and stable nanoparticle systems.

## 3.6 Electrical Conductivity

The four-point probe method for polyurea-based nanocomposites with copper and silver nanoparticles (TBT and TDA series) was used to assess the electrified performance of the device at room temperature (Table (3-12), Figures (3-18) and (3-19). To further examine the stability of the conductive response, the coefficient of variation of conductivity (CV%) was calculated for each sample using the following relation [162]:

$$\boldsymbol{CV}(\%) = \frac{\textbf{standard deviation of conductivity}}{\boldsymbol{mean\ conductivity}} \times \mathbf{100}$$

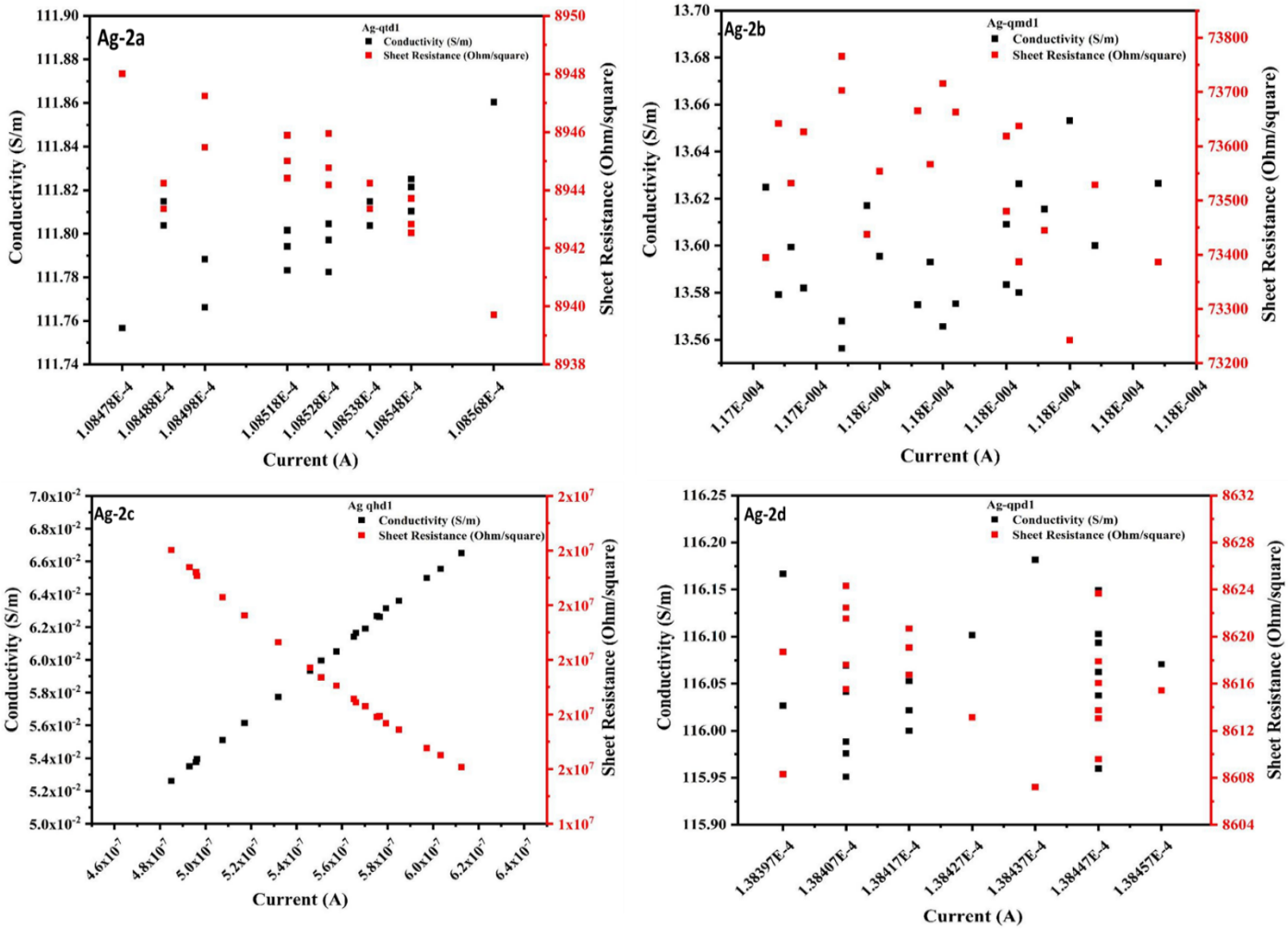


Figure (3-18): Electrical conductivity of polyurea/silver nanocomposites derived from monomer 2.

Following the addition of the dopant, or a quantity of the produced nanoparticles, an improvement in the values of all polymers was noted. This was accomplished by utilizing copper and silver, which are regarded as good conductors. We observe that the buildup of tiny impurity molecules within the polymer's crystal structure is the cause of the progressive rise in conductivity values of polymers with increasing impurity. The presence of a tiny impurity causes a section of the polymer's active crystal lattice to become electrically conductive by interfering with it. Therefore, the fraction of the conductive polymer increases as the contaminant percentage increases, until we achieve a rapid increase in conductivity at a particular impurity concentration. We refer to this position as the percolation point. The entire polymer crystal lattice then becomes conductive as conductivity gradually rises with increasing impurity. No matter how much impurity is added after this, the conductivity value stays constant [158], [159]. The findings indicate that the two main factors influencing the increase in conductivity as the impurity percentage rises are the spatial organization of the polymer's

crystal lattice and the degree of alternation in the polymer chain, which relates to the concentration of active centers [164]. The coefficient of variation (CV%) for the TBT-based polyurea composite (2a-d) varied significantly between samples, ranging from 0.02% to 7.09%. Specifically, samples 2a and 2d showed low CV% values (0.02% and 0.05%, respectively) and reliable and consistent electrical performance. However, samples 2b and 2c showed reduced stability even while their measurable conductivity was still there, as evidenced by their higher CV% values (0.18% and 7.09%).

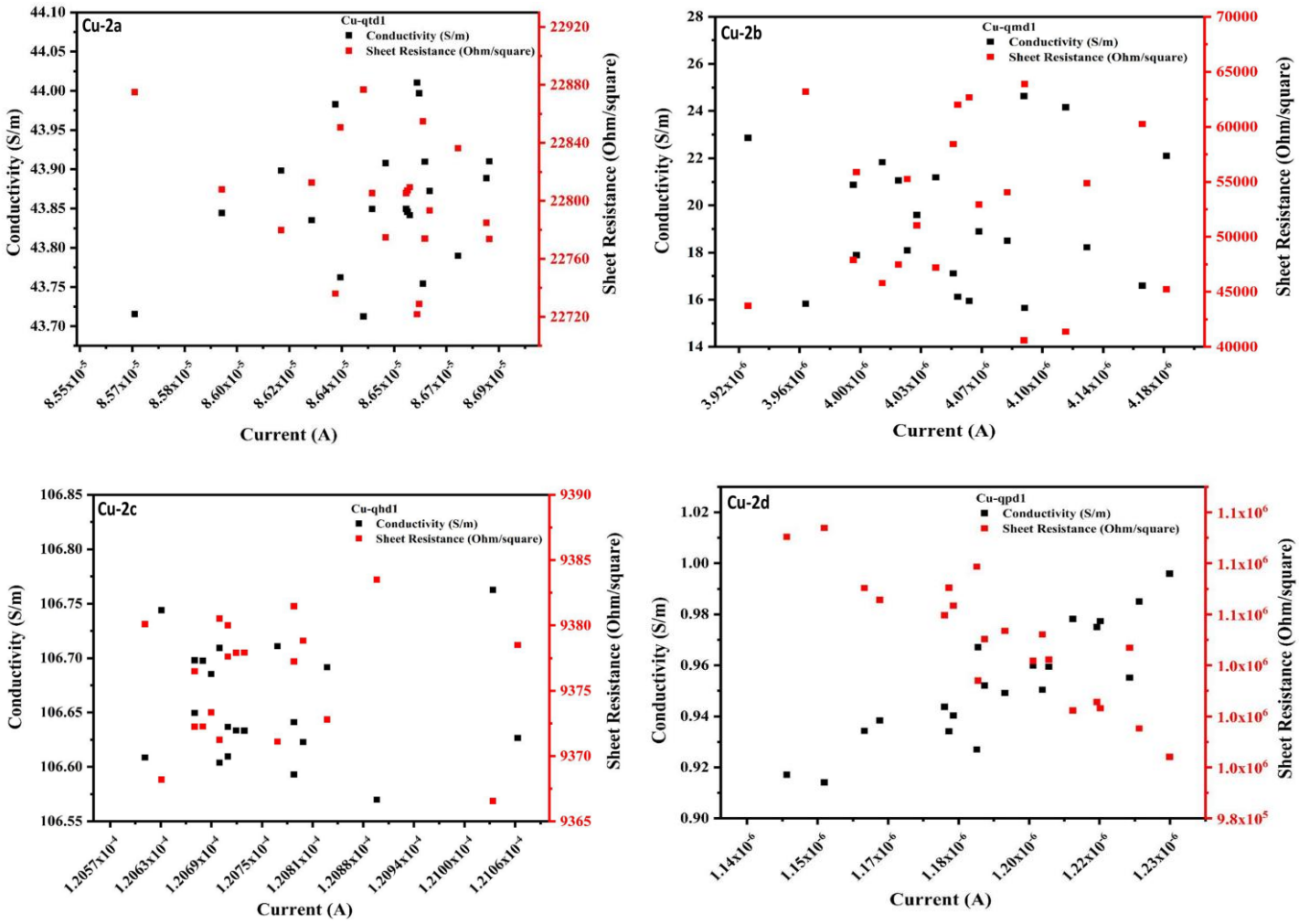


Figure (3-19): Electrical conductivity of polyurea/copper nanocomposites derived from monomer 2.

Likewise, the Cu-based nanocomposites (2a-2d) had CV% values ranging from 0.04% to 14.26%. Sample 2a showed a very low CV% value (0.19%), indicating great electrical stability, while sample 2b recorded the highest CV% value (14.26%), showing significant conductivity variability. Samples 2c and 2d showed low levels of stability, as demonstrated by their small CV% values (0.04% and 2.29%, respectively). Compared to their copper nanoparticle

counterparts, silver nanoparticles containing composite nanomaterials demonstrated superior electrical stability and conductivity. This superiority can be explained by the silver particles' higher electronic efficiency, high surface stability, and more uniform dispersion within the polyurea matrix, all of which help to create effective and continuous charge transport pathways throughout the polymeric structure.

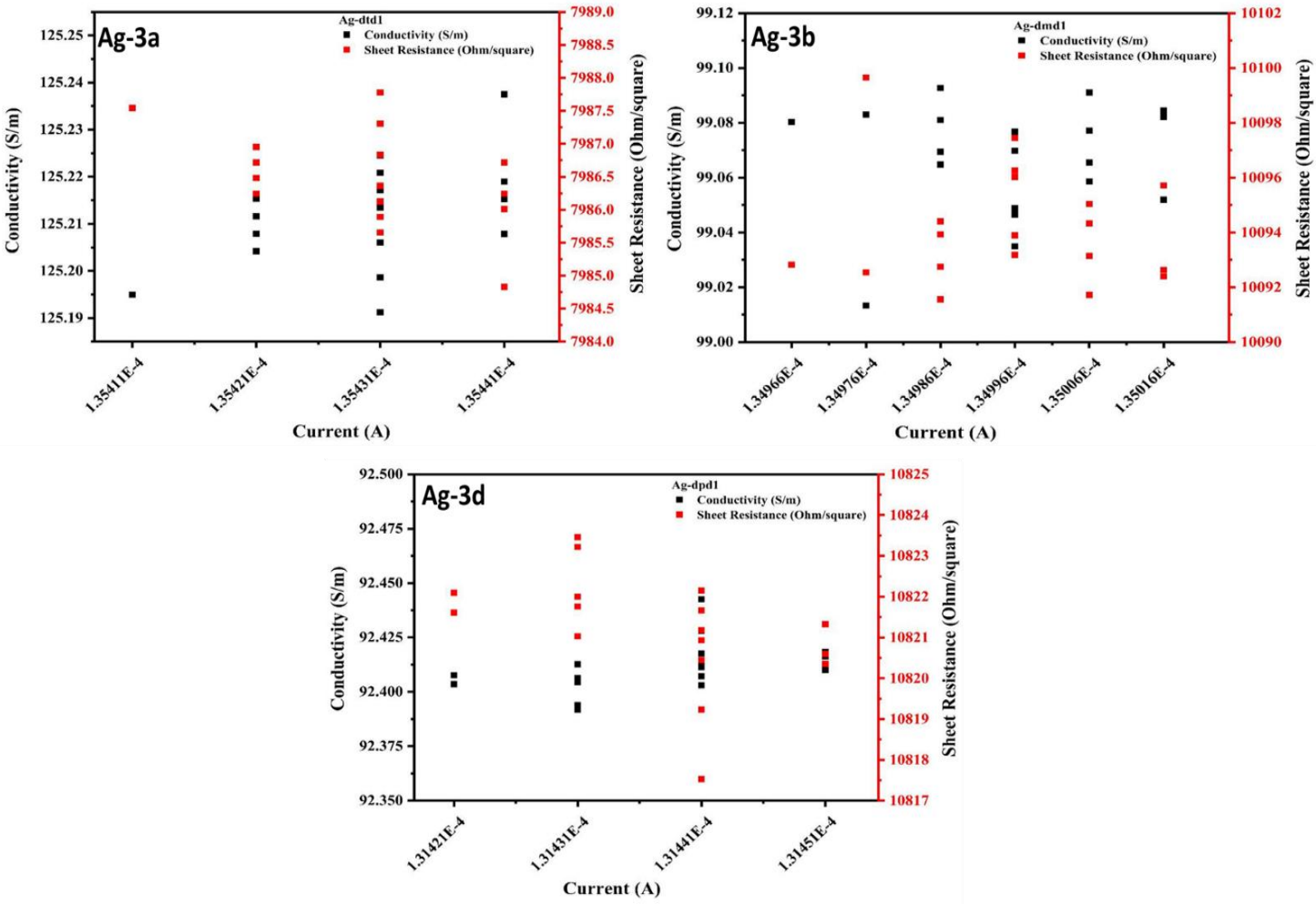


Figure (3-20): Electrical conductivity of polyurea/silver nanocomposites derived from monomer 3.

The electrical conductivity and sheet resistivity of silver-containing nano polymer samples (Ag-3a, Ag-3b, and Ag-3d) were assessed using the four-probe method, as seen in Figure (3-20). The diagrams' great precision, consistency, and repeatability are demonstrated by the fact that each point depicts an actual experimental measurement of the current value. The construction of an effective leakage network is suggested by Sample Ag-3a's maximum electrical capacity (125.2 S/m), which remained consistent throughout trials due to the uniform and regular dispersion of silver nanoparticles inside the polyurea matrix. Due to low

agglomeration and a comparatively uniform dispersion of metallic particles, sample Ag-3b revealed moderate conductance (99.1 S/m). On the other hand, sample Ag-3d had the highest surface resistivity (> 10 Ω/sq) and the lowest conductivity (92.4 S/m), suggesting limited charge transfer efficiency within the polymer matrix and weak nanoparticle interconnectivity. This result unequivocally demonstrates that the electrical transport mode is mostly determined by the molecular structure of the diamine segment in the polyurea chain. The degree of interaction between the metal particles and the polymer chain, and thus the effectiveness of conductive route construction, is directly influenced by the type of functional groups and the length of the chain. Additionally, the high quality and precision of the measurements are confirmed by the strong correlation of the points in each model, which shows the stability of the data and the low experimental variation (CV%).

Figure (3-21) illustration a heterogeneous distribution of copper particles within the polyurea matrix was indicated by sample Cu-3a moderate conductivity (36.6 S/m) and high sheet resistivity (28 kΩ/sq). Because of increased contact between copper and polymer chains and the creation of more effective electron transport routes, sample Cu-3b demonstrated a considerable improvement in conductivity (58 S/m) and a decrease in sheet resistivity (17 kΩ/sq). Even while the Cu-3d sample had the lowest surface resistivity (11 kΩ/sq) and the highest conductivity (85 S/m), this indicates that a very effective and uniform percolation network has formed within the polymer structure. The findings demonstrate a clear correlation between the conductivity order and the composition of the diamine segment in the polyurea chain, as variations in the functional groups impact the bonding efficacy between the metal particles and the polymer chain. The precision of the measurements and the stability of the constructed nanostructures are also demonstrated by the stability of the experimental points and the minimal dispersion in the data.

Direct comparison of the two systems reveals that silver particles generally exhibit higher electrical conductivity at similar loading ratios, while copper particles are more sensitive to the polymer's backbone structure, particularly the composition and structure of the diamine unit. This implies that the electrical behavior of the investigated nano polymers is dependent on the polymer chain's capacity to stabilize the metal particles, stop them from aggregating, and establish effective contact between the particles in order to generate ongoing electron transport pathways inside the matrix.

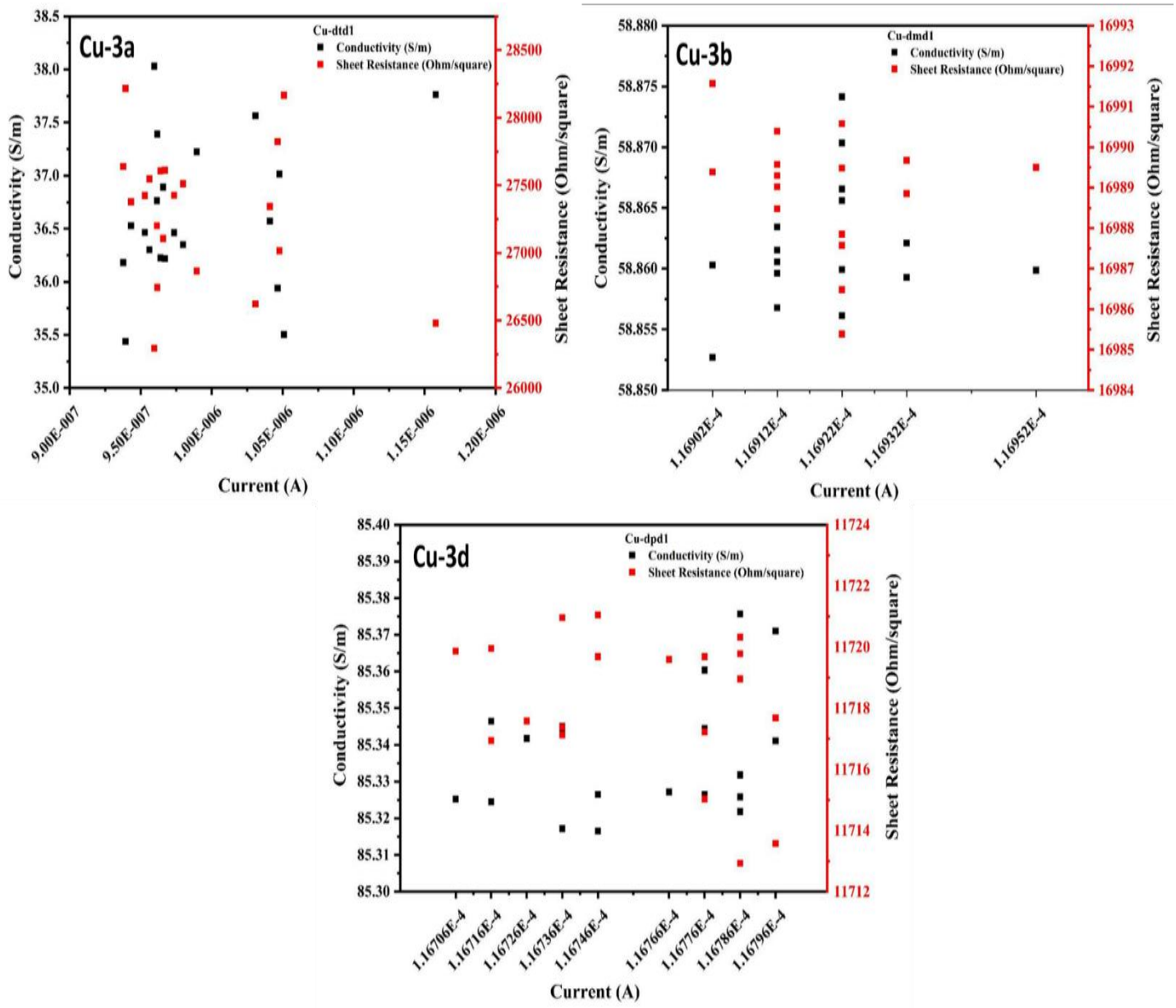


Figure (3-21): Electrical conductivity of polyurea/copper nanocomposites derived from monomer 3.

**Table (3-13): Electrical conductivity and stability of polyurea/silver and copper nanocomposites.**

| Composites | Mean conductivity (S/m) | Standard deviation (S/m) | CV% |
|---|---|---|---|
| Ag-TBT | | | |
| 2a | 111.80083 | 0.021843 | 0.02 |
| 2b | 13.59629 | 0.024534 | 0.18 |
| 2c | 0.059833 | 0.004243 | 7.09 |
| 2d | 116.0558 | 0.063228 | 0.05 |
| Ag-TDA | | | |
| 3a | 125.2115 | 0.010701 | 0.009 |
| 3b | 99.06712 | 0.01981 | 0.02 |
| 3d | 92.410688 | 0.010836 | 0.01 |
| Cu-TBT | | | |
| 2a | 43.85891603 | 0.082485 | 0.19 |
| 2b | 19.35933186 | 2.76026321 | 14.26 |
| 2c | 106.6565 | 0.051309 | 0.04 |
| 2d | 0.952717 | 0.021822 | 2.29 |
| Cu-TDA | | | |
| 3a | 36.64139492 | 0.67979 | 1.86 |
| 3b | 58.8618464 | 0.004668 | 0.008 |
| 3d | 85.339175 | 0.017833 | 0.02 |

## 3.7 Conclusion

1) Eight Schiff-base-derived polyurea polymers were successfully synthesized using two aromatic precursors (TBT and TDA) with four different diisocyanatos, followed by doping with silver and copper nanoparticles to prepare conductive polymeric inks with enhanced functional properties.
2) XRD and FT-IR analyses confirmed the successful formation of both the polymers and the metal nanoparticles, where the nanoparticles exhibited crystalline structures, while the spectra verified the disappearance of the isocyanate group and the formation of urea and Schiff-base linkages within the polymer chains.
3) XRD and FT-IR analyses confirmed the successful formation of both the polymers and the metal nanoparticles, where the nanoparticles exhibited crystalline structures, while the spectra verified the disappearance of the isocyanate group and the formation of urea and Schiff-base linkages within the polymer chains.
4) TEM, EDX, and ζ-potential analyses demonstrated homogeneous and stable nanoparticle dispersion, where silver-based systems exhibited smaller and more uniformly distributed nanoparticles, whereas copper-based systems formed interconnected structures that enhanced electron transport.
5) The prepared nanocomposites showed a significant improvement in electrical conductivity, with silver-doped polymers achieving the highest conductivity values, while copper-based systems demonstrated good electrical performance due to the formation of interconnected nanoscale channels, making these materials promising for flexible electronics, conductive coatings, sensors, and thermal management applications.

## 3.8 Recommendations

1- Optimization of nanoparticle loading levels: It is advisable to investigate various concentrations of Ag and Cu nanoparticles to determine the ideal loading that enhances conductivity and stability while reducing agglomeration.
2- Examination of electrical transport mechanisms: Future research should investigate the electron transport channels inside the polyurea matrix to elucidate the impact of nanoparticle dispersion and connection on electrical performance.
3- Evaluation of Biological Activity: It is recommended to evaluate the antibacterial or cytocompatibility properties of the nanocomposites to investigate their prospective applications in biomedical coatings and protective surfaces.
4- Characterization of mechanical properties: To better understand how the type and distribution of nanoparticles affect mechanical behavior, more research should examine tensile strength, Young's modulus, hardness, and stickiness.
5- Application-oriented and device integration studies: To assess the materials' performance under operating settings, they should be tested in useful applications such as printed electronics and conductive inks.

# *Reference*

[1] K. Ferji, “Basic concepts and tools of artificial intelligence in polymer science,” Polym. Chem., vol. 16, no. 21, pp. 2457–2470, 2025.

[2] J. Ni, Z., Jiao, H., Fei, C., Gu, H., Xu, S., Yu, Z., ... & Huang, “Evolution of defects during the degradation of metal halide perovskite solar cells under reverse bias and illumination,” *Nat. Energy*, vol. 7, no. 1, pp. 65–73, 2022.

[3] S. Ajitha, A. R., & Thomas, *Introduction: Polymer blends, thermodynamics, miscibility, phase separation, and compatibilization. In Compatibilization of polymer blends*. 2020.

[4] L. Luraghi, A., Peri, F., & Moroni, “Electrospinning for drug delivery applications: A review. ,” *J. Control. release*, vol. 334, pp. 463–484, 2021.

[5] U. S. Schubert, “From polymers or colloids to polymers and colloids,” *Colloid Polym. Sci.*, vol. 298, no. 2, pp. 1609–1610, 2020.

[6] J. Guo, T., Luo, L., Wang, L., Zhang, F., Liu, Y., & Leng, “Smart polymer microspheres: preparation, microstructures, stimuli-responsive properties, and applications,” ACS Nano, vol. 19, no. 9, pp. 18003–18036, 2025.

[7] R. Talreja, “Historical development of damage mechanics for composite materials,” In The History of Composites , Elsevier, 2026, pp. 845–869.

[8] A. M. Young, W. C., Budynas, R. G., & Sadegh, *Roark’s formulas for stress and strain*, vol. 7. 2002.

[9] V. S. Ivanov, *Radiation chemistry of polymers*. John Wiley & Sons, 2023.

[10] S. Razzaq, S., Asghar, A., & Iqbal, “Energy Harvesting Devices. In Advances in Hybrid Conducting Polymer Technology,” *Cham Springer Int. Publ.*, pp. 101–124, 2021.

[11] C. H. Mustafa, N. S., Omer, M. A. A., Garlnabi, M. E., Ismail, H. A., & Ch, “Reviewing of general polymer types, properties and application in medical field,” *Int J Sci Res*, vol. 5, no. 8, pp. 212–221, 2016.

[12] J. Gedde, U. W., Hedenqvist, M. S., Johansson, M., Berglund, L., & Wohlert, “Introduction to polymer science,” in In Fundamental polymer science, Cham: Springer Nature Switzerland, 2025, pp. 1–58.

[13] S. L. Lloyd, E. M., Vakil, J. R., Yao, Y., Sottos, N. R., & Craig, “Covalent mechanochemistry and contemporary polymer network chemistry: A marriage in the making,” *J. Am. Chem. Soc.*, vol. 145, no. 2, pp. 751–768, 2023.

[14] E. Saldívar-Guerra, E., & Vivaldo-Lima, “Introduction to polymers and polymer types,” Polym. Sci. Eng. Sustain., vol. 1, pp. 1–18, 2025.

[15] A. Kadhim, A. F., & Hashim, “Recent review on metal oxides nanostructures doped polystyrene for biological and industrial applications,” *World J. Adv. Res. Rev.*, vol. 17, no. 3, pp. 412–423, 2023.

[16] A. Hsissou, R., Seghiri, R., Benzekri, Z., Hilali, M., Rafik, M., & Elharfi, “Polymer composite materials: A comprehensive review,” *Compos. Struct.*, vol. 262, pp. 113–640, 2021.

[17] Ç. Yurdakul, M., Tok, M., Döner, G. S., & Kırbıyık Kurukavak, *Sustainable Polymer Composites for Automotive Industry. In Macro, Micro and Nanocomposites from Sustainable Sources: Shrinking Environmental Footprints*. Singapore: Springer Nature Singapore, 2026.

[18] T. A. Purohit, P., Bhatt, A., Mittal, R. K., Abdellattif, M. H., & Farghaly, "Polymer Grafting and its chemical reactions," *Front. Bioeng. Biotechnol.*, vol. 10, pp. 104–4927, 2023.

[19] N. Wang, A., Chen, C., Liao, L., Qian, J., Yuan, F. G., & Zhang, "Enhanced β-phase in direct ink writing PVDF thin films by intercalation of graphene," *J. Inorg. Organomet. Polym. Mater.*, vol. 30, no. 5, pp. 1497–1502, 2020.

[20] K. W. Kim, Y., Kim, M. S., Jeon, H. J., Kim, J. H., & Chun, "Mechanical performance of polymer materials for low-temperature applications," *Appl. Sci.*, vol. 12, no. 23, pp. 12–251, 2022.

[21] J. Jia, Y., Mao, Z., Huang, W., & Zhang, "Effect of temperature and crystallinity on the thermal conductivity of semi-crystalline polymers: A case study of polyethylene," *Mater. Chem. Phys.*, vol. 287, pp. 126–325, 2022.

[22] B. Gürbüz, E., & Sanyal, "Tuning of lattice thermal conductivity of amorphous Fe0. 85Zr0. 15 by nanostructured voids, pressure and temperature," *J. Non. Cryst. Solids*, vol. 616, pp. 122–430, 2023.

[23] H. Pispas, S., Anastasiadis, S. H., & Iatrou, "State-of-the-Art Polymer Science and Technology in Greece," *Polymers*, vol. 15, no. 5, pp. 12–64, 2023.

[24] P. Das, A., & Mahanwar, "A brief discussion on advances in polyurethane applications," *Adv. Ind. Eng. Polym. Res.*, vol. 3, no. 3, pp. 93–101, 2020.

[25] P. Pandya, H., & Mahanwar, "Fundamental insight into anionic aqueous polyurethane dispersions," *Adv. Ind. Eng. Polym. Res.*, vol. 3, no. 3, pp. 102–110, 2020.

[26] L. Lucherelli, M. A., Duval, A., & Avérous, "Biobased vitrimers: Towards sustainable and adaptable performing polymer materials," *Prog. Polym. Sci.*, vol. 127, pp. 101–515, 2022.

[27] L. V. Benavides Fernández, C. D., Guzmán Castillo, M. P., Quijano Pérez, S. A., & Carvajal Rodríguez, "Microbial degradation of polyethylene terephthalate: a systematic review.," *SN Appl. Sci.*, vol. 4, no. 10, p. 263, 2022.

[28] S. Ecochard, Y., & Caillol, "Hybrid polyhydroxyurethanes: How to overcome limitations and reach cutting edge properties," *Eur. Polym. J.*, vol. 137, pp. 109–915, 2020.

[29] F. Delebecq, E., Pascault, J. P., Boutevin, B., & Ganachaud, "On the versatility of urethane/urea bonds: reversibility, blocked isocyanate, and non-isocyanate polyurethane," *Chem. Rev.*, vol. 113, no. 1, pp. 80–118, 2013.

[30] D. Schlosser, "Sind konventionelle Kunststoffe mikrobiell abbaubar," *BIOspektrum*, vol. 24, no. 4, pp. 375–378, 2018.

[31] L. Zhong, W., Hu, D., Chen, Y., & Zhao, "Microwave-assisted physical foaming of

polymers: a review," *Polym. Rev.*, vol. 64, no. 4, pp. 1136–1175, 2024.

[32] A. R. A. Al-Samarrai, "Study of the physical properties of unsaturated polyester resin reinforced with natural materials as industrial alternatives," University of Tikrit, College of Science, 2004.

[33] A. G. Ragab, M. M., Othman, H., & Hassabo, "Natural polymers and their application in the textile sector," J. Text. Color. Polym. Sci., vol. 22, no. 2, pp. 93–113, 2025.

[34] W. J. Munati, "Study of the rheological behavior of a particulate polymer composite," University of Technology, Iraq, 2005.

[35] M. Monclús, L., Arp, H. P. H., Groh, K. J., Faltynkova, A., Løseth, M. E., Muncke, J., & Wagner, "Mapping the chemical complexity of plastics," *Nature*, vol. 643, no. 8071, pp. 349–355, 2025.

[36] T. Wu, W., Feng, H., Xie, L., Zhang, A., Liu, F., Liu, Z., ... & Xie, "Reprocessable and ultratough epoxy thermosetting plastic," *Nat. Sustain.*, vol. 7, no. 6, pp. 804–811, 2024.

[37] A. Munguia-Lopez, A. D. C., Sanchez-Zarco, X. G., & Owusu-Boateng, "Process Systems Engineering Approaches for Sustainable Plastics Management," Ind. Eng. Chem. Res., vol. 64, no. 27, pp. 13519–13535, 2025.

[38] C. Chen, "Epoxy Adhesive Technology: Latest Developments and New Trends," *Prog. Adhes. Adhes.*, vol. 8, pp. 251–282, 2024.

[39] M. A. Haque, F. M., Ishibashi, J. S., Lidston, C. A., Shao, H., Bates, F. S., Chang, A. B., ... & Hillmyer, "Defining the macromolecules of tomorrow through synergistic sustainable polymer research," *Chem. Rev.*, vol. 122, no. 6, pp. 6322–6373, 2022.

[40] S. Vickery, W., Coskun, H. I., Wang, J., & Sydlik, "Hands-on laboratory modules for polymer education within biomedical materials applications," J. Chem. Educ., vol. 102, no. 3, pp. 1160–1168, 2025.

[41] S. Boonyasaranai, B., Jakrawatana, N., Gheewala, S. H., Kurisu, K., & Phuphisith, "Assessment of Post-consumer Plastic Packaging Waste Flow in Chiang Mai: Challenges for Low-and High-value Plastic Waste Streams Towards a Circular Economy," Clean. Environ. Syst., pp. 100–424, 2026.

[42] C. W. Song, B., & Cho, "Applying polyvinyl alcohol to the preparation of various nanoparticles," *J. Pharm. Investig.*, vol. 54, no. 3, pp. 249–266, 2024.

[43] A. V. Patil, R. V., Inamdar, S. B., Das, S. Z., Akamanchi, K. K., Patil, K. G., Inamadar, A. V., Reddy, A. C., Raghu, K. R., & Kulkarni, "Tailor-made electrically responsive poly(acrylamide)-graft-pullulan copolymer-based transdermal drug delivery systems: Synthesis, characterization, in vitro and ex vivo evaluation," *J. Drug Deliv. Sci. Technol.*, vol. 56, pp. 101–525, 2020.

[44] X. Zhao, Y., Ma, T., Hu, L., Ren, X., Sun, X., & Yu, "Supramolecular interaction chemistry in polymer electrolytes towards stable lithium metal batteries," J. Energy Chem., vol. 107, pp. 154–169, 2025.

[45] K. B. Nagaraja, D. B., Buddha, R. S., Babu Naidu, K. C., & Basha, "Development and evaluation of a polymer composite material reinforced by Tectona grandis fiber, with

static analysis," *Polymers*, vol. 17, no. 5, p. 634, 2025.

[46] S. O. Yang, G. G., Choi, H. J., Han, K. H., Kim, J. H., Lee, C. W., Jung, E. I., ... & Kim, "Block copolymer nanopatterning for nonsemiconductor device applications," *ACS Appl. Mater. Interfaces*, vol. 14, no. 10, pp. 12011–12037, 2022.

[47] D. Gardoni, G., Menegon, R., Sponchioni, M., & Moscatelli, "Thermoresponsive Copolymers with Well-Defined Composition and Phase Separation Via Semi-Batch Free-Radical Polymerization in a Non-Polar Medium," *ACS Appl. Polym. Mater.*, vol. 6, no. 1, pp. 616–626, 2023.

[48] L. Kumar, P., & Unnikrishnan, *Pyroelectric and piezoelectric polymers. In Polymers in Energy Conversion and Storage*. 2022.

[49] K. Pasbakhsh, S. A. B., Mohotti, P., Palaniandy, D., & Auckloo, *Polyurea: Synthesis, properties, composites, production, and applications*. Elsevier, 2023.

[50] E. Sarcina, F., Signorile, M., & Salmoiraghi, "Polyurea Adhesives & Coatings," *Prog. Adhes. Adhes.*, vol. 9, pp. 521–560, 2025.

[51] P. Palaniandy, K., Auckloo, S. A. B., Chan, E.-S., & Pasbakhsh, *Raw materials, properties, and structure of polyurea.* Elsevier, 2023.

[52] D. Iqbal, P., Tripathi, N., Parthasarathy, M., Kumar, S., & Roy, "Polyurea spray coatings: Tailoring material properties through chemical crosslinking," *Prog. Org. Coatings*, vol. 123, pp. 201–208, 2018.

[53] S. Cai, M., Dongyu, "High mechanical performance polyurea/organoclay nanocomposites," *Compos. Sci. Technol.*, vol. 103, pp. 44–48, 2014.

[54] G. Do, S., Stepp, S., & Youssef, "Quasi-static and dynamic characterization of polyurea microspheres reinforced polyurea matrix composite," *Mater. Today Commun.*, vol. 25, pp. 101–464, 2020.

[55] P. L. N. Somarathna, H. C. C., Raman, S. N., Mohotti, D., & Fernando, "Polyurea in construction and building applications," in *In Polyurea*, Elsevier, 2023, pp. 239–272.

[56] C. Ding, L., Wang, Y., Lin, J., Ma, M., Hu, J., Qiu, X., ... & Feng, "Recent advances in polyurea elastomers and their applications in blast protection: a review," *J. Mater. Sci.*, vol. 59, no. 62, pp. 14893–14923, 2024.

[57] H. K. Mahar, M. E., Taimur, S., & Tareen, *Smart Glass Technology*. Cambridge Scholars Publishing, 2025.

[58] S. Zarour, R., Omar, A., & Abu-Reziq, "Preparation of poly(ethylene glycol) polyurea microcapsules using oil/oil emulsions and their application as microreactors," *Polymers*, vol. 13, no. 15, p. 2566, 2021.

[59] Y. Li, M., Li, G. E., Wang, C., Shi, R., Wang, J., Wang, S., Wang, Y., & Chen, "Synthesis and application of modified lignin polyurea binder for manufacturing a controlled-release potassium fertilizer," *Agronomy*, vol. 13, no. 10, p. 2641, 2023.

[60] H. Mahtabani, A., La Zara, D., Niittymäki, M., Anyszka, R., Rytöluoto, I., & He, "Molecular layer deposition of polyurea on silica nanoparticles and its application in

dielectric nanocomposites," *J. Phys. Chem. C*, vol. 127, no. 24, pp. 11736–11747, 2023.

[61] J. C. Du, J., Canamas, P., Guichardon, P., Ibaseta, N., Montagnier, B., & Hubaud, "Adaptability of polyurea microcapsules loaded with octyl salicylate for sunscreen application: Influence of shell thickness of microfluidic-calibrated capsules on UV absorption efficiency," vol. 6, no. 5, 2023.

[62] Y. Li, L., Shen, H., Zhang, Z., Xu, S., Liu, Y., Zhang, H., Tang, L., Peng, H., Wang, F., Li, G., Li, H., & Liu, "Improve the insulation performance of air-insulated gaps: Application of polyurea materials on the ground potential side of transmission line," *High Volt.*, vol. 10, no. 3, pp. 726–737, 2025.

[63] C. A. Charles, J. A., & Harper, *Handbook of plastic processes*. John Wiley & Sons, 2005.

[64] M. J. M. Gaskell, D. R., & Krane, *An introduction to transport phenomena in materials engineering*. 2024.

[65] B. Erba, A., Desmarais, J. K., Casassa, S., Civalleri, B., Donà, L., Bush, I. J., ... & Kirtman, "A program for computational solid state physics and chemistry," *J. Chem. Theory Comput.*, vol. 19, no. 20, pp. 6891–6932, 2022.

[66] J. Ding, L., Yu, Z. D., Wang, X. Y., Yao, Z. F., Lu, Y., Yang, C. Y., ... & Pei, "Polymer semiconductors: synthesis, processing, and applications," *Chem. Rev.*, vol. 123, no. 12, pp. 7421–7497, 2023.

[67] A. K. Majeed, "Structural and dielectric properties of (Bi1-xSrxFeO3) ferrites prepared using sol-gel auto combustion method," College of Science, University of Diyala, Diyala, Iraq, 2014.

[68] R. Kulkarni, M. D., Swati, S. S., & Shirsat, "Optical and structural properties of zinc oxide nanoparticles," *Int. J. Adv. Res. Phys. Sci.*, vol. 2, no. 1, pp. 14–18, 2015.

[69] M. S. Dresselhaus, *Solid State Physics Optical Properties of Solids*. International Monographs on Physics, 2022.

[70] E. Atta, A., Al-Harbi, N., Alotaibi, B. M., Uosif, M. A. M., & Abdeltwab, "Structural characteristics and dielectric properties of irradiated polyvinyl alcohol/sodium iodide composite films," *Inorg. Chem. Commun.*, vol. 159, pp. 111–651, 2024.

[71] J. Z. Zhou, Y., Zhang, J., Ren, G., Zhang, B. Y., & Ou, "Illuminating quantum phenomena in 2d materials: The power of optical spectroscopy," *Adv. Opt. Mater.*, vol. 13, no. 31, pp. 17–14, 2025.

[72] Z. Xing, C., Jiang, W., Li, M., Wang, M., Xiao, J., & Xu, "Application of atomic force microscopy in bitumen materials at the nanoscale: A review," *Constr. Build. Mater.*, vol. 342, pp. 12–8059, 2022.

[73] M. Wang, "Identification and evaluation of optimal fiber shape for transverse thermal conductivity of unidirectional composites," *J. Eng. Fiber. Fabr.*, vol. 19, 2024.

[74] C. B. McCrum, N. G., Buckley, C. P., & Bucknall, *Principles of polymer engineering*. Oxford university press, 2026.

[75] D. R. Askeland, *The science and engineering of materials*, 6th ed. Cengage Learning, 2011.

[76] J. Ma, Y., Wang, W., Miao, H., Han, S., Fu, Y., Chen, Y., & Hao, "Physicochemical synergistic effect of microwave-assisted Co-pyrolysis of biomass and waste plastics by thermal degradation, thermodynamics, numerical simulation, kinetics, and products analysis," *Renew. Energy*, vol. 223, pp. 12–26, 2024.

[77] ASTM International, "Standard terminology relating to plastics.," 2003.

[78] ASTM International, "Standard terminology relating to thermophysical properties," 2003.

[79] J. Menczel, J. D., & Grebowicz, "Handbook of Differential Scanning Calorimetry: Techniques, Instrumentation, Inorganic, Organic and Pharmaceutical Substances," *Butterworth-Heinemann*, 2023.

[80] C. Mazzotta, E., Di Giulio, T., & Malitesta, "Electrochemical sensing of macromolecules based on molecularly imprinted polymers: challenges, successful strategies, and opportunities," *Anal. Bioanal. Chem.*, vol. 414, no. 18, pp. 5165–5200, 2022.

[81] E. Saldívar-Guerra, E., & Vivaldo-Lima, "Introduction to polymers and polymer types," *Polym. Sci. Eng. Sustain.*, vol. 1, pp. 1–18, 2025.

[82] Y. Zhang, X., Zheng, J., Liu, H., & Wu, "Lifetime Prediction of PVC-P Geomembranes Immersion in Water at Elevated Temperatures," *Polymers*, vol. 17, no. 11, pp. 14–70, 2025.

[83] I. Ipatova, V., Bliznyuk, U., Borshchegovskaya, P., Bolotnik, T., Chernyaev, A., Gloriozov, I., ... & Rodin, "(2025). Effect of E-Beam and X-Ray Irradiation on Radiation–Chemical Yield and Reaction Rate of Volatile Organic Compound Transformations," *Molecules*, vol. 30, no. 21, p. 4226, 2025.

[84] H. T. Y. Sheng, S. J., & Sheng, "Effects of geometrical characteristics of surface roughness on droplet wetting," *J. Chem. Phys.*, vol. 127, pp. 234–704, 2007.

[85] K. Cai, M., Jianchen, J., Murugadoss, V., Jiang, J., Gao, X., Lin, Z., Huang, M., Guo, J., Alsareii, S. A., Algadi, H., & Kathiresan, "Waterborne polyurethane and its nanocomposites: A mini-review for anti-corrosion coating, flame retardancy, and biomedical applications," *Adv. Compos. Hybrid Mater.*, vol. 5, no. 2, pp. 641–650, 2022.

[86] J. Seiffert, S., & Sprakel, "Physical chemistry of supramolecular polymer networks," *Chem. Soc. Rev.*, vol. 41, no. 2, pp. 909–930, 2022.

[87] Q. Zheng, T. X. N., Xu, Y., & Zhao, "Dynamic covalent polymer networks: A molecular platform for designing functions beyond chemical recycling and self-healing," *Chem. Rev.*, vol. 121, no. 3, pp. 1716–1745, 2021.

[88] S. Holgate, *Understanding solid state physics*. Amsterdam, Netherlands: Elsevier, 2021.

[89] L. Huang, "Advances in multicolor electrochromic devices based on inorganic materials.," *J. Mater. Chem. C*, vol. 11, no. 30, pp. 10107–10120, 2023.

[90] B. Zhong, Z., Wang, X., & Tan, “Porous organic polymers for CO2 capture and catalytic conversion,” Chem. Eur. J., vol. 31, no. 13, pp. 2024–4089, 2025.

[91] F. Das, O., Gedde, U., Hedenqvist, M. S., Hakkarainen, M., & Nilsson, *Applied polymer science*. Springer, 2021.

[92] S. N. Murad, M. A. B. A., Iraqi, A., Aziz, S. B., & Abdullah, “Conducting polymers for optoelectronic devices and organic solar cells: A review,” *Polymers*, vol. 12, no. 11, p. 2627, 2020.

[93] T. Onggar, C., Kruppke, I., & Cherif, “Techniques and processes for the realization of electrically conducting textile materials from intrinsically conducting polymers and their application potential,” *Polymers (Basel).*, vol. 12, no. 12, p. 2867, 2020.

[94] M. Arslan, M. A., Acik, G., & Tasdelen, “The emerging applications of click chemistry reactions in the modification of industrial polymers,” *Polym. Chem.*, vol. 10, no. 28, pp. 3806–3821, 2019.

[95] W. Barford, *Electronic and optical properties of conjugated polymers*. International Monographs on Physics, 2013.

[96] J. Bai, J., Wu, D., Shelley, T., Schubel, P., Twine, D., Russell, J., ... & Zhang, “A comprehensive survey on machine learning driven material defect detection,” ACM Comput. Surv., vol. 57, no. 11, pp. 1–36, 2025.

[97] T. Plisko, “Effect of the addition of polyacrylic acid of different molecular weights to coagulation bath on the structure and performance of polysulfone ultrafiltration membranes,” *Polymers (Basel).*, vol. 15, no. 7, p. 1664, 2023.

[98] A. Scaccabarozzi, “Doping approaches for organic semiconductors,” *Chem. Rev.*, vol. 122, no. 4, pp. 4420–4492, 2021.

[99] A. Kukhta, C. K. L. N., & Marks, “Molecular design strategies toward improvement of charge injection and ionic conduction in organic mixed ionic–electronic conductors for organic electrochemical transistors,” *Chem. Rev.*, vol. 122, no. 4, pp. 4325–4355, 2022.

[100] C. J. Nandihalli, T. M. N., & Liu, “Polymer based thermoelectric nanocomposite materials and devices: Fabrication and characteristics,” *Nano Energy*, vol. 78, pp. 105–186, 2020.

[101] J. F. Tadesse, M. G., Ahmmed, A. S., & Lübben, “Review on conductive polymer composites for supercapacitor applications,” *J. Compos. Sci.*, vol. 8, no. 2, 2024.

[102] G. Vinogradov, “Subsonic and supersonic polaron dynamics in polyacetylene,” *Synth. Met.*, vol. 299, pp. 117–477, 2023.

[103] A. Roy, J. D. P., Anandan, G. T., Nayak, N., & Kumar, “Raman snapshots of side-chain dependent polaron dynamics in polythiophene films,” *J. Phys. Chem. B*, vol. 127, no. 2, pp. 567–576, 2023.

[104] P. Chen, L., Ma, Y., & Guo, “In operando optical characterization of organic mixed ionic–electronic conductors for unraveling charge transport and doping dynamics, A perspective,” *J. Chem. Phys.*, vol. 163, no. 3, 2025.

[105] J. C. Bittencourt, “Synthesis and characterization of ionomers and Poly (fullerene) s for promising application in organic electronics,” 2023.

[106] K. Safarov, T., Kodirov, O., & Beknazarov, “Synthesis Of Polyacetylene And Stabilization Of Polyvinyl Chloride With Polyacetylene,” *Nvpubhouse Libr. Am. J. Appl. Sci. Technol.*, vol. 5, no. 10, pp. 70–78, 2025.

[107] Y. Lu, J., & Chen, “Prospects of organic electrode materials for practical lithium batteries,” *Nat. Rev. Chem.*, vol. 4, no. 3, pp. 127–142, 2020.

[108] X. Zhang, R. W. M., Nautiyal, A., Du, H., Wei, Z., & Zhang, “Electropolymerization of polyaniline as high-performance binder free electrodes for flexible supercapacitor,” *Electrochim. Acta*, vol. 376, pp. 13–8037, 2021.

[109] B. Dai, “Overview of MXene and conducting polymer matrix composites for electromagnetic wave absorption,” *Adv. Compos. Hybrid Mater.*, vol. 5, no. 2, pp. 704–754, 2022.

[110] Chen, X., Peng, L., Liu, Y., Gao, X., Zhang, Y., Tang, C., Zhai, Z., Yang, L., Wu, W., & He, “Conjugated polymers based on metalla-aromatic building blocks,” *Proc. Natl. Acad. Sci.*, vol. 119, no. 29, 2022.

[111] C.-X. Song, C. H. X., Zhang, C.-X., & Zhao, “Inverse CO2/C2H2 separation in a pillared-layer framework featuring a chlorine-modified channel by quadrupole-moment sieving,” *Sep. Purif. Technol.*, vol. 297, pp. 119–608, 2021.

[112] J. Peng, X., Lozano, M., Su, J., Wang, L., Soler-Polo, D., Tuloup, T., ... & Lu, “Breaking Peierls theorem in polyacetylene chains via topological design,” 2025.

[113] S. Chen, Y., Xie, Y., Yan, X., Cohen, M. L., & Zhang, “Topological carbon materials: A new perspective,” *Phys. Rep.*, vol. 868, pp. 1–32, 2020.

[114] G. Li, D., Low, J. Z., Wilhelm, J., Liao, G., Gunasekaran, S., Prindle, C. R., Starr, R. L., “Highly conducting single-molecule topological insulators based on mono- and di-radical cations,” *Nat. Chem.*, vol. 14, no. 9, pp. 1061–1067, 2022.

[115] M. Heiligtag, F. J., & Niederberger, “The fascinating world of nanoparticle research,” *Mater. Today*, vol. 16, no. 7, pp. 262–271, 2013.

[116] P. Singh, P., Desu, P. K., Nakkala, R. K., Kondi, V., Devi, S., Alam, M. S., Hamid, H., Athawale, R. B., & Kesharwani, “Nanotechnology-based approaches applied to nutraceuticals,” *Drug Deliv. Transl. Res.*, vol. 12, no. 3, pp. 485–499, 2022.

[117] A. Shah, M. A. S., Shaikh, M. N., Khan, M. Y., Alfasane, M. A., Rahman, M. M., “Present status and future prospects of jute in nanotechnology: A review,” *Chem. Rec.*, vol. 21, no. 7, pp. 1631–1665, 2021.

[118] S. Harish, V., Tewari, D., Gaur, M., Yadav, A. B., & Swaroop, “Review on nanoparticles and nanostructured materials: Bioimaging, biosensing, drug delivery, tissue engineering, antimicrobial, and agro-food applications,” *Nanomaterials*, vol. 12, no. 3, p. 457, 2022.

[119] A. Santamaria, “Historical overview of nanotechnology and nanotoxicology,” in *In Nanotoxicity Methods Protoc*, 2012, ch. Humana, pp. 1–12.

[120] P. Yadav, D., Jangeer, S., Parashar, R., Sharma, G., Meena, P., Meena, M. K., "A critical review on nanoparticles synthesis: Physical, chemical and biological perspectives," *Int. J. Creat. Res. Thoughts,* vol. 11, pp. 838–848, 2023.

[121] N. Szczyglewska, P., Feliczak-Guzik, A., "Nanotechnology general aspects: A chemical reduction approach to the synthesis of nanoparticles," *Molecules,* vol. 28, no. 13, p. 4932, 2023.

[122] G. Khanna, D., Kaur, A., "Algae-based metallic nanoparticles: Synthesis, characterization and applications," *J. Microbiol. Methods,* vol. 163, pp. 105–656, 2019.

[123] A. Valov, D., & Lipa, "Engineering a Commodity Plastic with Built in Degradation Triggers via Resonant Activation," 2025.

[124] P. Zhou, J., Zou, K., Tao, J., Liu, J., Liu, Y., Duan, L., ... & Liu, "Using multi-scale interaction mechanisms in yolk-shell structured C/Co composite materials for electromagnetic wave absorption," *J. Mater. Sci. Technol.,* vol. 215, pp. 36–44, 2025.

[125] G. Yao, S., Ramakrishna, S., & Chen, "Recent advances in metal–organic frameworks based on electrospinning for energy storage," *Adv. Fiber Mater.,* vol. 5, no. 5, pp. 1592–1617, 2023.

[126] Y. Lu, G., Tian, T., & Wang, "Advanced electrospinning technology applied to polymer-based sensors in energy and environmental applications," *Polymers,* vol. 16, no. 6, p. 839, 2024.

[127] G. Du, S., Song, L., Xiong, J., Li, N., Xi, Z., Wang, L., Jin, D., "Coaxial electrospun TiO2/ZnO core–sheath nanofibers film: Novel structure for photoanode of dye-sensitized solar cells," *Electrochim. Acta,* vol. 78, pp. 392–397, 2012.

[128] E. Anžlovar, A., & Žagar, "Cellulose structures as a support or template for inorganic nanostructures and their assemblies," *Nanomaterials,* vol. 12, no. 11, p. 1837, 2022.

[129] Z. S. Qin, J., Yang, Z., Xing, F., Zhang, L., Zhang, H., & Wu, "Two-dimensional mesoporous materials for energy storage and conversion: current status, chemical synthesis and challenging perspectives.," *Electrochem. Energy Rev.,* vol. 6, no. 1, p. 9, 2023.

[130] M. M. Poolakkandy, R. R., & Menamparambath, "Soft-template-assisted synthesis: A promising approach for the fabrication of transition metal oxides," *Nanoscale Adv.,* vol. 2, no. 11, pp. 5015–5045, 2020.

[131] K. Yamauchi, Y., & Kuroda, "Rational design of mesoporous metals and related nanomaterials by a soft-template approach," *Chem. – An Asian J.,* vol. 3, no. 4, pp. 664–676, 2008.

[132] C. A. Hurst, S. J., Payne, E. K., Qin, L., & Mirkin, "Multisegmented one-dimensional nanorods prepared by hard-template synthetic methods," *Angew. Chemie Int. Ed.,* vol. 45, no. 17, pp. 2672–2692, 2006.

[133] M. Khan, N. A., Ali, S., Latif, S., "Biological synthesis of nanoparticles and their applications in sustainable agriculture production," *Nat. Sci.,* vol. 14, no. 6, pp. 226–234, 2022.

[134] S. A. Heif, M., & Helo, "Civil liability arising from the use of nanotechnology in the medical field: A comparative study between Jordanian, Emirati and Egyptian legislation," *J. Leg. Ethical Regul. Issues*, vol. 25, no. 1, 2022.

[135] K. Raghav, S. D., Yadav, P. K., *Nanotechnology for a sustainable future*. Amsterdam, Netherlands: Elsevier, 2020.

[136] P. Das, N., Panda, S., Das, D. K., Nayak, S. K., Parthasarathy, S., Kirgiz, M. S., & Patnaik, "Polymer nanocomposites: Innovations in material design and applications," in *In Exploring nanomaterial synthesis, characterization, and applications*, 2025, pp. 169–196.

[137] F. Camargo, P. H. C., Satyanarayana, K. G., & Wypych, "Nanocomposites: Synthesis, structure, properties and new application opportunities," *Mater. Res.*, vol. 12, pp. 1–39, 2009.

[138] Y. Zhu, C., Du, D., Eychmüller, A., & Lin, "Engineering ordered and nonordered porous noble metal nanostructures: Synthesis, assembly, and their applications in electrochemistry," *Chem. Rev.*, vol. 115, no. 16, pp. 8896–8943, 2015.

[139] O. Ahmad, S., Munir, S., Zeb, N., Ullah, A., Khan, B., Ali, J., Bilal, M., "Green nanotechnology: A review on green synthesis of silver nanoparticles—An ecofriendly approach," *Int. J. Nanomedicine*, vol. 14, pp. 5087–5107, 2019.

[140] K. Bharadwaj, "Green synthesis of gold nanoparticles using plant extracts as beneficial prospect for cancer theranostics," *Molecules*, vol. 26, no. 21, p. 6389, 2021.

[141] H. Xu, L., Wang, Y.-Y., Huang, J., Chen, C.-Y., Wang, Z.-X., & Xie, "Silver nanoparticles: Synthesis, medical applications and biosafety," *Theranostics*, vol. 10, no. 20, pp. 89–96, 2020.

[142] G.-W. Zhang, D., Ma, X.-L., Gu, Y., Huang, H., & Zhang, "Green synthesis of metallic nanoparticles and their potential applications to treat cancer," *Front. Chem.*, vol. 8, p. 799, 2020.

[143] K. B. Oo, W., Park, J. H., Sonia, Z. A., Win, M. Z., Cho, D., & Yi, "Modification of Copper-Ceria Catalyst via Reverse Microemulsion Method and Study of the Effects of Surfactant on WGS Catalyst Activity," *Catalysts*, vol. 13, no. 6, p. 951, 2023.

[144] R. S. Powar, N. S., Patel, V. J., Pagare, P. K., & Pandav, "Cu nanoparticle: Synthesis, characterization and application," *Chem. Methodol.*, vol. 3, pp. 457–480, 2019.

[145] & B. Reddy, R. K., Kumar, H. D., Lee, S.-M., Seshaiah, K., "Synthesis, characterization of thiosemicarbazone metal complexes and antioxidant activity in different in vitro model systems," *J. Serbian Chem. Soc.*, vol. 78, no. 2, pp. 229–240, 2013.

[146] B. A. Saeed, B. M. S., Al-jadaan, S. A. N., & Abbas, "Pharmacological and biological evaluation of 5,5'[(1,4-phenelene) bis (1,3,4-thiadiazol-2-amine)]," In Journal of Physics, 2019.

[147] A. S. Esfahanizadeh, M., & Mehdipour, "Preparation and properties of thermally stable polyureas containing ether and ketone units," *J. Appl. Chem. Res.*, 2015.

[148] E. Shahwan, T. A. E., Sirriah, S. A., Nairat, M., Boyacı, E., & Eroğlu, "Green synthesis

of iron nanoparticles and their application as a Fenton-like catalyst for the degradation of aqueous cationic and anionic dyes," *Chem. Eng. J.*, vol. 172, no. 1, pp. 258–266, 2011.

[149] J.-R. Sierra-Ávila, R., Pérez-Alvarez, M., Cadenas-Pliego, G., Ávila-Orta, C. A., Betancourt-Galindo, R., "Synthesis of copper nanoparticles coated with nitrogen ligands," *J. Nanomater.*, vol. 2014, no. 1, pp. 361–791, 2014.

[150] D. Sirohi, S., Mittal, A., Nain, R., Jain, N., Singh, R., Dobhal, S., ... & Parida, "Effect of nanoparticle shape on the conductivity of Ag nanoparticle poly (vinyl alcohol) composite films," *Polym. Int.*, vol. 68, no. 12, pp. 1961–1967, 2019.

[151] A. M. El-Saghier, A. M., Abdul-Baset, A., El-Hady, O. M., & Kadry, "Synthesis of some new thiadiazole/thiadiazine derivatives as potent biologically active compounds," *Sohag J. Sci.*, vol. 8, no. 3, pp. 371–375, 2023.

[152] R. Toader, G. A., Rusen, E., Teodorescu, M., Diacon, A., Stanescu, P. O., Rotariu, T., "Novel polyurea polymers with enhanced mechanical properties," *J. Appl. Polym. Sci.*, vol. 133, no. 38, 2016.

[153] G. Ruan, T., Li, P., Wang, H., Li, T., & Jiang, "Identification and prioritization of environmental organic pollutants: From an analytical and toxicological perspective," *Chem. Rev.*, vol. 123, no. 17, pp. 10584–10640, 2023.

[154] S. Zhang, X.-F., Liu, Z.-G., Shen, W., & Gurunathan, "Silver nanoparticles: Synthesis, characterization, properties, applications, and therapeutic approaches," *Int. J. Mol. Sci.*, vol. 17, no. 9, p. 1534, 2016.

[155] Razafindralambo, H., Sun, Y. Z., Vasantharaj, S., Ghafarifarsani, H., Hoseinifar, S. H., & Raeeszadeh, M. Vijayaram, S., "Applications of green synthesized metal nanoparticles a review. Biological Trace Element Research," vol. 202, no. 1, pp. 360–386, 20AD.

[156] E. A. Mohamed, "Green synthesis of copper & copper oxide nanoparticles using the extract of seedless dates," *Heliyon*, vol. 6, no. 1, pp. 31–95, 2020.

[157] M. Lekkerkerker, H. N., Tuinier, R., & Vis, *Colloids and the depletion interaction*. Springer Nature, 2024.

[158] A. K. Liebchen, B., & Mukhopadhyay, "Interactions in active colloids," *J. Phys. Condens. Matter*, vol. 34, no. 8, 2022.

[159] Malvern Instruments, "Zeta potential: An introduction in 30 minutes," *Worcestershire, UK: Malvern Instruments*, 2015.

[160] D. K. Naser, K. A., Abbas, A. K., & Aadim, "Zeta potential of Ag, Cu, ZnO, CdO and Sn nanoparticles prepared by pulse laser ablation in liquid environment," *Iraqi J. Sci.*, vol. 61, no. 7, pp. 2570–2581, 2020.

[161] A. H. Saied, E., Basher, N. S., Badr, B. M., Elkady, F. M., Mostafa, A. G., Ibrahim, N. A., ... & Hashem, "Eco-friendly biosynthesis of manganese oxide-silver bimetallic nanoparticles using Cucumis melo peel extract: characterization, antioxidant, antimicrobial, and antiviral activities," *Bioresour. Bioprocess.*, vol. 13, no. 1, p. 19, 2026.

[162] M. A. Gonçalves, L. A., de Souza, E. G., Nóbrega, L. H., Bier, V. A., Maggi, M. F., Bazzi, C. L., & Uribe-Opazo, "Spatial and temporal variability of soil apparent electrical conductivity," *Precis. Agric.*, vol. 26, no. 1, p. 10, 2025.

[163] Y. Ren, Z., Fang, F., Yan, N., & Wu, "State of the art in defect detection based on machine vision," *Int. J. Precis. Eng. Manuf. Technol.*, vol. 9, no. 2, pp. 661–691, 2022.

[164] Z. L. Dong, K., Peng, X., & Wang, "Fiber/fabric-based piezoelectric and triboelectric nanogenerators for flexible/stretchable and wearable electronics and artificial intelligence," *Adv. Mater.*, vol. 32, no. 5, 2020.

## الخلاصة

لقد جذبت المتراكبات البوليمر/الجسيمات النانوية اهتمامًا علميًا كبيرًا في العقود الأخيرة نظرًا لخواصها البنيوية والحرارية والكهربائية القابلة للتعديل، مما يجعلها واعدة للتطبيقات التكنولوجية المتقدمة. في هذا السياق، تركز الدراسة الحالية على تحضير وتوصيف ثمانية بوليمرات بولي يوريا مشتقة من مونومرات قاعدة شيف، باستخدام مونومرات عطرية مختارة لأربعة أنواع مختلفة من الداي إيزوسيانات (MDI، TDI، PDI، وHDI). تم تطعيم هذه البوليمرات لاحقًا بالجسيمات النانوية الفضية والنحاسية لتحقيق موصلية كهربائية عالية مع الحفاظ على استقرار حراري ممتاز.

المونومر الأول، ثنائي ثيوسيميكاربازون تيريفثالدهيد (TBT)، فقد تم تحضيره عبر تفاعل تيريفثالدهيد مع ثيوسيميكاربازيد في الإيثانول، وفق الصيغة البنيوية التالية:

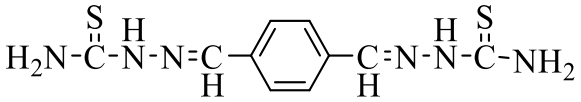

Terephthaldehyde bis(thiosemicarbazone) (TBT)

أما المونومر الثاني، 5,5′-[(1,4-فينيلين) ثنائي (1,3,4-ثياديازول-2-أمين)] (TDA)، فقد تم تحضيره من خلال تفاعل حمض التيريفثاليك مع الثيوسيميكاربازيد باستخدام حمض الكبريتيك المركز، وفق الصيغة البنيوية التالية:

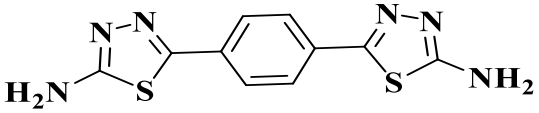

5,5′-[(1,4-phenene) bis(1,3,4-thiadiazol-2-amine)] (TDA)

لقد مثلت هذه المونومرات البنية الأساسية في تفاعلات التكثيف مع الداي إيزوسيانات المختارة في N-ميثيل-2-بيروليدون الجاف (dry-NMP)، مما أدى إلى تكوين بوليمرات بولي يوريا. وقد تم تحضير بوليمرات البولي يوريا من المونومر TBT:

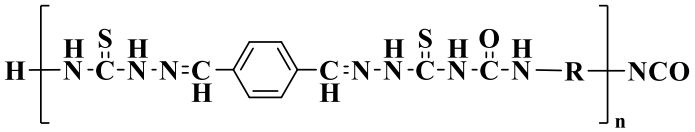

R= 2a= 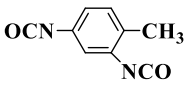 , 2b= 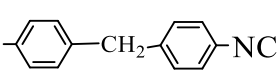 , 2c= 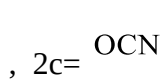 ,

2d= 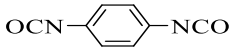

أما بوليمرات البولي يوريا التي تم تحضيرها من المونومر TDA:

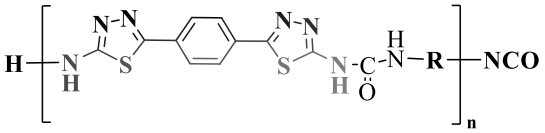

R= 3a= 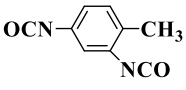 , 3b= 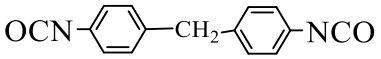 , 3c= 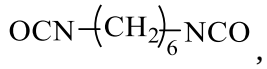 ,

3d= 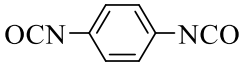

تم تحضير المركبات النانوية الهجينة لبولي يوريا عن طريق دمج الجسيمات النانوية الفضية والنحاسية في مصفوفة البوليمر باستخدام التشتت بالموجات فوق الصوتية. أكدت مطيافية الأشعة تحت الحمراء (FT-IR) تكوين روابط البولي يوريا بنجاح، في حين أظهرت التحليلات الحرارية الوزنية (TGA) سلوك تحلل حراري متعدد المراحل مع استقرار حراري مرتفع، خصوصًا في البوليمرات المبنية على PDI. كما أكدت تحليلات حيود الأشعة السينية (XRD) الطبيعة البلورية للجسيمات النانوية المدمجة، بينما أظهرت ملاحظات المجهر الإلكتروني الماسح ذو الدقة العالية (FESEM) والمجهر الإلكتروني النافذ (TEM) توزيعًا نسبيًا متجانسًا للجسيمات النانوية الفضية وتكوّن مسارات معدنية مترابطة بواسطة الجسيمات النحاسية، مما ساهم بشكل كبير في تحسين الموصلية الكهربائية. علاوة على ذلك، أكدت تحليلات الطيفية بالطاقة المشتتة للأشعة (EDX) وتحليل الجهد السطحي (Zeta potential) فعالية دمج الجسيمات النانوية واستقرارها الغروي العالي، خصوصًا في المركبات المحتوية على النحاس والنظم المبنية على PDI. أظهرت القياسات الكهربائية تحسنًا ملحوظًا في الموصلية مقارنة بالبوليمرات الأصلية، مع أداء متفوق للمركبات النانوية المعتمدة على الفضة، مما يبرز إمكاناتها للتطبيق في الإلكترونيات المرنة، والأحبار الموصلة، وأنظمة إدارة الحرارة.

*جمهورية العراق*

*وزارة التعليم العالي والبحث العلمي*

*جامعة ميسان*

*كلية العلوم*

*قسم الكيمياء*

# تحضير ودراسة الخواص الكهربائية والحرارية لبعض بوليمرات البولي يوريا المتراكبة

**رسالة مقدمة الى**

**كلية العلوم/ جامعة ميسان كجزء من متطلبات نيل**

**شهادة الماجستير في العلوم – الكيمياء**

الطالبة

**زينب كاظم حمود**

بكالوريوس علوم كيمياء/ جامعة ميسان (٢٠١٩)

**بإشراف**

**ا.م.د. أحمد مجيد عباس**

**ا.م.د. منذر عبد الحسن**

**١٤٤٧ هـ**

**٢٠٢٦ م**